The coupled chemo-mechanical degradation of cement-based materials

A thesis submitted in fulfillment of the requirements for the degree of

Doctor of Philosophy

Zhongcun Zuo

School of Civil, Environmental and Mining Engineering

Faculty of Engineering, Computer and Mathematical Sciences

University of Adelaide

January 2020

This thesis is dedicated to
my loved ones.

Statement of Originality

I certify that this work contains no material which has been accepted for the award of any other degree or diploma in my name, in any university or other tertiary institution and, to the best of my knowledge and belief, contains no material previously published or written by another person, except where due reference has been made in the text. In addition, I certify that no part of this work will, in the future, be used in a submission in my name, for any other degree or diploma in any university or other tertiary institution without the prior approval of the University of Adelaide and where applicable, any partner institution responsible for the joint-award of this degree.

I acknowledge that copyright of published works contained within this thesis resides with the copyright holder(s) of those works.

I also give permission for the digital version of my thesis to be made available on the web, via the University's digital research repository, the Library Search and also through web search engines, unless permission has been granted by the University to restrict access for a period of time.

I acknowledge the support I have received for my research through the provision of an Australian Government Research Training Program Scholarship.

Signed:_____

Date:_____

Acknowledgements

I would like to sincerely express my appreciation and thanks to my principle supervisor Dr. Terry Bennett and co-supervisor Dr. Mohamed Ali Sadakkathulla for initiating the present research project with their great foresight and offering me this golden opportunity. During my PhD candidature, they provide me all available technical supports that are essential in this project, and spare no effort to train me as a qualified independent researcher, from which I will benefit in the rest of my life. Specifically, I would like to acknowledge the inspiration of numerical modelling and Matlab coding from Dr. Terry Bennett, and the guidance of chemical degradation on cement-based materials from Dr. Mohamed Ali Sadakkathulla.

I gratefully acknowledge the financial support of the Australian Government Research Training Program Scholarship for letting me concentrate fully on the research work. I would like to extend this appreciation to staff in University of Adelaide for their assistance with the successful completion of my study.

Great thanks to my friends who ever chat and share, go hiking and crabbing, play video games and basketball, et cetera, with me. When I first touched down at Adelaide Airport, I was riddled with discomfort and anxiety. With their company, I can gradually settle down thereafter and get on the right track of my research.

Last but not least, my most sincere appreciation to every member in my family for unconditionally supporting and even tolerating my wayward choices. Their concern and love make me never dare to let them down. The growing sense of guilt for my absence from their lives drives me through the "Darkest Hour" of my PhD candidature.

List of Publications

1) Zhongcun Zuo and Terry Bennett : Simulation of the degradation of oilwell cement for the prediction of long-term performance, *Construction and Building Materials, Volume 202, 30 March 2019, Pages 669-680.*

2) Zhongcun Zuo and Terry Bennett : Numerical simulation of the interaction between chemical and mechanical damage for cementitious materials, *ACMSM25, 2020, 395-406.*

3) Zhongcun Zuo and Terry Bennett : Modelling and numerical simulations of the coupled chemo-mechanical degradation behaviour of cement-based materials, submitted to *Journal of Engineering Mechanics.*

4) Zhongcun Zuo and Terry Bennett : The chemo-mechanical effect of calcium carbonate precipitation for cement-based materials exposed to carbonated brine, *International Journal of Greenhouse Gas Control* (ready for submission).

Abstract

The thesis is devoted to study the degradation mechanisms of cement-based materials in contact with aggressive aqueous solutions, including the process of chemical reactions between cement constituents and pore solution with intruded ion spices, the subsequent variation of elastic moduli due to constituents transformation and the overall mechanical behaviour based on the nonlinearity of chemically degraded material. The proposed methodology presents the integrated solution for cement-based materials under requirements of various serving conditions, long duration lifetime and multi failure criteria.

The reactive transport model is employed to reproduce the dissolution and precipitation of cement constituents with thermodynamic equilibrium and kinetic laws. The Mori-Tanaka micromechanical model accommodates solid phases of cement-based materials with micromechanical behaviour and evaluate the elastic properties of the material in the present study. The post-peak behaviour of the material due to microcracks propagation is captured with the displacement based non-local damage model, and subsequently the overall flexural performance.

The process of chemical degradation of ordinary Portland cement (OPC) is predominated by the portlandite dissolution and calcium silicate hydrate (C-S-H) decalcification, and the diffusion-controlled progress is slow in real service conditions. The long-term performance of cement-based materials exposed to aqueous solutions is simulated up to 1000 years by reactive transport model with the calibrated parameters. The chemical reactions between cement constituents and diffused ion species result in porosity change, which is adopted to determine the relation of the corrosion depth versus square root of time. The corrosion rate can be reduced by the precipitation of calcium carbonate in cement matrix exposed to carbonate ions enriched solutions.

The dissolution and precipitation of cement constituents render the variation of material microstructure, and subsequently the relevant change of elasticity. The Mori-Tanaka scheme is employed to evaluate the elastic moduli of chemically degraded cement-based materials, which can cause the microcracks under external loading due to the stiffness reduction. The propagation of mechanical damage is evaluated by the non-local continuum damage model, and converted into porosity change of the material, which in turn promotes the progress of chemical degradation. The fully coupled chemo-mechanical simulation is able to demonstrate the instantaneous interaction between chemical degradation and mechanical damage, which can result in marked differences with the non-coupled case.

The calcium carbonate precipitation is a common phenomenon in cement-based materials, and plays an important role in chemo-mechanical degradation. Magnesium ions can be incorporated into the amorphous calcium carbonate reducing its solubility. The formation of amorphous calcium magnesium carbonate is observed on the surface of cement-based materials exposed to aqueous solution rich in magnesium, of which the sealing effect is demonstrated by both experiments and numerical simulations. The calcium carbonate layer forms within cement matrix without the presence of magnesium in the leaching solutions, and can cease the progress of chemical degradation by clogging the pore space. The interaction of pH and CO_2 concentration causes the dissolution/re-precipitation of calcium carbonate, presenting a shifting calcium carbonate layer towards the interior of the material. The influences of cement constituents transformation, including the precipitated calcium carbonate, is evaluated by the aforementioned methodology, which is subsequently applied to investigate the overall mechanical performance.

The proposed methodology accommodates the dissolution/precipitation of cement constituents and relevant mechanical behaviour, is suggested to be applied to other chemo-mechanical related projects in future studies.

Keywords : Cement Durability; Coupled Degradation; Calcium Carbonate; Elasticity Change; Microstructure; Non-Local Damage; Reactive Transport Model.

Contents

1 Introduction **1**

1.1 Background 1

1.2 Objectives 4

1.3 Outline of thesis 5

References 8

2 The long-term chemical degradation **13**

2.1 Introduction 16

2.2 Modelling approach 18

2.2.1 Transport equations 18

2.2.2 Surface complexation model 20

2.2.3 Thermodynamic equilibrium 23

2.2.4 Kinetics 24

2.3 Modelling calibration and validation 25

2.3.1 Introduction of experiments 26

2.3.2 Determination of simulated degradation front 26

2.3.3 Parameter sensitivity and model calibration 28

2.3.4 Modelling validation 30

2.3.5 General discussion 31

2.4 Long term simulations 32

2.4.1 Simulation of leaching by deionised water 33

2.4.2 Simulation of leaching by groundwaters 36

2.4.3 Validation of the model . . . 39
2.5 Conclusions . . . 40
References . . . 42

3 Coupled chemo-mechanical degradation 49
3.1 Introduction . . . 52
3.2 Modelling methodology of coupled degradation . . . 55
3.2.1 Chemical degradation modelling . . . 56
3.2.1.1 Transport equations . . . 56
3.2.1.2 Thermodynamic equilibrium . . . 56
3.2.1.3 Kinetics . . . 57
3.2.2 Mechanical damage modelling . . . 57
3.2.2.1 Damage evaluation modelling . . . 57
3.2.2.2 Displacement based non-local damage model . . . 58
3.2.3 Constitutive laws of the coupled damage . . . 59
3.3 The influence of leaching on the mechanical performance . . . 63
3.3.1 Chemical System . . . 63
3.3.2 Leaching induced reduction of elasticity . . . 64
3.3.3 The mechanical behaviour of a leached mortar beam . . . 66
3.4 The simulation of coupled chemical and mechanical degradation . . . 71
3.4.1 The coupled chemo-mechanical degradation on leached mortar beam . . . 72
3.4.2 The residual mechanical behaviour of mortar beams with coupled and non-coupled degradation . . . 77
3.5 Conclusions . . . 79
References . . . 81

4 The chemo-mechanical effect of carbonation 87
4.1 Introduction . . . 90

4.1.1 Mechanisms of CCP 90
4.1.2 The chemo-mechanical effect of CCP on cement-based materials 92
4.1.3 Scope and aim 93
4.2 The formation of ACMC in cement-based materials 94
4.2.1 The interpretation of experiments 95
4.2.2 The numerical simulation of the surface ACMC layer 96
4.2.3 General discussion 99
4.3 The pore-clogging behaviour of CCP in cement-based materials . . . 101
4.4 The effect of CCP on mechanical behaviour 106
4.4.1 The precipitation/dissolution of calcite layer in cement-based material 106
4.4.2 The residual elasticity of cement-based material exposed to carbonated brine 109
4.4.3 The mechanical behaviour of cement-based material exposed to carbonated brine 115
4.5 Conclusions 117
References 119

5 Conclusions and recommendations **127**
5.1 Conclusions 127
5.2 Recommendations 129

List of Tables

2.1 The surface complexation reactions considered in the reactive transport model. 22

2.2 The dissolution/precipitation of cement minerals 24

2.3 Chemical reactions in pore solution 25

2.4 Dissolution/precipitation reaction kinetic data for cement minerals . . 25

2.5 Initial proportion of cement minerals as volume fractions of the solid phase 29

2.6 Parameters for sensitivity testing 29

2.7 The composition of groundwaters 36

3.1 The chemical formulae and thermodynamic data of the incorporated cement minerals in the chemical system 64

3.2 The volume fractions (%) of compositions for cement paste and mortar adopted in simulations of section 3.3.2 65

3.3 Intrinsic elastic properties of solid phases in cement-based material . 67

3.4 The volume fractions (%) of compositions for mortar adopted in simulations of section 3.3.3 68

4.1 The chemical compositions of aqueous solutions in experiments [46]. 95

4.2 The volume fractions (%) of solid phases for cement paste adopted in simulations. 97

4.3 The chemical input data of the considered solid phases in simulations. 98

4.4 The concentrations of dissolved CO_2 in leaching solutions in experiments [3]. 101

4.5 Intrinsic elastic moduli of minerals in cement paste. 110

List of Figures

2.1 Schematic diagram of the model in simulations. 27

2.2 Identification of the corrosion front from mineral volume fractions and porosity profiles. 27

2.3 The effect on corrosion rate on initial porosity, cement composition and diffusion coefficient. 30

2.4 The validation of corrosion rate for pH=0 and 2. 31

2.5 Profiles of porosity for simulation of well cement exposed to pH=0 hydrochloric solution. 31

2.6 Schematic diagram of the model in long term simulations. 32

2.7 Profiles of a) porosity; and change in mineral volume fractions for b) portlandite and c) C-S-H, exposed to deionised water, with depth. . . 33

2.8 The concentration of Ca^{2+} for leaching of deionised water 34

2.9 Profiles of pH and minerals change in volume fractions at a) 100 b) 400 c) 550 and d) 1000 years exposed to deionised water. 35

2.10 Profiles of pH at varying depths and change in portlandite volume fraction at the non-exposed end of the model. 35

2.11 The corrosion rates of different waters in 1000 years 37

2.12 The simulated porosity and calcite profiles for highcarbonate and saline water after 1000 years 37

2.13 Profiles of cement minerals variation exposed to a) high carbon groundwater b) low carbon groundwater c) clay groundwater and d) saline groundwater at 1000 years. 38

2.14 The pH profiles after 1000 years for different groundwaters 39

3.1 Schematic flow diagram of the coupling scheme for chemical and mechanical damage proposed in present work. 55

3.2 Schematic diagram of the evolution of Young's modulus and elastic threshold with chemical and mechanical damage. 62

3.3 Schematic diagram of the one-dimensional model for cement-based material subject to 6M NH_4NO_3 leaching. 65

3.4 Profiles of minerals in volume fraction for (a) paste and (b) mortar exposed to 6M NH_4NO_3 solution for 15 days. 66

3.5 Profiles of Young's modulus for paste and mortar subject to 6M NH_4NO_3 solution leaching for 15 days. 67

3.6 Schematic diagram of the model for the mortar beam subject to 6M NH_4NO_3 leaching and subsequently three-point bending test. 68

3.7 Profiles of (a) C-S-H(Intact), (b) C-S-H(Leached), (c) portlandite in volume fractions and (d) Young's modulus (GPa) for the mortar beam exposed to 6M NH_4NO_3 solution for 114 days. 69

3.8 Comparison of force versus displacement curves between three-point bending simulation and experiment for (a) the intact mortar beam and (b) the one exposed to 6M NH_4NO_3 solution for 114 days. 70

3.9 Schematic diagram of the model for the mortar beam subject to the displacement loading and 6M NH_4NO_3 leaching. 71

3.10 Profiles of (a) C-S-H(Intact), (b) C-S-H(Leached), (c) portlandite in volume fractions and (d) Young's modulus (GPa) of the mortar beam simultaneously subject to the imposed displacement of 1.8×10^{-2} mm and 6M NH_4NO_3 solution for 114 days. 72

3.11 Profiles of the (a) mechanical and (b) chemical damage parameters for the mortar beam simultaneously subject to the imposed displacement of 1.8×10^{-2} mm and 6M NH_4NO_3 solution for 114 days. 73

3.12 Profiles of equivalent strain of the mortar beam subject to the imposed displacement of 1.8×10^{-2} mm and 6M NH_4NO_3 solution for the coupled damage simulation of (a) 40, (b) 80, (c) 114 days and (d) non-coupled damage simulation after 114 days leaching; (e) the comparison of equivalent strain in the lower central cross section between cases. . 76

3.13 Profiles of damage parameters of the mortar beam subject to the total imposed displacement of (a) 3.5×10^{-2} mm and (b) 4.5×10^{-2} mm after the coupled degradation of a displacement of 1.8×10^{-2} mm and 6M NH_4NO_3 solution leaching for 114 days; and profiles of damage parameters of the mortar beam subject to the imposed displacement of (c) 3.5×10^{-2} mm and (d) 4.5×10^{-2} mm after 114 days leaching of 6M NH_4NO_3 solution. 78

4.1 Schematic flow diagram of the one-dimensional domain of cement paste subject to leaching solution. 98

4.2 Profiles of the surface element (SE) and the outermost element (OE) of cement paste for the system in figure 4.1 subject to the hard tap water in table 4.1 for 2 days, including the content of ACMC and porosity of SE, and portlandite and C-S-H(Intact) of OE. 99

4.3 Profiles of calcite, portlandite and C-S-H(Leached) in the outermost element of cement paste subject to the demineralized water in table 4.1 for 300 hours. 99

4.4 Profiles of Ca/Si ratio and calcite in simulation by 45 days, and Ca/Si ratio measured in experiment in the case of 30 mM dissolved CO_2. . . 103

4.5 Profiles of Ca/Si ratio and calcite in simulation by 20 days, and Ca/Si ratio measured in experiment in the case of 10 mM dissolved CO_2. . . 103

4.6 Profiles of Ca/Si ratio and calcite in simulation by 45 days, and Ca/Si ratio measured in experiment in the case of 0.01 mM dissolved CO_2. . 104

4.7 The depth of reaction zone versus the square root of time for 30 mM, 10 mM and 0.01 mM dissolved CO_2 in experiments and simulations. . 105

4.8 Schematic diagram of the simulation for cement paste beam leached by carbonated brine (pH=3.7 and 30 mM dissolved CO_2) 107

4.9 Profiles of calcite volume fractions in the cement paste beam exposed to carbonated brine (pH=3.7 and 30 mM dissolved CO_2) for (a) 150 days, (b) 500 days, (c) 900 days and (d) 1400 days. 108

4.10 The volume fractions of (a) C-S-H(Intact), (b) C-S-H(Leached), (c) portlandite and (d) Young's modulus (GPa) of the cement paste beam exposed to carbonated brine (pH=3.7 and 30 mM dissolved CO_2) for 150 days. 111

4.11 The volume fractions of (a) C-S-H(Intact), (b) C-S-H(Leached), (c) portlandite and (d) Young's modulus (GPa) of the cement paste beam exposed to carbonated brine (pH=3.7 and 30 mM dissolved CO_2) for 500 days. 112

4.12 The volume fractions of (a) C-S-H(Intact), (b) C-S-H(Leached), (c) portlandite and (d) Young's modulus (GPa) of the cement paste beam exposed to carbonated brine (pH=3.7 and 30 mM dissolved CO_2) for 900 days. 113

4.13 The volume fractions of (a) C-S-H(Intact), (b) C-S-H(Leached), (c) portlandite and (d) Young's modulus (GPa) of the cement paste beam exposed to carbonated brine (pH=3.7 and 30 mM dissolved CO_2) for 1400 days. 114

4.14 Schematic diagram of the four-point bending test for cement paste beam leached by carbonated brine (pH=3.7 and 30 mM dissolved CO_2). 115

4.15 Curves of force versus displacement in the four-point bending test for cement paste beam subject to carbonated brine (pH=3.7 and 30 mM dissolved CO_2) after different time durations. 116

Chapter 1

Introduction

The durability of cement-based materials involves a complex chemical and physical process, especially for infrastructures exposed to aqueous solutions carrying aggressive ion species. The external environment poses a threat to the integrity of the material by triggering a series of chemical reactions with cement constituents, which weakens material properties with regard to serviceability.

The chemical degradation is the source for initiating the deterioration of cement-based materials, and occurs in various processes depending on the compositions in external solutions. Water plays an essential role in chemical degradation as both reaction medium and participant. Under this context, the universal chemical reaction is the dissolution of cement constituents regardless of the composition of aqueous solutions, which results in the change of microstructure and elastic properties for the material. Therefore, the investigation of chemical degradation for cement-based materials should base on the water-induced chemical reactions, meanwhile consider other simultaneous reactions according to the specific type of ion species in the external environment. The dissolution/precipitation of cement minerals within material matrix can significantly influence the transport and mechanical properties, and subsequently lead to microcracks under external loading by affecting the equilibrium of initial condition. It is inevitable to accommodate the mechanisms of both chemical reactions and mechanical damage to study the degradation of cement-based materials.

1.1 Background

The progress of chemical degradation is determined by the diffusion of ion species in the pore space of cement matrix [1], therefore the diffusion-controlled process is relatively slow, up to thousands of years [2]. In order to reduce time cost, various

experimental methods have been employed to accelerate the degradation of cement-based materials in laboratory environment, for instance, increasing the concentration of ion species [1, 3], applying the external electric field [4] and aggravating the physical boundary conditions [5]. The existing experimental outcomes demonstrate the mechanisms of cement degradation in significantly shortened duration, which verifies the efficiency of methods for the accelerated degradation. However, the extrapolation of these outcomes to real service life and engineering applications is infeasible due to the unsubstantial laboratory setting.

In terms of predicting the long-term degradation, the corrosion depth of cement-based materials is normally adopted as a principal indicator, and analytically proportional to the square root of time due to the diffusion-controlled feature of degradation [6]. In experiments, phenolphthalein can be applied on the cut surface of specimens to indicate the corrosion depth on the basis of pH dependence, which is not accurate since chemical degradation occurs before the pH of pore solution significantly decreases [7].

With the availability of computational methods, numerical modelling of chemical degradation is developed to investigate the performance of cement-based materials. The initial model is proposed to simulate the ion transport and subsequent matrix dissolution of cement in a phenomenological method [8, 9], which simplifies chemical reaction with the equilibrium of calcium concentrations. In this sense, the model is unable to reproduce chemical reactions specifically and incorporate the precipitation of cement minerals. Reactive transport modelling accommodates both ion transport and aquatic chemistry, and has been widely applied to chemical related studies of porous media [10–12]. The chemical reaction is evaluated based on thermodynamic equilibrium and kinetic constraint, which offers a convincing solution [13].

The coupled degradation for cement-based materials involves modelling of chemical reaction, mechanical damage and coupling scheme, any module of which can potentially be improved and subsequently enhance the overall solution.

In existing studies, reactive transport model has gradually replaced the phenomenological method to simulate the chemical degradation in detail. In addition, the proper development of microcracks is a crucial aspect for influencing the process of reactive transport, and essential to investigate the overall mechanical behaviour [14]. The non-local damage techniques [15, 16] can describe the material non-linearity for capturing the post-peak behaviour of mechanical performance, which however has not been widely realized.

The interaction between chemical and mechanical degradation requires that the model is able to immediately feed back either of the degradation outcomes to the coupled process. Therefore, the integrated coupling scheme is necessary to overcome the inadequacy of existing studies to achieve the fully coupled degradation for cement-based materials. For the aforementioned phenomenological method, the chemical degradation is straightforwardly linked to porosity and/or Young's modulus [17–22], which is a practical simplification but insufficient to reveal fundamental mechanisms. With the output of reactive transport model, the residual amount of each solid phase in cement material is obtained as the result of chemical degradation, which needs to be converted to residual mechanical properties. To achieve this, the micromechanical behaviour of each solid phase is supposed to be taken into account to precisely evaluate the elastic moduli of the degraded material. The micromechanical models, such as Mori-Tanaka [23], generalized self-consistent [24] and interaction direct derivation schemes [25], are available for the evaluation of material elasticity.

Subsequently, the weakened material is unable to maintain the initial equilibrium, and results in mechanical damage under external loading, which can increase voids within the material matrix. The microcracks can change transport properties and promote the reactive transport process as the feedback to chemical degradation [11, 14, 21, 22]. The incorporation of mechanical damage needs to be consistent with the chemical model, of which the methods are generally to update porosity of material matrix or the tensors of transport and stiffness properties. In terms of capturing the post-peak behaviour, non-local damage modelling is suggested in literature [11], but has not been widely adopted yet for the coupled chemo-mechanical degradation.

The coupled chemo-mechanical degradation varies with specific circumstances, since the composition of external solutions determines the undergoing chemical reactions and subsequent impacts on material properties. The precipitation of calcium carbonate in cement-based materials is a universal phenomenon in natural environment due to the abundance of CO_2 [7], and has great potential in industrial applications, for example, carbon capture and storage [3, 26], cement/concrete restoration [27–29], and geological disposal [30].

The crystallization pathway of calcium carbonate is highly dependent on compositions in aqueous solutions, and can exert different influences on the process of cement degradation. The amorphous calcium carbonate is normally a precursor for the crystallization of $CaCO_3$ [31–33], which can be affected by the pH value of reactive solution [34]. Vaterite is demonstrated to be the precursor prior to the transformation

from amorphous calcium carbonate to calcite [35, 36]. With the presence of magnesium ions, Mg/Ca ratio in the reactive solution plays an important role in amorphous calcium carbonate crystallization [34, 36], since magnesium ions can exert a stabilizing effect due to high dehydration energy [37, 38], and the formation of amorphous calcium magnesium carbonate occurs in the condition of Mg/Ca ratio $\geq$ 1:8. In terms of cement-based materials exposed to carbonated brine, the experiments [3, 39] demonstrate that the formation of ACMC layer seals the water/cement interface and protects cement matrix from further chemical degradation.

The clogging effect due to the formation of $CaCO_3$ layer within material matrix is of interest [40–44] for ceasing/reducing chemical reactions. Meanwhile, the concentration of external aqueous solutions can result in the dissolution and re-precipitation of the carbonate layer presenting a trend of shifting inwards [3]. The calcium carbonate has been proven to be effective in enhancing elasticity of cement-based materials [45, 46]. Therefore, the evaluation of residual elastic moduli and coupled behaviour become more complicate than the case of non-carbonation.

1.2 Objectives

In the present project, the study is implemented with three-level objectives, which represent innovations of coupled chemo-mechanical degradation for cement-based materials.

Objective 1 : The long-term performance for cement-based materials subject to chemical degradation

- Investigation of chemical degradation process of cement-based materials up to 1000 years with numerical modelling for overcoming difficulties of extrapolating accelerated experimental outcomes.
- Determination of corrosion depth by dissolution/precipitation of cement minerals, and evaluation of corrosion rate for cement-based materials leached by various groundwater.

Objective 2 : The fully coupled chemo-mechanical degradation for cement-based materials

- Incorporation of reactive transport model, non-local damage and micromechanical model for consummating aquatic chemistry, microstructural behaviour and microcracks propagation in coupled chemo-mechanical degradation.
- Fully coupling the interaction between chemical and mechanical degradation process, and exploring the significance by contrast to the non-coupled case.

Objective 3 : The chemo-mechanical behaviour of cement-based materials exposed to carbonate brine

- Investigation of the formation and subsequent effect of carbonate layer for cement-based materials exposed to magnesium rich carbonated brine.
- Evaluation of the chemo-mechanical behaviour of calcium carbonate precipitation within cement matrix with regard to the interaction of pH and CO_2 concentration.

1.3 Outline of thesis

The deterioration of cement-based materials subject to both aggressive environmental conditions and mechanical loading is studied in this thesis, which consists of three manuscripts in Chapter 2 - 4. Each of the chapters is titled as the generalization of whole content of the corresponding manuscript in consistence with the framework of thesis.

In Chapter 2, the long-term performance for cement-based materials subject to chemical degradation is studied to achieve Objective 1. The mechanism of the long-term chemical degradation for oilwell cement is investigated with reactive transport model, demonstrating the process of the complicated dissolution/precipitation of cement minerals under the chemical attack of aggressive solutions. The portlandite is the first solid phase dissolving in the reactions at a pH value of approximate 12.5, and adopted to identify the degradation front. The depletion of portlandite can cause the rapid decline of pH and subsequently promote the dissolution of C-S-H. The parameters of oilwell cement are calibrated with available experimental data to evaluate the corrosion depth. The long-term performance of cement subject to various underground water is investigated for a nominal service life of 1000 years. The relation between corrosion depth and the square root of time is captured in simulations. The

deionized water poses a greater threat to cement-based materials comparing the corrosion rate with that of underground water, which is further demonstrated as a result of the chemical reactions between ion spices in underground water and those in pore solution of cement. In the carbonate rich case, the precipitation of calcium carbonation is captured and demonstrates a protective effect to the material by reducing or even clogging the pore space. The chemical degradation studied in this chapter is the preliminary work for the modelling of the coupled degradation.

In Chapter 3, the fully coupled chemo-mechanical degradation for cement-based materials is studied to achieve Objective 2. A displacement based non-local damage model is developed in Matlab to evaluate the propagation of microcracks, which is coupled with the reactive transport model to simulate the interaction between chemical reactions and mechanical loads. The significant reduction of Young's modulus of cement-based materials subject to leaching is evaluated by Mori-Tanaka scheme, and the evolution of elastic threshold is assumed to be the same as the way of mechanical damage. Since the chemically induced stiffness loss is validated with experimental results on the material level, the three-point bending test is simulated on the partially leached mortar beam to evaluate the residual structural performance with the mechanical damage model. The numerical modelling is subsequently focusing on the mutual effect between chemical degradation and mechanical damage of cement-based materials subject to the aggressive aqueous solutions to couple the two mechanisms in the duration of 114 days. The fully coupled chemo-mechanical modelling, and performed in a staggered manner, and evaluates the chemical degradation and mechanical equilibrium of the mortar beam on an eight-day cycle. The overall propagation of microcracks in the coupled case exhibits a different pattern with that in non-coupled case. It is noteworthy that the coupled chemo-mechanical degradation can generate the greater degradation and localized in a convex area, which can retard the propagation of mechanical damage in reloading stage by contrast to the non-coupled case. The proposed methodology of coupled chemo-mechanical degradation is able to evaluate the microscale variation and effect of the material constituents and the macroscale structural behaviour, and is practical to evaluate durability of engineering materials for the chemo-mechanical degradation related infrastructures.

In Chapter 4, the chemo-mechanical behaviour of cement-based materials exposed to carbonate brine is studied to achieve Objective 3. The coupled chemo-mechanical damage model is applied to the effect of calcium carbonate precipitation for cement-based materials. Carbon dioxide dissolves into water and generates aggressive ion

species which can cause reactions of both dissolution and precipitation. The formation of calcium carbonate depends on the compositions of the aqueous solution to which the material is exposed. The magnesium ions can promote the nucleation of amorphous calcium carbonate and the transformation to crystalline, which is investigated and demonstrated with contrast experiments in this chapter. The protective effect of amorphous calcium magnesium carbonate for cement-based materials is simulated by numerical modelling. In the absence of magnesium ions, the interaction of pH and CO_2 concentration of pore solution is demonstrated to be consistent with experimental outcomes. In order to comprehensively understand the dissolution and re-precipitation of calcium carbonate layer within material matrix, the detailed analysis of the weakening and strengthening effect is performed with the coupled chemo-mechanical modelling, and extended to the overall flexural performance for beams.

References

[1] Edward N. Matteo and George W. Scherer. Experimental study of the diffusion-controlled acid degradation of Class H Portland cement. *International Journal of Greenhouse Gas Control*, 7:181 – 191, 2012.

[2] M.D.C. van der Kuip, T. Benedictus, N. Wildgust, and T. Aiken. High-level integrity assessment of abandoned wells. *Energy Procedia*, 4:5320 – 5326, 2011.

[3] Edward N. Matteo, Bruno Huet, Carlos F. Jové-Colón, and George W. Scherer. Experimental and modeling study of calcium carbonate precipitation and its effects on the degradation of oil well cement during carbonated brine exposure. *Cement and Concrete Research*, 113:1 – 12, 2018.

[4] Yaoling Luo, Chong Wang, Zheng Fang, Lujun Xiao, and Qianpu Zeng. The tsa degradation process of cement-based materials in the electrical field environment. *Construction and Building Materials*, 206:703 – 716, 2019.

[5] Nadine Neuville, Eric Lécolier, Georges Aouad, Alain Rivereau, and Denis Damidot. Effect of curing conditions on oilwell cement paste behaviour during leaching: Experimental and modelling approaches. *Comptes Rendus Chimie*, 12(3–4):511 – 520, 2009.

[6] Haifeng Yuan, Patrick Dangla, Patrice Chatellier, and Thierry Chaussadent. Degradation modelling of concrete submitted to sulfuric acid attack. *Cement and Concrete Research*, 53:267 – 277, 2013.

[7] H. F. W. Taylor. *Cement chemistry*. Thomas Telford, London, second edition, 1997.

[8] B. Gérard. Contribution des couplages mécanique-chimie-transfert dans la tenue a long terme des ouvrages de stockage de déchets radioactifs. *PhD Thesis, Laboratoire de Méchanique et Technologie, E.N.S. de Cachan, in French*, 1996.

[9] A. Delagrave, B. Gérard, and J. Marchand. *Modelling the calcium leaching mechanisms in hydrated cement pastes*. In: K. Scrivener, J. Young (Eds.), Mechanics of Chemical Degradation of Cement-Based Systems. Chapman & Hall, London, pp. 30—37, 1997.

[10] Bruno M. Huet, Jean H. Prévost, and George W. Scherer. Quantitative reactive transport modeling of portland cement in CO_2-saturated water. *International Journal of Greenhouse Gas Control*, 4(3):561 – 574, 2010.

[11] E. Stora, B. Bary, Q.-C. He, E. Deville, and P. Montarnal. Modelling and simulations of the chemo-mechanical behaviour of leached cement-based materials: Interactions between damage and leaching. *Cement and Concrete Research*, 40(8):1226 – 1236, 2010.

[12] Fabien Georget, Jean H. Prévost, and Bruno Huet. Reactive transport modelling of cement paste leaching in brines. *Cement and Concrete Research*, 111:183 – 196, 2018.

[13] Tianfu Xu, Eric Sonnenthal, Nicolas Spycher, and Karsten Pruess. *TOUGHREACT : A new code of the TOUGH family of nonisothermal multiphase reactive geochemical transport in variably saturated geologic media.* Lawrence Berkeley National Laboratory, Berkeley, California, 2003.

[14] Caroline Le Bellégo, B. Gérard, and G. Pijaudier-Cabot. Coupled mechanical and chemical damage in calcium leached cementitious structures. *Journal of Engineering Mechanics*, 129(3):333 – 341, 2003.

[15] Gilles Pijaudier-Cabot and Zdeněk P. Bažant. Nonlocal damage theory. *Journal of Engineering Mechanics*, 113(10):1512–1533, 1987.

[16] R. H. J. Peerlings, R. De Borst, W. A. M. Brekelmans, and J. H. P. De Vree. Gradient enhanced damage for quasi-brittle materials. *International Journal for Numerical Methods in Engineering*, 39(19):3391–3403, 1996.

[17] G. Pijaudier-Cabot, B. Gérard, and L. Molez. *Damage mechanics of concrete structures subjected to mechanical and environmental actions.* In: R. de Borst, N. Bićanić, H. Mang, G. Meschke (Eds.), Computational Modelling of Concrete Structures. Balkema, Rotterdam, pp. 559-–566, 1998a.

[18] G. Pijaudier-Cabot, B. Gérard, N. Burlion, and L. Molez. *Localisation of damage in quasi-brittle materials and influence of chemically activated damage.* In: R. de Borst, E. van der Giessen (Eds.), Material Instabilities in Solids. John Wiley & Sons, Chicester, pp. 441-–456, 1998b.

[19] Caroline Le Bellégo, B. Gérard, and G. Pijaudier-Cabot. Chemo-mechanical effects in mortar beams subjected to water hydrolysis. *Journal of Engineering Mechanics*, 126(3):266–272, 2000.

[20] V.H. Nguyen, B. Nedjar, and J.M. Torrenti. Chemo-mechanical coupling behaviour of leached concrete: Part ii: Modelling. *Nuclear Engineering and Design*, 237(20):2090 – 2097, 2007.

[21] Detlef Kuhl, Falko Bangert, and Günther Meschke. Coupled chemo-mechanical deterioration of cementitious materials. part I: Modeling. *International Journal of Solids and Structures*, 41(1):15–40, 2004.

[22] Dawei Hu, Hui Zhou, Fan Zhang, and Jianfu Shao. Modeling of short- and long-term chemomechanical coupling behavior of cement-based materials. *Journal of Engineering Mechanics*, 140(1):206 – 218, 2014.

[23] T Mori and K Tanaka. Average stress in matrix and average elastic energy of materials with misfitting inclusions. *Acta Metallurgica*, 21(5):571 – 574, 1973.

[24] Eveline Herve and Andre Zaoui. n-Layered inclusion-based micromechanical modelling. *International Journal of Engineering Science*, 31(1):1 – 10, 1993.

[25] Q.-S. Zheng and D.-X. Du. An explicit and universally applicable estimate for the effective properties of multiphase composites which accounts for inclusion distribution. *Journal of the Mechanics and Physics of Solids*, 49(11):2765 – 2788, 2001.

[26] Ribooga Chang, Semin Kim, Seungin Lee, Soyoung Choi, Minhee Kim, and Youngjune Park. Calcium carbonate precipitation for CO_2 storage and utilization: A review of the carbonate crystallization and polymorphism. *Frontiers in Energy Research*, 5:17, 2017.

[27] J. Cowie and F. P. Glasser. The reaction between cement and natural waters containing dissolved carbon dioxide. *Advances in Cement Research*, 4(15):119–134, 1992.

[28] C. Edvardsen. Water permeability and autogenous healing of cracks in concrete. *ACI Materials Journal*, 96:448–454, 1999.

[29] A. Neville. Autogenous healing - A concrete miracle? *Concrete International*, 24:76–82, 2002.

[30] Rita G.W. Vasconcelos, Nicolas Beaudoin, Andrea Hamilton, Neil C. Hyatt, John L. Provis, and Claire L. Corkhill. Characterisation of a high ph cement backfill for the geological disposal of nuclear waste: The nirex reference vault backfill. *Applied Geochemistry*, 89:180 – 189, 2018.

[31] Eva Loste, Rory M. Wilson, Ram Seshadri, and Fiona C. Meldrum. The role of magnesium in stabilising amorphous calcium carbonate and controlling calcite morphologies. *Journal of Crystal Growth*, 254(1):206 – 218, 2003.

[32] Brian Jones and Xiaotong Peng. Amorphous calcium carbonate associated with biofilms in hot spring deposits. *Sedimentary Geology*, 269-270:58 – 68, 2012.

[33] Attila Demény, Péter Németh, György Czuppon, Szabolcs Leél-Őssy, Máté Szabó, Katalin Judik, Tibor Németh, and József Stieber. Formation of amorphous calcium carbonate in caves and its implications for speleothem research. *Scientific Reports*, 6:155–164, 2016.

[34] J.D. Rodriguez-Blanco, S. Shaw, P. Bots, T. Roncal-Herrero, and L.G. Benning. The role of pH and Mg on the stability and crystallization of amorphous calcium carbonate. *Journal of Alloys and Compounds*, 536:S477 – S479, 2012.

[35] J.D. Rodriguez-Blanco, S. Shaw, and L.G. Benning. The kinetics and mechanisms of amorphous calcium carbonate (ACC) crystallization to calcite, via vaterite. *Nanoscale*, 3(1):265–271, 2011.

[36] Bettina Purgstaller, Vasileios Mavromatis, Adrian Immenhauser, and Martin Dietzel. Transformation of Mg-bearing amorphous calcium carbonate to mg-calcite – in situ monitoring. *Geochimica et Cosmochimica Acta*, 174:180 – 195, 2016.

[37] Yael Politi, David R. Batchelor, Paul Zaslansky, Bradley F. Chmelka, James C. Weaver, Irit Sagi, Steve Weiner, and Lia Addadi. Role of magnesium ion in the stabilization of biogenic amorphous calcium carbonate: A structure-function investigation. *Chemistry of Materials*, 22(1):161–166, 2010.

[38] P. Bots, L.G. Benning, R.E.M. Rickaby, and S. Shaw. The role of SO_4 in the switch from calcite to aragonite seas. *Geology*, 39(4):331–334, 04 2011.

[39] M. Schwotzer, T. Scherer, and A. Gerdes. Protective or damage promoting effect of calcium carbonate layers on the surface of cement based materials in aqueous environments. *Cement and Concrete Research*, 40(9):1410 – 1418, 2010.

[40] Andrew Duguid, Mileva Radonjic, and George Scherer. Degradation of well cements exposed to carbonated brine. *In: 4th Annual Conference on Carbon Capture and Sequestration. Monitor and Exchange Publications and Forum, Washington, DC.*, 2005.

[41] Juan Manuel Galíndez and Jorge Molinero. Assessment of the long-term stability of cementitious barriers of radioactive waste repositories by using digital-image-based microstructure generation and reactive transport modelling. *Cement and Concrete Research*, 40(8):1278 – 1289, 2010.

[42] Barbara G. Kutchko, Brian R. Strazisar, David A. Dzombak, Gregory V. Lowry, and Niels Thaulow. Degradation of well cement by CO_2 under geologic sequestration conditions. *Environmental Science & Technology*, 41(13):4787–4792, 2007.

[43] Marcus Wigand, John P. Kaszuba, J. William Carey, and W. Kirk Hollis. Geochemical effects of CO_2 sequestration on fractured wellbore cement at the cement/caprock interface. *Chemical Geology*, 265(1):122 – 133, 2009.

[44] Anna V. Saetta and Renato V. Vitaliani. Experimental investigation and numerical modeling of carbonation process in reinforced concrete structures: Part I: Theoretical formulation. *Cement and Concrete Research*, 34(4):571 – 579, 2004.

[45] A. Fabbri, J. Corvisier, A. Schubnel, F. Brunet, B. Goffé, G. Rimmelé, and V. Barlet-Gouédard. Effect of carbonation on the hydro-mechanical properties of portland cements. *Cement and Concrete Research*, 39(12):1156 – 1163, 2009.

[46] Ján Jerga. Physico-mechanical properties of carbonated concrete. *Construction and Building Materials*, 18(9):645 – 652, 2004.

Chapter 2

The long-term chemical degradation

In this chapter, the study of long-term chemical degradation is presented as a published journal paper which is

Zhongcun Zuo and Terry Bennett : Simulation of the degradation of oilwell cement for the prediction of long-term performance, *Construction and Building Materials, Volume 202, 30 March 2019, Pages 669-680.*

The paper is available at

https://www.sciencedirect.com/science/article/pii/S0950061819300625

Statement of Authorship

Title of Paper	Simulation of the degradation of oilwell cement for the prediction of long-term performance
Publication Status	☑ Published ☐ Accepted for Publication ☐ Submitted for Publication ☐ Unpublished and Unsubmitted work written in manuscript style
Publication Details	Zhongcun Zuo & Terry Bennett (March 2019). Simulation of the degradation of oilwell cement for the prediction of long-term performance, Construction and Building Materials, 202, 669-680.

Principal Author

Name of Principal Author (Candidate)	Zhongcun Zuo
Contribution to the Paper	Undertook literature review, determined research theme, developed the theoretical proof for numerical modelling, performed simulations and interpretation of results, and wrote the manuscript.
Overall percentage (%)	60%
Certification:	This paper reports on original research I conducted during the period of my Higher Degree by Research candidature and is not subject to any obligations or contractual agreements with a third party that would constrain its inclusion in this thesis. I am the primary author of this paper.
Signature	Date 20/1/2020

Co-Author Contributions

By signing the Statement of Authorship, each author certifies that:

i. the candidate's stated contribution to the publication is accurate (as detailed above);

ii. permission is granted for the candidate in include the publication in the thesis; and

iii. the sum of all co-author contributions is equal to 100% less the candidate's stated contribution.

Name of Co-Author	Terry Bennett
Contribution to the Paper	Supervised the selection of research theme, helped with data analysis, and revised the manuscript.
Signature	Date 20/1/2020

Simulation of the degradation of oilwell cement for the prediction of long-term performance

Abstract

The cement sheath surrounding a wellbore forms an important barrier to maintain well integrity beyond the service life of a well. The understanding of the potential degradation of well cement, as a result of exposure to groundwater, is therefore necessary to determine if this barrier remains intact or remedial action is required at some time in the future. A reactive transport model of a well cement is developed and calibrated to accelerated laboratory tests. The calibrated model of cement is subsequently exposed to different groundwater compositions for a simulated time period of 1000 years. The results of these simulations demonstrate that the groundwater composition affects the long term degradation through the dissolution of portlandite and C-S-H. The precipitation of calcite has a protective effect by filling the pore space and subsequently reducing the intrusion of aggressive aqueous species in the surrounding formation.

Keywords : Long-Term Performance; Oil Well Cement; Corrosion Modelling.

2.1 Introduction

There are around 10000 hydrocarbon boreholes drilled onshore in Australia, and at least 4 million onshore hydrocarbon wells worldwide [1]. The oilwell structure consists of steel casing strings and cement annulus between each casing string and between the outermost casing string and the surrounding formation. Wells drilled to explore for and extract hydrocarbons will penetrate shallower strata before reaching the target horizons, therefore the outermost sheath of cement is vital in providing zonal isolation between different fluid bearing strata and the reservoir. In practice, the nominal annular thickness is determined by the size of casing and drill bit. For convenience of the placement of casing and cement, the drill bit is larger than the casing for several centimetres, whereas the actual thickness of the annulus may vary significantly due to the eccentricity of the casing [2].

Over the depth of a well, the cement sheath, between the steel casing and formation, will come into direct contact with fluid bearing strata. The formation fluids contain aqueous species which can be potentially chemically aggressive to the cement. These species can be transferred from the formation rock pore space into the cement pore space via the mechanisms of advection and diffusion, however diffusion is normally the predominant process for transport of chemical components. The chemical reactions that occur between the formation fluid and the cement are acid–base reactions, mineral dissolution and precipitation, surface complexation and ion exchange [3]. These reactions proceed from the interface of the cement and formation, progressing with time towards the steel casing. These reactions develop an altered zone of cement, the properties of which are generally poorer than those of the original cement. The chemical changes to the cement in turn change the porosity and permeability of the cement, which aggravates the penetration of aggressive species [4]. In the worse case scenario, the cement sheath could become a relatively high-permeability conduit for subsurface fluid to migrate [5] in the presence of a pressure gradient.

Various degradation experiments have been conducted to investigate the transport and chemical reactions of solutes within well cement. In these experiments, the cement specimens were immersed in brine with high concentration of aqueous species to cause significant change in the composition and properties of cement. Le Saoût et al. [6] conducted leaching tests and subsequently performed chemical analyses on the near surface of the altered zone of cement samples to determine the variation of cement composition after one year of immersion in a solution of neutral pH and 0.35 M NaCl. Matteo and Scherer [7] performed uniaxial chemical attack of cement samples

with hydrochloric acid for a period of 50 hours. The corrosion rate was measured and the dependence of temperature and pH were determined. Neuville et al. [8], using the same brine composition as Le Saoût et al. [6], characterised the chemical and physical properties of oilwell cement after 3 months of leaching at elevated temperature and pressure. The process of the cement degradation observed in these tests was invariably accelerated by the strong acid and/or high concentration of the brine to enable observable cement degradation in a relatively short time duration.

Accelerated experiments have been demonstrated to be effective to realise cement degradation in a laboratory setting, however comparison and extrapolation of the results to real service conditions and time scales are troublesome. The diffusion–controlled chemical degradation progress is relatively slow, even under high temperatures, it would take 10,000 years for the degradation of less than 1 meter of cement [9]. Reactive transport modelling has been used to evaluate long term chemical variations, for example the water–rock interaction of Yellowstone [10] and the thermal–hydrological–chemical effects at Yucca Mountain [11] in geothermal systems.

In the context of wells, simulations involving the carbonation of oilwell cement have been conducted in the feasibility studies of CO_2 sequestration [12–15]. These works primarily focus on the transport and solubility of CO_2 in the subsurface and not specifically on the degradation of cement. Huet et al. [16] focussed attention on the process of cement carbonation by applying reactive transport modelling to predict the changes in the properties of cement, and validated the results with accelerated experiments [17].

The evaluation of the durability of cementitious materials has been considered as a relevant issue in a broad range of industry sectors. According to the available literature, the simulation of Galíndez and Molinero [18] shows the mineralogical transformations of cement after exposed to a leaching solution for 1000 years. In the study of Jacques et al. [19], a simplified system model of cement was adopted for the evaluation of degradation front. Grandia et al. [20] simulated the fronts of the chemical degradation with an integrated cement model, however, the process of mineral formation was not implemented. In terms of the relationship between degradation depth and time, Yuan et al. [21] predicted the degradation rate based on a linear relationship between the degradation depth and the square root of time. The quantitative measurement of long–term degradation needs to be studied further, due to the complexity of physical and chemical processes involved. Reactive transport models can incorporate specific cement composition, and solve the chemical degradation on the basis

of thermodynamic equilibrium and kinetic constraints. The mass transport, including ion diffusion and adsorption, determines the amount of ion species reacting with cement matrix in each time step. The key parameters in the transport model need to be calibrated by experiments, which requires an experimental outcome available for quantitative comparison with that of simulation. In this study, the experimental outcome is degradation depth, and subsequently is adopted as the parameter for the evaluation of long–term degradation. The aim of this paper is to develop a method, from parameter calibration by experiment to simulation of long–term degradation, to evaluate the degradation depth and rate of oilwell cement after exposure to formation waters for up to 1000 years.

An overview of the reactive transport modelling approach is given in section 2.2 before the model is employed to simulate accelerated tests in section 2.3. The accelerated tests are used to investigate the sensitivity of, and calibrate, the model parameters for cement used in long term simulations. Long term simulations of cement degradation are performed in section 2.4 with the cement exposed to differing formation waters.

2.2 Modelling approach

The evaluation of cement degradation requires the coupling of chemical reactions with ion transport processes. Reactive transport modelling [22] of geochemistry can be applied to porous and fractured media with physical and chemical heterogeneity, and accommodate any number of chemical species present in liquid, gas and solid phases. The chemicals in the brine are transported by advection and diffusion, allowing the dissolved minerals and other species to be carried in solution through the pore space.

2.2.1 Transport equations

The process of chemical degradation of cementitious materials exposed to acidic solutions is diffusion-controlled [7]. The transport of aggressive species, the reactants of chemical degradation, is governed by diffusion. Since the Coulombic force among charged ion species can have an impact on the diffusion, the Nernst-Planck model offers a better description meeting the actual process of ion transport phenomenon [23–25]. Huet et al. [16] considered that the electrical coupling between the species was likely to be a second order effect compared to the tortuosity of cementitious materials. Arnold et al. [26] compared Fickian with Nernst-Planck model

with three leachants: deionized water, ammonium nitrate and waste form solutions. The ammonium nitrate case of Nernst-Planck model exhibit greater departure from that of Fickian model as opposed to the other two cases, the speciation of NH_4 and NO_3 proving to be the primary factor for the differences. Arnold et al. [26] just concluded that electrical coupling between ionic species is significant for the case of strong nitrate solutions, which is commonly adopted accelerated agent to boost the rate of degradation. In terms of the other two leachants that match the practical service conditions better, the differences of simulated results between Fickian and Nernst-Planck model are slight or even negligible.

In this study, Fickian diffusion model is employed, and the diffusive flux of species i in aqueous solution is defined as

$$J_i = -D_e \frac{\partial C_i}{\partial x} \tag{2.1}$$

$$D_e = \phi \tau_0 \tau D_0 \tag{2.2}$$

where D_e is the effective diffusion coefficient of species i, C_i is the concentration of species i, ϕ is porosity, D_0 is the diffusion coefficient of ion species in bulk water, $\tau_0\tau$ is the tortuosity including a porous medium dependent factor τ_0 and a coefficient τ that depends on water saturation S_l. The tortuosity is calculated from the Millington and Quirk model [27] as

$$\tau_0 \tau = \phi^{1/3} S_l^{7/3} \tag{2.3}$$

Ion species in aqueous solution are electrically charged, and tend to separate from each other due to different diffusive velocity. The faster ions are retarded under the action of Coulombic force, while the slower ions are expedited in turn [25]. The diffusion coefficient is set as an average value, which is the approach adopted for well cement degradation [12, 16], and is commonly used in other applications [28, 29].

The general governing equation of 1D transport model is described as

$$\frac{\partial M_i}{\partial t} = -\frac{\partial J_i}{\partial x} + q_i \tag{2.4}$$

where M_i is mass accumulation term for species i in aqueous solution, and x is the diffusive distance. q_i is the source/sink term of species i and expressed as

$$q_i = q_{is} + q_{il} + q_{ia} \tag{2.5}$$

where q_{is}, q_{il} and q_{ia} denote releasing or capturing species i as a result of mineral dissolution/precipitation, aqueous complexation and physical adsorption on the surface of C-S-H particles.

The mineral precipitation and dissolution render the volume variation of solid phase in matrix, eventually resulting in porosity change. The porosity is calculated as

$$\phi = 1 - \sum_{m=1}^{N_m} fr_m \tag{2.6}$$

where N_m is the total number of minerals, and fr_m, volume fraction, is the volume proportion of mineral m in the medium [30]. As a result of mineral precipitation and dissolution, the volume fraction of each mineral varies in the course of simulation, and subsequently the porosity is calculated in each time step by equation (2.6).

The mass accumulation M_i is defined as the product of porosity ϕ and the concentration C_i, homogenizing the transport equation for porous medium. Therefore, equation (2.4) is expressed as

$$\frac{\partial \phi C_i}{\partial t} = D_e \frac{\partial^2 C_i}{\partial x^2} + q_{is} + q_{il} + q_{ia} \tag{2.7}$$

2.2.2 Surface complexation model

In cementitious materials, the physical sorption of aqueous species on calcium silicate hydrate (C-S-H) has been studied in experiments [31–34]. Dzombak and Morel [35] developed the diffuse layer model, the surface complexation model, to describe the physical and chemical reactions between solutes and the specific surface sites. In this model, two layers of charge are formed at the solid/liquid interface: a surface layer and a diffuse layer of counterions. The surface layer is comprised of specifically sorbed ions, and the diffuse layer consists of nonspecifically sorbed ions. The surface charge density $\sigma(C \cdot m^{-2})$ is considered as a function of the sorption densities of surface sites

$$\sigma = F \left[\Gamma_H - \Gamma_{OH} + \sum (Z_m \Gamma_M) + \sum (Z_A \Gamma_A) \right] \tag{2.8}$$

where F is the Faraday constant ($96485C \cdot mol^{-1}$), and Z is the valance of a sorbing ion. The sorption densities of surface sites ($mol{\cdot}m^{-2}$) of protons, hydroxyl ions, sorbed cations and anions are denoted by Γ_H, Γ_{OH}, Γ_M and Γ_A individually. Specifically, the ions, for example OH_2^+, O^-, OM^+, A^-, constitute the surface layer, and the surface charge density is

$$\sigma = \frac{F}{AS}\left[\left(\equiv XOH_2^+\right) + \left(\equiv XOM^+\right) - \left(\equiv XO^-\right) - \left(\equiv XA^-\right)\right] \tag{2.9}$$

where A is the specific surface area ($m^2 \cdot g^{-1}$) , S is solid concentration ($g \cdot m^{-3}$). The term in bracket is the concentration of surface complexes ($mol \cdot kg^{-1}$).

For a symmetrical electrolyte with valence Z, the surface charge density based on the Gouy–Chapman theory is related to the surface potential Ψ_o (V) by

$$\sigma_d = (8000RT\varepsilon\varepsilon_o c)^{\frac{1}{2}} \cdot sinh\left(Z\Psi_o F/2RT\right) \tag{2.10}$$

where R is the molar constant ($8.354J \cdot mol^{-1} \cdot K^{-1}$), T is the absolute temperature (K), ε is the relative dielectric constant of water ($\varepsilon = 78.5 \quad at \quad 25°C$), ε_o is the permittivity of free space ($8.854 \times 10^{-12} CV^{-1}m^{-1}$) and c is the molar electrolyte concentration (mol).

The equivalent relationship of charge balance of the diffuse layer model is

$$\sigma + \sigma_d = 0 \tag{2.11}$$

Therefore, substituting equation (2.9) and (2.10) into equation (2.11) can obtain

$$\begin{aligned} &\frac{F}{AS}\left[\left(\equiv XOH_2^+\right) + \left(\equiv XOM^+\right) - \left(\equiv XO^-\right) - \left(\equiv XA^-\right)\right] \\ &+ (8000RT\varepsilon\varepsilon_o c)^{\frac{1}{2}} \cdot sinh\left(Z\Psi_o F/2RT\right) = 0 \end{aligned} \tag{2.12}$$

With the diffuse layer model, the surface potential and the total number of adsorbed ions for a C-S-H surface subjected to an ionic solution can be obtained. The solid solution model of Kulik and Kersten [36] was adopted by Lothenbach et al. [37] to model C-S-H in cementitious materials. The C-S-H surface site density correlated

with the surface charge density is the crucial parameter in the model. The crystal structure of the C-S-H phase, which determines the number of types of surface sites, has been generally considered as the Tobermorite or Jennite [38]. Two surface sites, silanol ($\equiv SiOH$) and silandiol ($\equiv Si\,(OH)_2$), have been studied by Pointeau et al. [39]. Viallis-Terrisse et al. [32] conceived that the whole surface of C-S-H is comprised of one type of surface site ($\equiv SiOH$). Heath et al. [40] presumed that silanol ($\equiv SiOH$) and calcium ($\equiv CaOH$) sites consists of the C-S-H surface. Since the C-S-H surface site have been not thoroughly expounded, with the available data of equilibrium constants and specific surface area, silanol ($\equiv SiOH$) is considered as the only surface site for the physical ion adsorption in this study.

The complexation reactions involved in this study are tabulated in table 2.1. The specific surface site (A) of C-S-H is the specific surface area 500 $m^2 \cdot g^{-1}$ [32], and the sorption density (Γ_{C-S-H}) is 8×10^{-6} $mol \cdot m^{-2}$ [34].

The equilibrium of ion adsorption can be described by the equilibrium constant K. For example, the equilibrium constant of calcium ion adsorption is

$$K = \frac{[\equiv SiOCa^{2+}]\,\{H^+\}}{[\equiv SiOH]\,\{Ca^{2+}\}} exp\left(\frac{-F\Psi_o}{RT}\right) \tag{2.13}$$

where the activity of ions is denoted with $\{\}$.

Table 2.1: The surface complexation reactions considered in the reactive transport model.

Surface complexation reactions	Log(K)	Reference
$\equiv SiOH \rightleftharpoons \equiv SiO^- + H^+$	-12.7	[41]
$\equiv SiOH + Na^+ \rightleftharpoons \equiv SiONa + H^+$	-13.745	[41]
$\equiv SiOH + K^+ \rightleftharpoons \equiv SiOK + H^+$	-13.745	[41]
$\equiv SiOH + Ca^{2+} \rightleftharpoons \equiv SiOCa^+ + H^+$	-9.4	[41]
$\equiv SiOH + Ca^{2+} + SO_4^{2-} \rightleftharpoons \equiv SiOCaSO_4^- + H^+$	-8.5	[42]
$\equiv SiOH + Cl^- \rightleftharpoons \equiv SiOHCl^-$	-0.35	[41]

2.2.3 Thermodynamic equilibrium

The precipitation/dissolution of cement minerals is considered as the reaction between ion species and cement matrix. The mineral saturation is calculated by

$$\Omega_m = K_m^{-1} \prod_{j=1}^{N_c} C_j^{\nu_{mj}} \gamma_j^{\nu_{mj}} \quad m = 1, ..., N_p \tag{2.14}$$

where K_m is the equilibrium constant, C_j $(mol \cdot kg^{-1})$ is molal concentration of the j-th primary species, ν_{mj} is the stoichiometric coefficient of the primary species, γ_j is the activity coefficient of species j, N_c and N_p are the number of primary species and minerals respectively. The equilibrium of minerals in aqueous solution is determined by the mineral saturation index

$$SI_m = log\Omega_m \tag{2.15}$$

When $SI_m = 0$, the mineral is at equilibrium. The minerals is unsaturated and can dissolve, if $SI_m < 0$. The minerals is supersaturated and can precipitate, if $SI_m > 0$.

The interaction between primary species in solution is aqueous complexation. The concentration of aqueous complexes is calculated by

$$C_i = K_i^{-1} \gamma_i^{-1} \prod_{j=1}^{N_c} C_j^{\nu_{ij}} \gamma_j^{\nu_{ij}} \quad i = 1, ..., N_x \tag{2.16}$$

where C_i $(mol \cdot kg^{-1})$ is the molal concentration of the aqueous complexes i, γ_i and γ_j are the activity coefficients, K_i is the equilibrium constant, N_x is the number of considered aqueous complexes. The activity coefficient is defined by HKF equation [43].

The dissolution/precipitation of cement minerals and aqueous complexes reactions are tabulated in table 2.2 and 2.3. The thermodynamic data are taken from the database: data0.ymp.R5.dat, of EQ3/6 [44].

Table 2.2: The dissolution/precipitation of cement minerals

Minerals reactions	Log(K)	Reference
$Ca(OH)_2 + 2H^+ \rightleftharpoons Ca^{2+} + 2H_2O$	22.5444	[44]
$Ca_{1.7}SiO_{6.317}H_{5.234} + 3.4H^+ \rightleftharpoons 1.7\ Ca^{2+} + 4.317H_2O + SiO_2$	28.0022	[44]
$CaCO_3 + H^+ \rightleftharpoons Ca^{2+} + HCO_3^- + H_2O$	1.8490	[44]
$Ca_6Al_2(SO_4)_3(OH)_{12}{:}26H_2O + 12H^+ \rightleftharpoons 2Al^{3+} + 6Ca^{2+} + 3SO_4^{2-} + 38H_2O$	56.8823	[44]
$3CaOAl_2O_3(CaCO_3){:}11H_2O + 13H^+ \rightleftharpoons 2Al^{3+} + 4Ca^{2+} + HCO_3^- + 17H_2O$	80.5669	[44]

2.2.4 Kinetics

The chemical reaction is under kinetic constraints. The reaction rate of Lasaga et al. [45] is adopted

$$r_n = f(c_1, c_2, ..., c_{N_c}) = \pm k_n A_n \mid 1 - \Omega_n^{\theta} \mid^{\eta} \quad n = 1, ..., N_q \tag{2.17}$$

where k_n is the rate constant ($mol \cdot m^{-2} \cdot s^{-1}$), A_n is the specific reactive surface area ($m^2 \cdot g^{-1}$), Ω_n is the mineral saturation, N_q is the number of minerals . θ and η are determined by experiments, and usually are set to equal to one.

The fluid transport equations are linked to the chemical reactions via updates to the porosity (and dependent variables such as permeability) that occur as a result of dissolution and precipitation of chemical species. The rates of mineral precipitation and dissolution exponentially depend on hydrogen ion concentration.

$$k_{adj} = k(10^{-pH_c}/10^{-pH_1})^{\text{slope}_1} \quad \text{if } pH_c < pH_1 \tag{2.18}$$

$$k_{adj} = k(10^{-pHc}/10^{-pH_2})^{\text{slope}_2} \quad \text{if } pH_c > pH_2 \tag{2.19}$$

where k is the original rate constant, k_{adj} is the rate constant adjusted for pH, pH_c is the current (calculated) pH. In the acid region an exponent of $\text{slope}_1 = 1$ is specified for pH_c lower than $\text{pH}_1 = 4$ in equation (2.18). When pH_c is higher than $\text{pH}_2 = 8$, the exponent is $\text{slope}_2 = 0.5$ in equation (2.19). Between pH_1 and pH_2, the rates are assumed to remain independent of pH [22].

The temperature dependency of the reaction rate constants is expressed via the Arrhenius equation.

$$k = k_{25} exp\left[-\frac{E_a}{R}\left(\frac{1}{T} - \frac{1}{298.15}\right)\right] \tag{2.20}$$

where E_a is the activation energy, k_{25} is the rate constant at $25°C$, R is the gas constant, T is absolute temperature. A fuller description of the general methodology

Table 2.3: Chemical reactions in pore solution

Aqueous reactions	Log(K)	Reference
$H_2O \rightleftharpoons H^+ + OH^-$	-13.9951	[44]
$CO_{2(aq)} + H_2O \rightleftharpoons H^+ + HCO_3^-$	-6.3447	[44]
$CO_3^{2-} + H^+ \rightleftharpoons HCO_3^-$	10.3288	[44]
$AlSO_4^+ \rightleftharpoons Al^{3+} + SO_4^{2-}$	-3.0100	[44]
$CaCl^+ \rightleftharpoons Ca^{2+} + Cl^-$	0.6960	[44]
$CaCl_{2(aq)} \rightleftharpoons Ca^{2+} + 2Cl^-$	0.6440	[44]
$CaCO_{3(aq)} + H^+ \rightleftharpoons Ca^{2+} + HCO_3^-$	7.0020	[44]
$CaHCO_3^+ \rightleftharpoons Ca^{2+} + HCO_3^-$	-1.0467	[44]
$CaSO_{4(aq)} \rightleftharpoons Ca^{2+} + SO_4^{2-}$	-2.1111	[44]
$CaOH^+ + H^+ \rightleftharpoons Ca^{2+} + H_2O$	12.8330	[44]
$CaHSiO_3^+ + H^+ \rightleftharpoons Ca^{2+} + H_2O + SiO_{2(aq)}$	8.5752	[44]
$HSiO_3^- + H^+ \rightleftharpoons H_2O + SiO_{2(aq)}$	9.953	[44]
$HSO_4^- \rightleftharpoons H^+ + SiO_{2(aq)}$	-1.9791	[44]
$HCl_{(aq)} \rightleftharpoons H^+ + Cl^-$	0.6700	[44]
$KCl_{(aq)} \rightleftharpoons K^+ + Cl^-$	1.4950	[44]
$KHSO_{4(aq)} \rightleftharpoons H^+ + K^+ + SO_4^{2-}$	-0.8140	[44]
$KSO_4^- \rightleftharpoons K^+ + SO_4^{2-}$	-0.8800	[44]
$NaOH_{(aq)} + H^+ \rightleftharpoons Na^+ + H_2O$	14.7950	[44]
$NaCO_3^- + H^+ \rightleftharpoons Na^+ + HCO_3^-$	9.8140	[44]
$NaHCO_{3(aq)} \rightleftharpoons Na^+ + HCO_3^-$	-0.1541	[44]
$NaHSiO_3 + H^+ \rightleftharpoons Na^+ + H_2O + SiO_{2(aq)}$	8.3040	[44]
$NaSO_4^- \rightleftharpoons Na^+ + SO_4^{2-}$	-0.7000	[44]

to solve the chemical interactions of multicomponent systems has been published by Bethke [46].

The kinetic data for the cement minerals are listed in table 2.4.

Table 2.4: Dissolution/precipitation reaction kinetic data for cement minerals

Minerals	Chemical formula	A(cm^2/g)	k_{25}(mol/m^2s)	E_a(kJ/mol)	Reference
Calcite	$CaCO_3$	10	1.600×10^{-09}	41.87	[47]
C-S-H:1.7	$Ca_{1.7}SiO_{6.317}H_{5.234}$	152	2.818×10^{-12}	39.6	[7] [48]
Portlandite	$Ca(OH)_2$	10	6.450×10^{-06}	39.6	[7] [49]
Ettringite	$Ca_6Al_2(SO_4)_3(OH)_{12}$:$26H_2O$	10	3.162×10^{-12}	39.6	[7] [48]
Monocarbonate	$3CaOAl_2O_3(CaCO_3)$:$11H_2O$	10	3.162×10^{-14}	39.6	[7] [50]

2.3 Modelling calibration and validation

The model calibration and validation procedure is described in this section. The accelerated tests used for calibration are first described along with the experimental

measurement of the degradation front and corrosion depth. The determination of the degradation front from a numerical simulation is next described for subsequent use in model parameter sensitivity analysis and calibration. The calibrated model parameters are employed in validation simulations with acidic solutions of different pH values.

2.3.1 Introduction of experiments

In order to measure the rate of acid corrosion, Matteo and Scherer [7] conducted accelerated leaching experiments for cement degradation. In their experiments, polypropylene centrifuge tubes were adopted as both cement mould and reaction vessel. In flow-through experiments, 1M hydrochloric acid was imposed on the top of the specimen over a range of flow rates from 7.5 to 300 mL/h at ambient temperature to examine the effect on the rate of corrosion due to accumulation of leachate in the reactor and at the cement/acid interface. They demonstrated that a flow rate of $\geq$ 75 mL/h could be considered as a constant boundary condition, which is the worst-case scenario for the corrosion rate of cement.

The corrosion depth was identified by the colour–changed depth. The cement close to the cement/acid interface changed appearance to a brown colour, and a white layer was formed between this and the unaltered cement. As the cement comes into contact with the aggressive solution, portlandite is the first phase to dissolve [51], followed in sequence by ettringite, C-S-H and monocarbonate. Duguid [17] demonstrated that the cement changed colour, to a brownish hue, after the dissolution of portlandite on reacting with acidic solution. Thus, the corrosion depth of the experiment could be determined as the distance between the cement/acid interface and the dissolution front of portlandite [52, 53].

2.3.2 Determination of simulated degradation front

To numerically replicate the experiments, a 1D model was adopted, the geometry of which was a cuboid with 0.5 $\times$ 0.5 mm of section and 5 mm of length. The domain was divided into 50 elements along the length as shown in figure 2.1. The boundary was represented by a large reservoir (by means of a zone of 10^{50} m^3) where the brine solution with concentration measured in the experiments was imposed. The cement composition of Geloni et al. [12] was adopted here with an initial porosity of 0.3 [8].

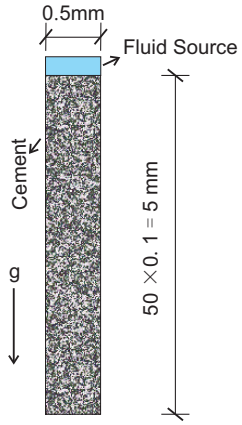

Figure 2.1: Schematic diagram of the model in simulations.

A 50 hour simulated duration was conducted to demonstrate the determination of the degradation front from the numerical model. In figure 2.2 the profile of porosity and minerals (portlandite and C-S-H) is shown. The change of volume fraction is the ratio of the variation of a solid phase volume to the total element volume, with the sign indicating precipitation or dissolution. The algebraic sum of volume fraction change for each mineral is the change of porosity and therefore when the summation is negative, dissolution dominates the reaction process and the porosity increases.

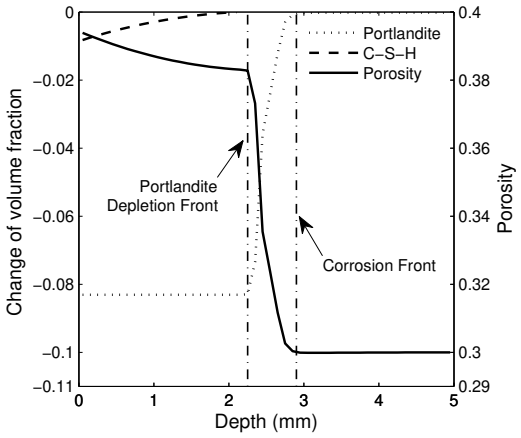

Figure 2.2: Identification of the corrosion front from mineral volume fractions and porosity profiles.

In figure 2.2 the change of volume fraction and porosity is shown at the end of the simulation time. Examining the change of volume fraction of portlandite, dissolution of the mineral to a depth of approximately 2.2 mm can be observed followed by a zone of ongoing portlandite depletion. From approximately 2.9 mm depth, onwards, the cement was unaltered, as indicated by both no change in the volume fractions

of the minerals or the porosity. The distance from the cement/acid interface to the corrosion front was taken to be the corrosion depth.

It is noteworthy that the process of C-S-H dissolution did not begin until complete depletion of portlandite, indicated in figure 2.2 as the portlandite depletion front, and was accompanied with a further change in the porosity.

2.3.3 Parameter sensitivity and model calibration

The calibration of model parameters was determined using a parameter sensitivity study. In the reactive transport model, the chemical species enter into cement matrix, and subsequently react with cement minerals. The thermodynamic and kinetic data are long tested, and the investigation of this kind data goes beyond the scope of the study. The process of kinetically-controlled chemical reactions would be influenced by the transport mechanisms. The validation and calibration are focussed upon the related parameters of transport mechanism. According to equation (2.1) and (2.2), the diffusion coefficient in free water, the intrinsic property of ion, determines the diffusion flux in the interstitial solution of cementitious materials. The porosity influences the effective diffusion coefficient as described by equation (2.2) and (2.3). The initial porosity determines the ion diffusion before degradation, which influences the initial state of the ion transport in the simulation. As described in section 2.2.3 and 2.2.4, the equilibrium constant and kinetic data represent the chemical performance of each cement mineral. In the process of degradation, the proportion of minerals can be reflected in the porosity change due to differences in resistance to chemical attack, and subsequently impact the ion transport during simulation. Therefore, the cement composition, porosity and the diffusion coefficient all have a major effect on the rate of degradation.

The composition of unhydrated cement and the condition of hydration in Matteo and Scherer's experiment [7] are not available for this study. The present work is not intended to involve the uncertain evolution of the process of hydration of specific cement, but to determine a reasonable hydrated cement composition as the starting point for the subsequent long term degradation. The typical composition of an API Class G High Sulphate Resistant grade commercial oilwell cement in the study of Geloni et al. [12] was adopted as CEM-O in table 2.5. Considering the presence of carbonate ion, monosulfate is replaced by monocarbonate [51].

The influence of cement composition on the resistance to degradation has been investigated [54], demonstrating that a cement with a low C_3S content has a better per-

formance in acidic environments after hydration. Durning and Hicks [55] concluded that the reduction or complete elimination of portlandite in cement is of importance to increase the resistance of cement to chemical attack in acidic environments. According to hydration reactions [56, 57], the hydration of C_3S could render higher ratio of portlandite and C-S-H than that of C_2S. Therefore, adjusting the content of C_3S and C_2S, the hydrated cement paste contains different amount of portlandite. Based on this statement, a reasonable range of portlandite and C-S-H volume fractions were assumed for sensitivity analysis, and tabulated in table 2.5.

Table 2.5: Initial proportion of cement minerals as volume fractions of the solid phase

Materials	Calcite	C-S-H:1.7	Portlandite	Ettringite	Monocarbonate
CEM-O	0.0138	0.8183	0.1187	0.026	0.0231
CEM-I	0.0138	0.7683	0.1687	0.026	0.0231
CEM-II	0.0138	0.8683	0.0687	0.026	0.0231

The initial porosity will affect the effective diffusion coefficient of aqueous species [16, 58], which influences the transport rate of aggressive species and subsequently the process of degradation. Neuville et al. [8] analysed oilwell cement specimens after curing, the porosity was found to be around 0.3. In the sensitivity analysis values 0.2, 0.3 and 0.4 were adopted.

Three values of the diffusion coefficient were chosen for a temperature of 25°C in this study. In previous studies [12, 16], the diffusion coefficient in free water was set to an average value for all aqueous species. Geloni et al. [12] set the diffusion coefficient to 8×10^{-10} m^2/s at 50°C.

The key parameters explored are shown in table 2.6.

Table 2.6: Parameters for sensitivity testing

Cement composition	Initial porosity	Diffusion coefficient(m^2/s)
CEM-I	P1=0.2	D1=1×10^{-10}
CEM-O	P2=0.3	D2=2×10^{-10}
CEM-II	P3=0.4	D3=4×10^{-10}

The cement composition of CEM-O was employed as a reference in the first simulation test, with the initial porosity P2 and diffusion coefficient D2 in table 2.6.

Figure 2.3 shows the evolution of the corrosion depth with the square root of time. The dependence and sensitivity of the corrosion depth on the initial porosity, cement

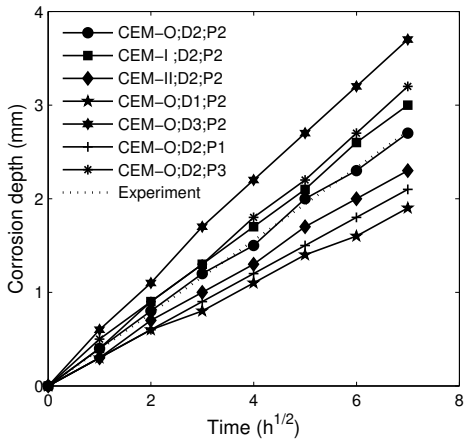

Figure 2.3: The effect on corrosion rate on initial porosity, cement composition and diffusion coefficient.

composition and diffusion coefficient are shown. Whilst the chemical composition of the cement and the porosity had an effect on the corrosion rate, within the parameter ranges investigated, the diffusion coefficient was the most sensitive of the parameters.

The combination of cement composition CEM-O, initial porosity P2 and diffusion coefficient D2 represented the best match to the experimental data and were subsequently adopted for validation of the model to a change in pH of acid solution.

2.3.4 Modelling validation

In the experimental programme of Matteo and Scherer [7] in section 2.3.1, flow-through tests under different pH values were also performed, and were employed here to serve as a validation for the calibrated model. Based on the parameter calibration in section 2.3.3, the initial set-up of the model was determined. The comparison of corrosion rate is shown in figure 2.4. As the pH increased, the cement degradation slowed down dramatically and the corrosion rate measured experimentally was captured in the simulations.

The modification of the cement is shown after a 50 hour simulation time. In figure 2.5, the porosity change demonstrated the degradation front moving downwards from the top of the model with time. The degraded porosity increased from the initial value 0.3 to around 0.384 within 4 hours, and then remained relatively stable at this level. At the end of the simulation, the maximum porosity was approximately 0.394.

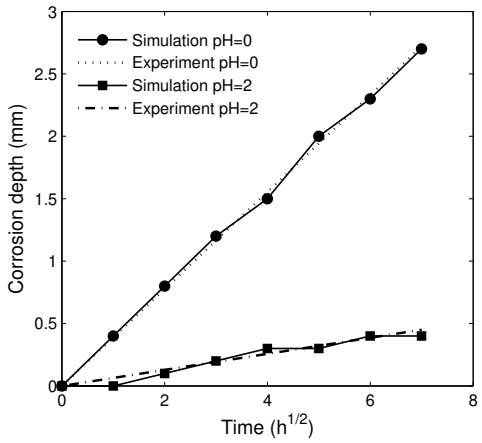

Figure 2.4: The validation of corrosion rate for pH=0 and 2.

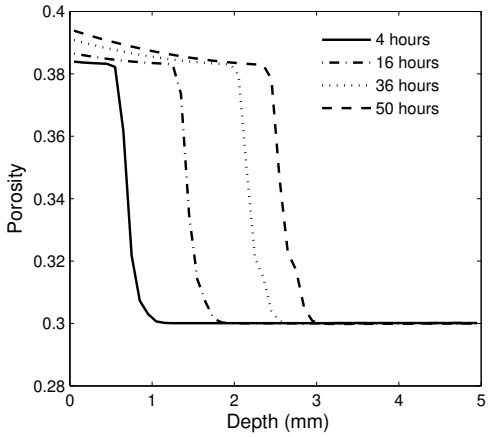

Figure 2.5: Profiles of porosity for simulation of well cement exposed to pH=0 hydrochloric solution.

2.3.5 General discussion

The hydrochloric acid attack of cement was simulated using a reactive transport model, and the evolution of composition and porosity of cement were addressed. The dissolution of cement minerals, such as portlandite and C-S-H can be found in experiments [52, 53, 59]. This model is capable of simulating the variation of solid phases as shown in figure 2.2. The assessment of the corrosion rate of materials is performed, and compared with the experimental results in the sensitivity analysis. The best match of corrosion rate in figure 2.3 demonstrates that the model can properly capture the effective diffusion coefficient for ion transport in the course of degradation by equation 2.1 - 2.3. The variation of the pH value of pore solution, which is most commonly caused by the exposure to acidic solution, has been shown

to affect the degradation process [7, 60]. When the model was applied to different concentrations of hydrochloric acid, the change in the corrosion rate is successfully captured by the model and matches with the experiment results by the model of pH dependency in section 2.2.4.

In long term degradation, with more complicated dissolution/precipitation of cement minerals, the corresponding porosity change influences the ion diffusion the same way as the accelerated case. The validated pH dependency of chemical reaction rate can reasonably correlate experiments of the strong acidic solution with simulations for the actual service condition. The calibration and validation of the model in this section can build confidence to evaluate the durability of oil well cement.

2.4 Long term simulations

Long duration simulations were performed to forecast the condition of a cement sheath over a realistic lifespan of a well. A 1000-year lifespan was simulated employing the material properties determined from the calibration and validation work performed in section 2.3. The model of cement sheath was exposed to different groundwater compositions, to investigate the influence of carbonate and sulphate concentrations on the degradation and transport mechanisms. Simulations with deionised water are used as a baseline comparison.

The geometry of the model is a cuboid with 5×5 mm of section and 100 mm of length. The domain was divided into 100 elements along the length as shown in figure 2.6. The initial length of time steps is 1×10^{-3} second. The time step size will be doubled if the converged state of the last step was reached within 4 Newton-Raphson iterations.

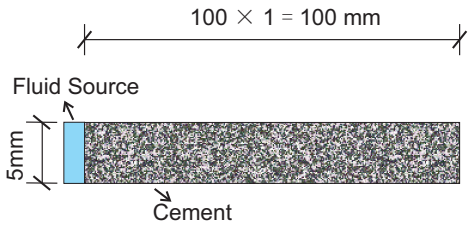

Figure 2.6: Schematic diagram of the model in long term simulations.

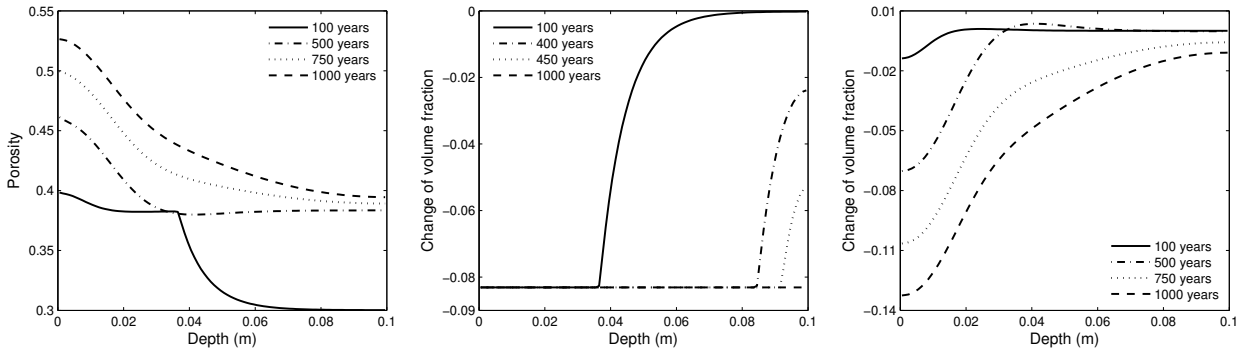

(a) (b) (c)

Figure 2.7: Profiles of a) porosity; and change in mineral volume fractions for b) portlandite and c) C-S-H, exposed to deionised water, with depth.

2.4.1 Simulation of leaching by deionised water

The cement sheath degradation with exposure to neutral deionised solution is simulated here. Figure 2.7a shows the porosity profiles of the cement at different ages. The porosity profile at 100 years displays a near horizontal section owing to the the exhaustion of portlandite (shown in figure 2.7b) which has leached from the cement pore space into the surrounding environment. A dissolution front at a depth of 0.04 m depth can be identified in figure 2.7a, between the depleted zone (0-0.04 m) and an intact zone from a depth of approximately 0.07 m onwards.

In the later service life, the porosity continues to increase, with a second 'front' observed in figure 2.7a as the C-S-H dissolves as shown in figure 2.7c. This 'front' has started to develop at 100 years, but is more pronounced at later time periods with the maximum porosity of 0.53 reached at 1000 years (figure 2.7a).

Exposure to deionised water causes concentration gradients of ion species, and then induces ion diffusion from the interior of the cement to the exposed surface. Loss of ions in the cement pore solution could promote the dissolution of solid phases in hydrated cement systems, such as portlandite and C-S-H [61].

The dissolution of portlandite and C-S-H started at the exposed surface, and extended to the interior, as shown in figures 2.7b and 2.7c. Consequently, the concentration of calcium ions in the pore solution increased to reach an equilibrium in the reactions of dissolution. A gradient of calcium concentration was formed between the pore solution and deionised water at the model boundary in figure 2.8, which drove the diffusion of calcium ions from the the cement.

The variation of pH and minerals with time is shown in figure 2.9. In figure 2.9a the

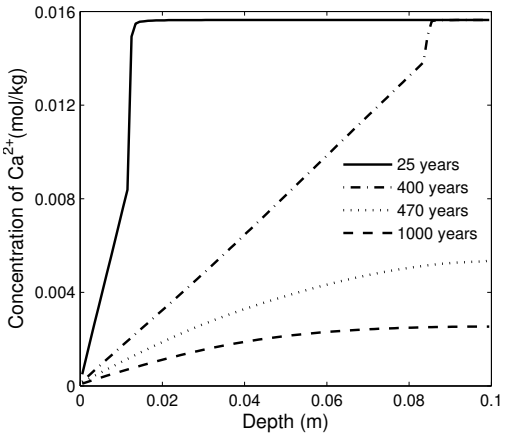

Figure 2.8: The concentration of Ca^{2+} for leaching of deionised water

pore solution pH is displayed along side the change in volume fractions of portlandite and C-S-H at 100 years. A clear zone of portlandite depletion can be observed up to a depth of almost 0.04 m, beyond this zone the pH remains constant. In the depletion zone the pH dropped markedly and the rate of pH reduction became even further pronounced as the C-S-H began to react in the first 0.015 m. This pattern is also evident in figure 2.9b at 400 years, with the initiation of C-S-H reactions occurring at a pH of approximately 11.9.

When alkali hydroxides are released, the pH of the pore solution is buffered by the first dissolved mineral of cementitous material [62], the portlandite ($Ca(OH)_2$), which stabilizes the pH value at approximately 12.5. The dissolution of the C-S-H takes place between pH 12.5 and 10.

Figures 2.9c and 2.9d display the change in volume fraction and corresponding pH after the portlandite has been exhausted. The pH of pore solution in the model displayed a significant decrease across the entire depth of the cement between 466 and 475 years of the simulation, as shown in figure 2.10. The change of portlandite volume fraction is displayed at 0.1 m depth, which demonstrates that the portlandite was exhausted at approximately 471 years. Prior to this time, the majority of hydrogen ions were consumed in the reactions with portlandite, and therefore the pH did not drop significantly. Hydrogen ions accumulated rapidly after the exhaustion of portlandite due to the slow reaction rate of other minerals.

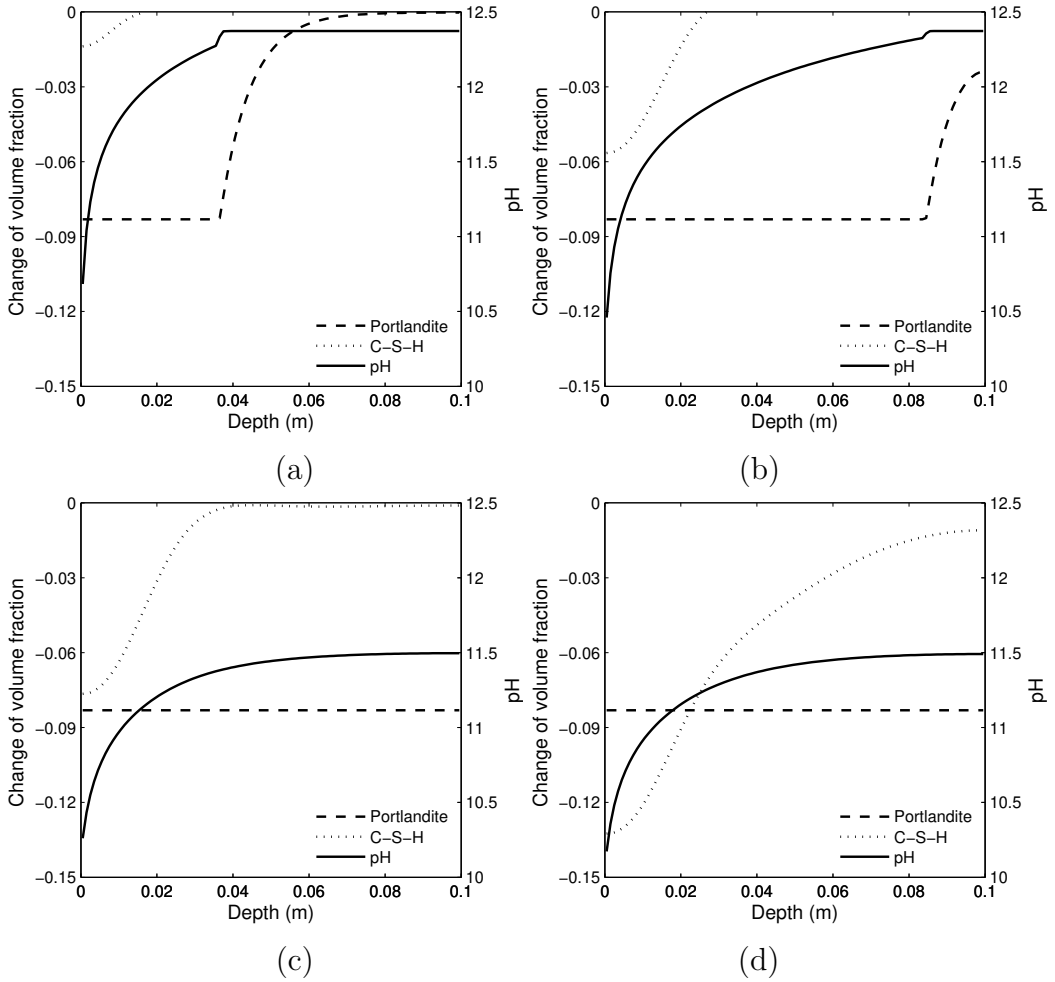

Figure 2.9: Profiles of pH and minerals change in volume fractions at a) 100 b) 400 c) 550 and d) 1000 years exposed to deionised water.

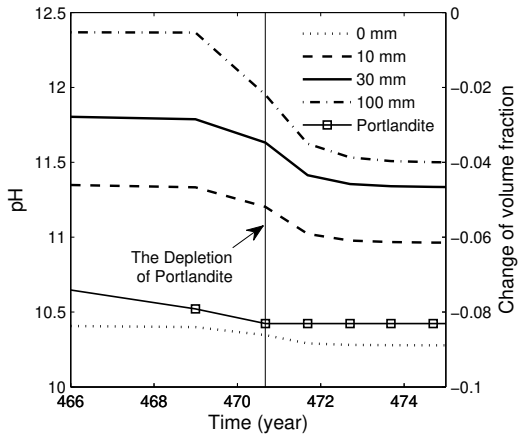

Figure 2.10: Profiles of pH at varying depths and change in portlandite volume fraction at the non-exposed end of the model.

2.4.2 Simulation of leaching by groundwaters

The composition of the groundwater that a cement sheath is exposed to affect the mineralogical changes and dissolution reactions of cement degradation [62]. A series of simulations with different groundwater compositions were performed to evaluate the sensitivity of the chemical degradation rate of cement. Four groundwater compositions [63] were chosen for the simulations as detailed in table 2.7.

Table 2.7: The composition of groundwaters

Species	Saline (mol/kg)	High-carbonate (mol/kg)	Low-carbonate (mol/kg)	Clay (mol/kg)
Na	3.7×10^{-1}	8.4×10^{-3}	8.2×10^{-2}	3.2×10^{-2}
K	4.4×10^{-3}	3.8×10^{-5}	2.5×10^{-4}	7.1×10^{-3}
Mg	5.7×10^{-3}	3.3×10^{-5}	6.8×10^{-4}	1.4×10^{-2}
Ca	2.9×10^{-2}	8.8×10^{-5}	4.8×10^{-2}	1.5×10^{-2}
Sr	2.0×10^{-3}	2.0×10^{-5}	9.9×10^{-4}	1.1×10^{-3}
Al	1.7×10^{-6}	4.6×10^{-7}	5.4×10^{-8}	6.9×10^{-9}
C	1.0×10^{-3}	2.8×10^{-3}	1.6×10^{-4}	3.0×10^{-3}
Si	2.5×10^{-4}	1.1×10^{-4}	7.6×10^{-5}	9.4×10^{-5}
Cl	4.2×10^{-1}	5.3×10^{-3}	1.7×10^{-1}	3.0×10^{-2}
S	1.2×10^{-2}	2.8×10^{-4}	6.4×10^{-3}	3.4×10^{-2}
pH	7.22	8.75	7.73	7.00

The corrosion rates of groundwater compositions and deionised water are exhibited in figure 2.11. In the first decade, the rates were approximately the same, owing to the near neutrality of waters, and gradually differed from each other over the following century displaying a nearly linear relationship between corrosion depth and square root of time under the influence of pH. With lower pH, the corrosion rate of the saline groundwater was slightly higher than that of the low-carbonate groundwater. It is worthy of note that the corrosion rates of the high-carbonate and clay groundwater compositions both began to decrease at approximately 250 years and eventually the corrosion came to a halt.

Figure 2.12 shows the porosity and changes in calcite volume fraction for high-carbonate and saline ground water compositions. With similar compositions, the high-carbonate and clay groundwater compositions resulted in a complete filling of the pore space, whereas some porosity was retained (although dramatically reduced) for the low-carbonate and saline waters. This reduced porosity was induced by the precipitation of calcite, which is the main reaction product of carbonation [64]. With the presence of carbonate ions, calcite precipitated as the dissolution of portlandite

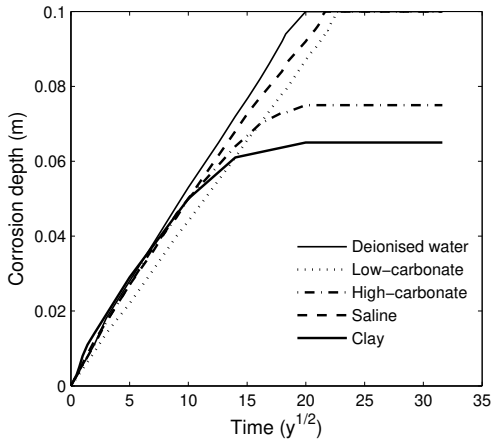

Figure 2.11: The corrosion rates of different waters in 1000 years

and C-S-H by the reaction between calcium and carbonate ions. The carbonation process caused a porosity decrease (clogging of the pore space) since the molar volume of calcite is larger [62]. The resulting effect of this reduced porosity was the formation of a layer near the cement/solution interface that served to protect the cement via a decrease in the rate of ion diffusion and subsequently reactions with the minerals. For high-carbonate content and clay water, the precipitation of calcite was elevated and the pore space near the surface became completely clogged. The cement furthest from the interface with groundwater remained intact (no porosity change) at the end of 1000–year simulation. With lower carbonate concentrations, the low-carbonate and saline waters did not have the effect of completely filling the pore space, however the porosity still decreased due to calcite precipitation.

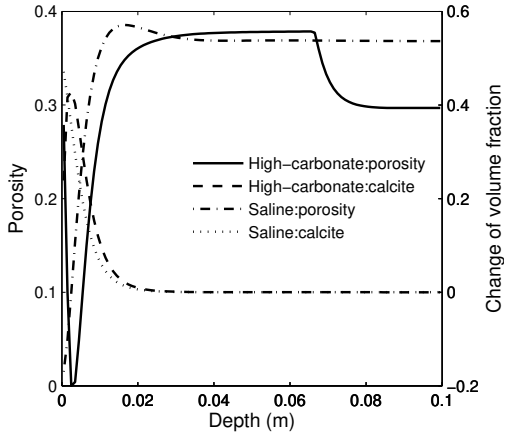

Figure 2.12: The simulated porosity and calcite profiles for highcarbonate and saline water after 1000 years

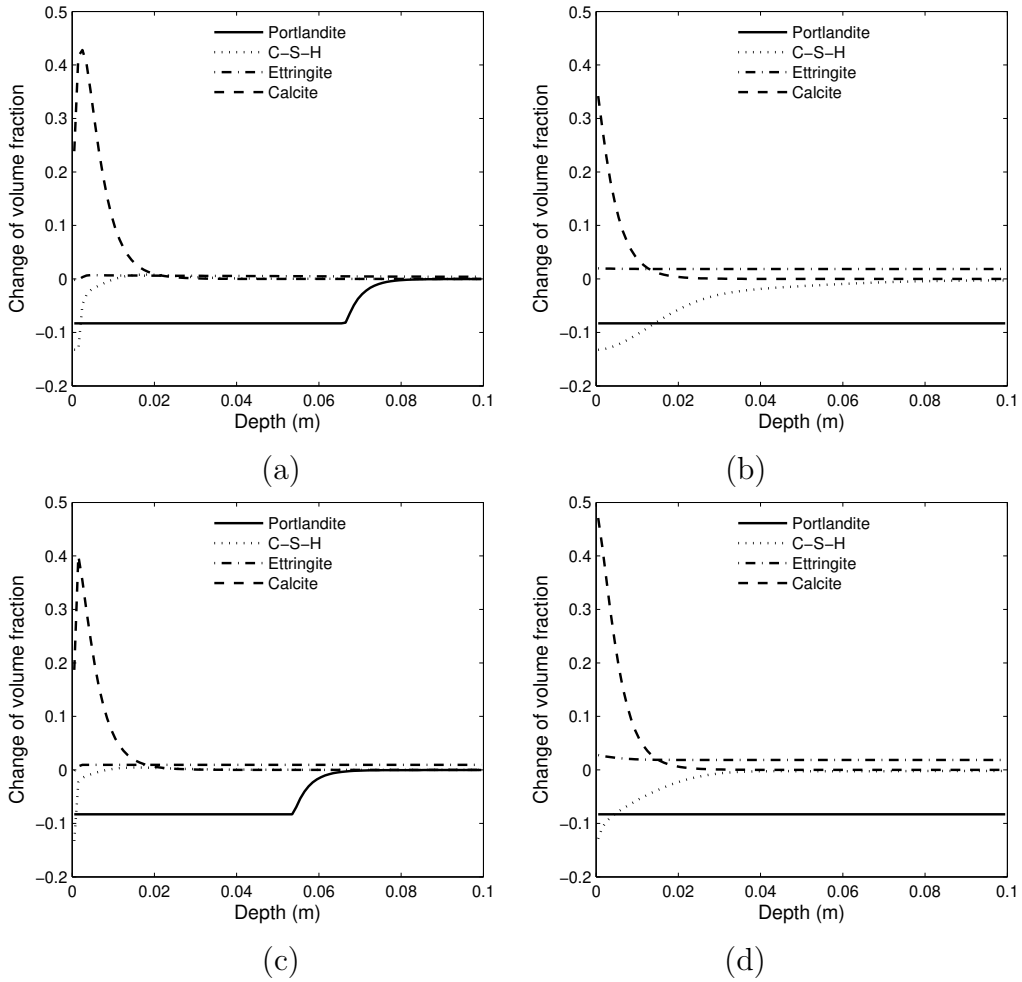

Figure 2.13: Profiles of cement minerals variation exposed to a) high carbon groundwater b) low carbon groundwater c) clay groundwater and d) saline groundwater at 1000 years.

The variation of cement minerals is shown in figures 2.13. In the high-carbonate and clay cases, only the C-S-H close to the surface dissolved, and portlandite remained intact away from the interface (figures 2.13a and 2.13c). The corrosion depth of C-S-H was markedly deeper in the low-carbonate and saline cases, with portlandite totally exhausted (figures 2.13b and 2.13d). The calcite layer formed at the cement/groundwater interface prevented sulphate ions from diffusing into the interior, and thus the precipitation of ettringite was not significant in all cases. However, the low-carbonate and saline groundwater both displayed more ettringite formation than the higher-carbonate cases.

As shown in the response to deionised waters in section 2.4.1, portlandite had an impact on the pH of the pore solution. The pH of the pore solution in the simulations with clay and high-carbonate groundwater was approximately 12.5, significantly higher than that of the lower-carbonate and saline cases, as shown in figure 2.14.

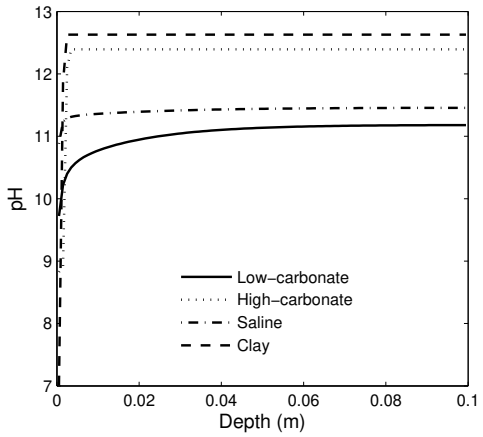

Figure 2.14: The pH profiles after 1000 years for different groundwaters

2.4.3 Validation of the model

Regarding the validation of the simulation over real service life, laboratory and field experiments are not realistic. However, the qualitative verification with existing studies can contribute to a further insight of the mechanism of long–term degradation.

In the experiment, Duguid et al. [17] conducted the flow–through test with carbonated brine, and observed a layer of calcite in acidic solution. It is concluded that the degradation rate of cement depends on the stability of the precipitated minerals. Thermodynamic equilibrium in section 2.2.3 accounts for the precipitation of cement minerals observed in this study, demonstrating that the stability of precipitated minerals ,for example calcite and ettringite, is determined by the value of the saturation index (SI_m). Galíndez and Molinero [18] studied the optimum design of injection grout, and the sensitivity analysis revealed that low carbonate groundwater can significantly accelerate the degradation rate, due to the absence of calcite layer. The result of the present study shows a good agreement with the above mentioned conclusions. The formation of a calcite layer has the prominent effect on the relation between the degradation depth and the square root of time as shown in figure 2.11.

The precipitation of ettringite could exert pressure on the pore wall. It has been clarified that ettringite is stable at ambient temperature and $pH > 10.7$ [65]. According to figure 2.14, pH of the interstitial solution for all cases are generally higher than 10.7, and the precipitation of ettringite is observed in figure 2.13. In the outer elements of the model in figure 2.13a and 2.13c, the absence of ettringite is captured, which is corresponding to the low pH value (8.9 and 7 separately) in the outer elements in figure 2.14. In the case of saline groundwater, pH is higher than 10.7 over

the whole model, the profile of ettringite in the outer elements shows a slight increase comparing with the inner elements, which represents the front of ettringite precipitation. For the low carbon case, the relatively low pH value of the outer elements (approximately 9.7) counteracts the effect of precipitating front in saline case, but not as much as that in high carbon and clay cases, demonstrating a generally a flat profile of ettringite.

2.5 Conclusions

The cement sheath surrounding a wellbore provides an important barrier to the transport of fluids between different fluid bearing strata in the presence of a pressure gradient. This barrier is required to perform both during the service life and beyond decommissioning.

A reactive transport model is adopted to simulate the process of chemical degradation of well cements in response to exposure to groundwater. Accelerated test results from the literature are employed to calibrate the model parameters of the composition, initial porosity and diffusion coefficient that determine the intrinsic characteristics of a cementitious material. The calibrated model is employed in long duration simulations, in order to forecast the performance of the cement sheath in the long term, which naturally cannot be performed in a laboratory or be acquired from field samples.

Portlandite is the first phase dissolving and depleting as the chemical reactions commence and is used to determine the corrosion depth. The dissolution of C-S-H starts subsequent to the exhaustion of portlandite, with a slower rate compared with that of portlandite. The degree of C-S-H dissolution decides the final porosity of the altered zone, and in turn the durability [57].

The quantitative relations between degradation depth and the square root of time for a variety of aqueous solutions are revealed. The deionised water poses more threat to cement than the other four types of groundwater presenting in a higher proportion of corrosion depth versus square root of time. The degradation process could be generalized as the depletion of portlandite and dissolution of C-S-H with the corresponding pH of the pore solution. A complex precipitation/dissolution phenomenon is observed in the simulations exposed to groundwater. The formation of calcite could serve as a protective layer near the exposed surface, reducing the porosity (or even clogging) and preventing the intrusion of aggressive species. The calcite layer and precipitation

of ettringite are validated by previous studies, which shows a good agreement with the conclusions.

The approach represented in this study offers a forecast of the chemical degradation associated with a range of potential groundwater compositions over real service life duration.

References

[1] R. J. Davies, S. Almond, R. S. Ward, R. B. Jackson, C. Adams, F. Worrall, L. G. Herringshaw, J. G. Gluyas, and M. A. Whitehead. Oil and gas wells and their integrity: Implications for shale and unconventional resource exploitation. *Marine and Petroleum Geology*, 56:239 – 254, 2014.

[2] E.B. Nelson. *Well Cementing*. Elsevier, first edition, 1990.

[3] William M. White. *Geochemistry*. John Wiley & Sons, Ltd., 2013.

[4] M. Alexander, Alexandra Bertron, and Nele De Nelie. *Performance of cement-based materials in aggressive aqueous environments*. Springer, 2013.

[5] Stefan Bachu and T. L. Watson. Evaluation of the potential for gas and CO_2 leakage along wellbores. *SPE 106817*, pages 115 – 126, 2009.

[6] G. Le Saoût, E. Lécolier, A. Rivereau, and H. Zanni. Chemical structure of cement aged at normal and elevated temperatures and pressures, Part II: Low permeability class G oilwell cement. *Cement and Concrete Research*, 36(3):428 – 433, 2006.

[7] Edward N. Matteo and George W. Scherer. Experimental study of the diffusion-controlled acid degradation of Class H Portland cement. *International Journal of Greenhouse Gas Control*, 7:181 – 191, 2012.

[8] Nadine Neuville, Eric Lécolier, Georges Aouad, Alain Rivereau, and Denis Damidot. Effect of curing conditions on oilwell cement paste behaviour during leaching: Experimental and modelling approaches. *Comptes Rendus Chimie*, 12(3–4):511 – 520, 2009.

[9] M.D.C. van der Kuip, T. Benedictus, N. Wildgust, and T. Aiken. High-level integrity assessment of abandoned wells. *Energy Procedia*, 4:5320 – 5326, 2011.

[10] Patrick F Dobson, Sonia Salah, Nicolas Spycher, and Eric L Sonnenthal. Simulation of water–rock interaction in the Yellowstone geothermal system using TOUGHREACT. *Geothermics*, 33(4):493 – 502, 2004.

[11] Patrick F Dobson, Timothy J Kneafsey, Eric L Sonnenthal, Nicolas Spycher, and John A Apps. Experimental and numerical simulation of dissolution and precipitation: Implications for fracture sealing at Yucca Mountain, Nevada. *Journal of Contaminant Hydrology*, 62–63:459 – 476, 2003.

[12] C. Geloni, T. Giordis, and A. Battistelli. Modelling of rocks and cement alteration due to CO_2 injection in an exploited gas reservoir. *Transport in porous media*, 90:183 – 200, 2011.

[13] L. André, P. Audigane, M. Azaroual, and A. Menjoz. Numerical modeling of fluid—rock chemical interactions at the supercritical CO_2–liquid interface during CO_2 injection into a carbonate reservoir, the Dogger aquifer (Paris Basin, France). *Energy Conversion and Management*, 48(6):1782 – 1797, 2007.

[14] Fabrizio Gherardi, Pascal Audigane, and Eric C. Gaucher. Predicting long-term geochemical alteration of wellbore cement in a generic geological CO_2 confinement site: Tackling a difficult reactive transport modeling challenge. *Journal of Hydrology*, 420 - 421:340 – 359, 2012.

[15] Thomas Giorgis, Michele Carpita, and Alfredo Battistelli. 2D modeling of salt precipitation during the injection of dry CO_2 in a depleted gas reservoir. *Energy Conversion and Management*, 48(6):1816 – 1826, 2007.

[16] Bruno M. Huet, Jean H. Prevost, and George W. Scherer. Quantitative reactive transport modeling of portland cement in CO_2-saturated water. *International Journal of Greenhouse Gas Control*, 4(3):561 – 574, 2010.

[17] Andrew Duguid, Mileva Radonjic, and George Scherer. Degradation of well cements exposed to carbonated brine. *In: 4th Annual Conference on Carbon Capture and Sequestration. Monitor and Exchange Publications and Forum, Washington, DC.*, 2005.

[18] Juan Manuel Galíndez and Jorge Molinero. Assessment of the long-term stability of cementitious barriers of radioactive waste repositories by using digital-image-based microstructure generation and reactive transport modelling. *Cement and Concrete Research*, 40(8):1278 – 1289, 2010.

[19] D. Jacques, J. Perko, S. Seetharam, and D. Mallants. Evaluating changes of transport properties of chemically degrading concrete using a coupled reactive transport model. *In: 1st International Symposium on Cement-Based Materials for Nuclear Wastes SFEN*, 2011.

[20] Fidel Grandía, Juan-Manuel Galindez, David Arcos, and Jorge Molinero. Quantitative modelling of the degradation processes of cement grout. *Svensk Kärnbränslehantering AB*, SKB TR-10-25, 2010.

[21] Haifeng Yuan, Patrick Dangla, Patrice Chatellier, and Thierry Chaussadent. Degradation modelling of concrete submitted to sulfuric acid attack. *Cement and Concrete Research*, 53:267 – 277, 2013.

[22] Tianfu Xu, Eric Sonnenthal, Nicolas Spycher, and Karsten Pruess. *TOUGHREACT: A new code of the TOUGH family of nonisothermal multiphase reactive geochemical transport in variably saturated geologic media.* Lawrence Berkeley National Laboratory, Berkeley, California, 2003.

[23] E. Samson, J. Marchand, J.-L. Robert, and J.-P. Bournazel. Modelling ion diffusion mechanisms in porous media. *International Journal for Numerical Methods in Engineering*, 46:2043 – 2060, 1999.

[24] E. Samson, J. Marchand, K.A. Snyder, and J.J. Beaudoin. Modeling ion and fluid transport in unsaturated cement systems in isothermal conditions. *Cement and Concrete Research*, 35(1):141 – 153, 2005.

[25] E. Samson and J. Marchand. Modeling the transport of ions in unsaturated cement-based materials. *Computers and Structures*, 85(23):1740 – 1756, 2007.

[26] Joshua Arnold, Ravindra Duddu, Kevin Brown, and David S. Kosson. Influence of multi-species solute transport on modeling of hydrated portland cement leaching in strong nitrate solutions. *Cement and Concrete Research*, 100:227 – 244, 2017.

[27] R. J. Millington and J. P. Quirk. Permeability of porous solids. *Transactions of the Faraday Society*, 57:1200 – 1207, 1961.

[28] Gour-Tsyh Yeh and Vijay S. Tripathi. A model for simulating transport of reactive multi-species components: Model development and demonstration. *Water Resources Research*, 27(3):3075 – 3094, 1991.

[29] Jan van der Lee, Laurent De Windt, Vincent Lagneau, and Patrick Goblet. Module-oriented modeling of reactive transport with hytec. *Computers and Geosciences*, 29(3):265 – 275, 2003.

[30] C. I. Steefel, C. A. J. Appelo, B. Arora, D. Jacques, T. Kalbacher, O. Kolditz, V. Lagneau, P. C. Lichtner, K. U. Mayer, J. C. L. Meeussen, S. Molins, D. Moulton, H. Shao, J. Šimůnek, N. Spycher, S. B. Yabusaki, and G. T. Yeh. Reactive transport codes for subsurface environmental simulation. *Computational Geosciences*, 19(3):445–478, Jun 2015.

[31] J.J. Beaudoin, V.S. Ramachandran, and R.F. Feldman. Interaction of chloride and C-S-H. *Cement and Concrete Research*, 20(6):875 – 883, 1990.

[32] Hélène Viallis-Terrisse, André Nonat, and Jean-Claude Petit. Zeta-potential study of calcium silicate hydrates interacting with alkaline cations. *Journal of Colloid and Interface Science*, 244(1):58 – 65, 2001.

[33] Y. Elakneswaran, T. Nawa, and K. Kurumisawa. Electrokinetic potential of hydrated cement in relation to adsorption of chlorides. *Cement and Concrete Research*, 39(4):340 – 344, 2009.

[34] Christophe Labbez, Isabelle Pochard, Bo Jönsson, and André Nonat. C-S-H/solution interface: Experimental and monte carlo studies. *Cement and Concrete Research*, 41(2):161 – 168, 2011.

[35] David A. Dzombak and Francois M. M. Morel. *Surface Complexation Modelling : Hydrous Ferric Oxide*. John Wiley & Sons, 1990.

[36] Dmitrii A. Kulik and Michael Kersten. Aqueous solubility diagrams for cementitious waste stabilization systems: Ii, end-member stoichiometries of ideal calcium silicate hydrate solid solutions. *Journal of the American Ceramic Society*, 84(1):3017 – 3026, 2001.

[37] Barbara Lothenbach, Thomas Matschei, Göril Möschner, and Fred P. Glasser. Thermodynamic modelling of the effect of temperature on the hydration and porosity of portland cement. *Cement and Concrete Research*, 38(1):1 – 18, 2008.

[38] I.G. Richardson. The calcium silicate hydrates. *Cement and Concrete Research*, 38(2):137 – 158, 2008.

[39] Ingmar Pointeau, Pascal Reiller, Nathalie Macé, Catherine Landesman, and Nathalie Coreau. Measurement and modeling of the surface potential evolution of hydrated cement pastes as a function of degradation. *Journal of colloid and interface science*, 300(1):33 – 44, August 2006.

[40] T. G. Heath, D. J. Ilett, and C. J. Tweed. Thermodynamic modelling of the sorption of radioelements onto cementitious materials. *Material Research Society Proceedings*, 412:443 – 449, 1995.

[41] Y. Elakneswaran, A. Iwasa, T. Nawa, T. Sato, and K. Kurumisawa. Ion-cement hydrate interactions govern multi-ionic transport model for cementitious materials. *Cement and Concrete Research*, 40(12):1756 – 1765, 2010.

[42] Anthony Soive and Van Quan Tran. External sulfate attack of cementitious materials: New insights gained through numerical modeling including dissolution/precipitation kinetics and surface complexation. *Cement and Concrete Composites*, 83:263 – 272, 2017.

[43] H.C. Helgeson, D.H. Kirkham, and D.C. Flowers. Theoretical prediction of the thermodynamic behavior of aqueous electrolytes at high pressures and temperatures: Iv. calculation of activity coefficients, osmotic coefficients, and apparent molal and standard and relative partial molal properties to 600°c and 5kb. *American Journal of Science*, 281:1249 – 1516., 1981.

[44] Thomas J. Wolery. EQ3/6, A software package for geochemical modeling of aqueous systems: package overview and installation guide. *Lawrence Livermoer Laboratory, Berkeley, California*, 1992.

[45] Antonio C. Lasaga, Josep M. Soler, Jiwchar Ganor, Timothy E. Burch, and Kathryn L. Nagy. Chemical weathering rate laws and global geochemical cycles. *Geochimica et Cosmochimica Acta*, 58(10):2361 – 2386, 1994.

[46] C. M. Bethke. *Geochemical biogeochemical reaction modelling.* Oxford University, New York, second edition, 2008.

[47] U. Svensson and W. Dreybrodt. Dissolution kinetics of natural calcite minerals in CO_2-water systems approaching calcite equilibrium. *Chemical Geology*, 100(1):129 – 145, 1992.

[48] Isabel Baur, Peter Keller, Denis Mavrocordatos, Bernhard Wehrli, and C.Annette Johnson. Dissolution-precipitation behaviour of ettringite, monosulfate, and calcium silicate hydrate. *Cement and Concrete Research*, 34(2):341 – 348, 2004.

[49] Cheryl E. Halim, Stephen A. Short, Jason A. Scott, Rose Amal, and Gary Low. Modelling the leaching of Pb, Cd, As, and Cr from cementitious waste using PHREEQC. *Journal of Hazardous Materials*, 125(1–3):45 – 61, 2005.

[50] Ana Trapote Barreira. Dissolution kinetics of C-S-H gel and durability of mortar. *Technical University of Catalonia*, 2015.

[51] H. F. W. Taylor. *Cement chemistry.* Thomas Telford, London, second edition, 1997.

[52] F. Adenot and M. Buil. Modelling of the corrosion of the cement paste by deionized water. *Cement and Concrete Research*, 22(2):489 – 496, 1992.

[53] Marc Mainguy, Claire Tognazzi, Jean Michel Torrenti, and Frédéric Adenot. Modelling of leaching in pure cement paste and mortar. *Cement and Concrete Research*, 30(1):83 – 90, 2000.

[54] H.T. Cao, L. Bucea, A. Ray, and S. Yozghatlian. The effect of cement composition and pH of environment on sulfate resistance of Portland cements and blended cements. *Cement and Concrete Composites*, 19(2):161 – 171, 1997.

[55] T. A. Durning and M. C. Hicks. Using microsilica to increase concrete's resistance to aggressive chemicals. *Concrete International*, 13(3):42 – 48, 1991.

[56] Shashank Bishnoi and Karen L. Scrivener. μic: A new platform for modelling the hydration of cements. *Cement and Concrete Research*, 39(4):266 – 274, 2009.

[57] Sara Goñi, Francisca Puertas, María Soledad Hernández, Marta Palacios, Ana Guerrero, Jorge S. Dolado, Bruno Zanga, and Fulvio Baroni. Quantitative study of hydration of C_3S and C_2S by thermal analysis. *Journal of Thermal Analysis and Calorimetry*, 102(3):965 – 973, 2010.

[58] K. Pruess, C. Oldenburg, and G. Moridis. TOUGH2 user's guide, version 2.0. *Lawrence Berkeley Laboratory Report LBL-43134, Berkeley, California*, 1999.

[59] P. Faucon, P. Le Bescop, F. Adenot, P. Bonville, J.F. Jacquinot, F. Pineau, and B. Felix. Leaching of cement: Study of the surface layer. *Cement and Concrete Research*, 26(11):1707 – 1715, 1996.

[60] E. Revertegat, C. Richet, and P. Gégout. Effect of pH on the durability of cement pastes. *Cement and Concrete Research*, 22(2):259 – 272, 1992.

[61] Fredrik P. Glasser, Jacques Marchand, and Eric Samson. Durability of concrete – Degradation phenomena involving detrimental chemical reactions. *Cement and Concrete Research*, 38(2):226 – 246, 2008.

[62] D. Jacques, L. Wang, E. Martens, and D. Mallants. Modelling chemical degradation of concrete during leaching with rain and soil water types. *Cement and Concrete Research*, 40(8):1306 – 1313, 2010.

[63] A. R. Hoch, G. M. N. Baston, F. P. Glasser, F. M. I. Hunter, and V. Smith. Modelling evolution in the near field of a cementitious repository. *Mineralogical Magazine*, 76:3055 – 3069, 2012.

[64] Anna V. Saetta and Renato V. Vitaliani. Experimental investigation and numerical modeling of carbonation process in reinforced concrete structures: Part I: Theoretical formulation. *Cement and Concrete Research*, 34(4):571 – 579, 2004.

[65] A. Gabrisová, J. Havlica, and S. Sahu. Stability of calcium sulphoaluminate hydrates in water solutions with various ph values. *Cement and Concrete Research*, 21(6):1023 – 1027, 1991.

Chapter 3

Coupled chemo-mechanical degradation

In this chapter, the study of coupled chemo-mechanical degradation is presented as a manuscript which is

Zhongcun Zuo and Terry Bennett : Modelling and numerical simulations of the coupled chemo-mechanical degradation behaviour of cement-based materials, submitted to *Computers & Structures*.

A conference paper is published as the preliminary work of this chapter, which is

Zhongcun Zuo and Terry Bennett : Numerical simulation of the interaction between chemical and mechanical damage for cementitious materials, *ACMSM25, 2020, 395-406*.

The conference paper is available at

https://doi.org/10.1007/978-981-13-7603-0_39

Statement of Authorship

Title of Paper	Modelling and numerical simulations of the coupled chemo-mechanical degradation behaviour of cement-based materials
Publication Status	☐ Published ☐ Accepted for Publication ☑ Submitted for Publication ☐ Unpublished and Unsubmitted work written in manuscript style
Publication Details	Zhongcun Zuo & Terry Bennett (2020). Modelling and numerical simulations of the coupled chemo-mechanical degradation behaviour of cement-based materials, submitted to Computers & Structures.

Principal Author

Name of Principal Author (Candidate)	Zhongcun Zuo
Contribution to the Paper	Undertook literature review, determined research theme, developed the theoretical proof for numerical modelling, performed simulations and interpretation of results, and wrote the manuscript.
Overall percentage (%)	75%
Certification:	This paper reports on original research I conducted during the period of my Higher Degree by Research candidature and is not subject to any obligations or contractual agreements with a third party that would constrain its inclusion in this thesis. I am the primary author of this paper.
Signature	Date 20/1/2020

Co-Author Contributions

By signing the Statement of Authorship, each author certifies that:

i. the candidate's stated contribution to the publication is accurate (as detailed above);

ii. permission is granted for the candidate in include the publication in the thesis; and

iii. the sum of all co-author contributions is equal to 100% less the candidate's stated contribution.

Name of Co-Author	Terry Bennett
Contribution to the Paper	Supervised the selection of research theme, helped with data analysis, and revised the manuscript.
Signature	Date 20/1/2020

Modelling and numerical simulations of the coupled chemo-mechanical degradation behaviour of cement-based materials

Abstract

The coupling of chemical reactions and mechanical damage is fundamental to investigate the durability of load bearing cement-based materials subject to aggressive environments. The present work is devoted to the incorporation of a reactive transport model and non-local damage model to integrate the complete process of chemical degradation and appropriate propagation of mechanical damage in the framework of coupled chemo-mechanical degradation. The chemical degradation of cement-based materials subject to leaching solution is principally concluded as the dissolution of portlandite and decalcification of C-S-H, and the reduction of Young's modulus is evaluated based on the microstructure of materials by Mori-Tanaka scheme. The displacement based non-local damage model is incorporated to capture the post-peak behaviour of the leached mortar beam in three-point bending test. The significance of coupling chemical and mechanical damage for the degraded beam is demonstrated by comparing the coupled damage with outcomes of the non-coupled case.

Keywords : Coupled Degradation; Cement Durability; Elasticity Reduction; Microstructure; Non-Local Damage; Reactive Transport Model.

3.1 Introduction

The coupling behavior of multi fields for infrastructures has been highlighted in recent studies to investigate degradation process [1–3]. The performance of cement-based materials can be determined by both the chemical alteration of the material as a result of interactions with the external environment [4] and the applied mechanical stresses. The evaluation of the material properties for infrastructures, such as the cement sheath of oil and gas wellbores, dams and nuclear waste storage, needs to be based on criteria for both mechanical damage and chemical degradation. Therefore, the coupled chemo-mechanical damage mechanism is required to assess the serviceability and durability of cement-based materials in such circumstances.

The exposure of cement-based materials to the surrounding aqueous environment enables the continued diffusion of external aggressive ion species into the pore space of the cement matrix throughout the service life. The ion transport subsequently results in the continuous transformation of the composition and microstructure of cement-based materials by affecting the chemical equilibrium between the pore solution and the cement minerals, which simultaneously leads to a reduction of the shielding capacity to ion transport and the elastic stiffness of cement matrix. The consequent mechanical damage due to the stiffness loss can in turn aggravate the deterioration of material integrity by promoting the process of ion species transport.

A phenomenological chemical model [5, 6] was proposed to simulate the process of leaching, and described the chemical matrix dissolution with the calcium concentrations of the skeleton material and pore solution. When the equilibrium between calcium ions in the pore solution and solid phases is achieved in this model, a reduced calcium concentration in the pore solution causes dissolution of the cement matrix. Whereas, if the calcium concentration increases, the solid phases remain unchanged, resulting in the absence of precipitation of cement minerals. This phenomenological model has been extensively incorporated to investigate the coupled chemo-mechanical damage of cement-based materials, of which the calcium leaching was presented in various methods for stiffness degradation and ion transport acceleration. The consequences of chemical deterioration on porosity and elasticity of cement paste were described as a function of calcium concentration with experimental data [7–10]. The change of calcium concentration from the phenomenological chemical model was employed to evaluate the chemically induced porosity change [11, 12]. In other studies [13, 14], the chemical damage process was represented by a variable with regard to the reaction extent. Subsequently, the porosity change or damage variable was

adopted to evaluate the residual stiffness, implying that the leaching process of different minerals can alter the mechanical stiffness of materials homogeneously. In terms of cement-based materials, the chemical reactions of mineral constituents with pore solution differ significantly [4], for instance portlandite dissolving firstly followed by monosulfate, ettringite and calcium silicate hydrate (C-S-H). Therefore, the residual stiffness of the degraded cement should be evaluated according to the specific amount of each cement mineral after dissolving/precipitating in the matrix. Furthermore, aquatic chemistry is the principal concern dominating the process of chemical degradation, and can be categorized as acid–base reactions, mineral dissolution and precipitation, surface complexation and ion exchange [15]. In this sense, a more comprehensive chemical module is beneficial to capture the degradation process of the material in aqueous environment.

Reactive transport modelling is capable of offering a more realistic solution by evaluating the aquatic chemistry on the basis of thermodynamic equilibrium and kinetic constraint, and has been increasingly adopted to evaluate the chemically induced deterioration for cement-based materials [16–19]. In chemical simulations, the reactions between cement minerals and pore solution are captured as the volume fraction variation of each solid phase, and the corresponding porosity change is applied to update the transport properties in subsequent time steps.

As chemical reactions proceed, the variation of volume fraction is determined by the solubility of each cement mineral, and subsequently affects the residual elastic modulus of the material. In order to evaluate the mechanical properties of a material, the microstructure of the material needs to be taken into account. The three-level division of microstructure for cement-based material was proposed by Heukamp [20] based on characteristic length scale. The Mori-Tanaka scheme [21] was employed to estimate the effective stiffness of C-S-H matrix and cement paste on level I and II separately, and then upscaled the Young's modulus of mortar/concrete on level III by the Hervé-Zaoui scheme [22]. Stora et al. [23] adopted a reactive transport model to simulate the leaching process within cement-based materials, and evaluated the elastic and transport properties with residual volume fractions of solid phases on the basis of the three-level microstructure. In contrast to the work of Heukamp, the level I consists of two layers of cement paste distinguished by the density of C-S-H, and the elastic properties were estimated by generalized self-consistent scheme (GSCS) [22], and the interaction direct derivation (IDD) [24] was incorporated to evaluate the properties of both cement paste layers on level II. The properties of mortar were

subsequently evaluated by GSCS on the level III. Stora et al. [17] evaluated the residual mechanical properties of the degraded mortar beam with the proposed method, which was subsequently employed to model three-point bending behaviour comparing with experimental results [25]. The simulated post-peak behaviour suffered convergence difficulties, for which the local damage model was considered as the principle reason. The convergence issue of three-point bending modelling was negated in the work of Le Bellégo et al. [26] by the use of non-local damage techniques coupled with the phenomenological chemical model. To achieve the simulation of fully coupled chemo-mechanical deterioration, the mechanical damage was converted to the variation of the effective diffusivity [12, 17], or the increment of porosity [11, 26] which was adopted to describe the transport equations.

The integration of a reactive transport model, non-local damage and a novel coupling technique is presented in this work, in order to incorporate the complex aquatic chemistry, alleviate the mesh objectivity and accommodate the chemical and mechanical degradation phenomena. The geochemical model [27] has been developed to investigate the reactive transport of non-isothermal multi-component fluid, and applied to physically and chemically heterogeneous porous media. Numerous non-local damage approaches exist in the literatures, categorized as the integral type model [28] and the gradient enhanced model [29], and the accumulated damage is obtained by using a non-local treatment to avoid mesh dependence. In this work, the displacement based non-local damage model [30–32] is adopted. The two moduli qualitatively provide the more realistic evaluations, and subsequently the fully coupled model is able to offer an enhanced solution for the chemo-mechanical degradation of cement-based materials.

In the present work, the reactive transport model evaluates the varying volume fractions of solid phases, which compose the porosity change, in the process of chemical degradation. The microstructure is considered as C-S-H matrix with inclusions, and the elastic Young's modulus is evaluated by Mori-Tanaka scheme [21] on the basis of volume fractions. In a similar approach to previous studies [11, 26], the microcracks derived from tensile stress are calculated as a scalar multiplier for the stiffness reduction, and converted to porosity increment for updating the transport properties in addition to the chemically induced porosity change. The chemical and mechanical damage parameters are subsequently incorporated in the constitutive model to demonstrate specifically the evolution and interaction of the two damage parameters for numerical implementation.

The methodologies of the reactive transport modelling, the displacement based non-local damage model and strain-stress based constitutive law in the coupling scheme are presented in section 3.2. The residual stiffness of chemically degraded cement-based materials is evaluated in section 3.3, and subsequently employed to simulate the flexural behaviour of the degraded mortar beam, which are contrasted with experimental outcomes. In section 3.4, the simulation of fully coupled chemo-mechanical degradation is conducted to investigate the instantaneous interaction between chemically and mechanically induced degradation, and compared with the results of the non-coupled case.

3.2 Modelling methodology of coupled degradation

The exposure of cement-based materials to external aqueous solution is considered as the commencement of the coupled chemo-mechanical degradation. For numerical modelling, starting with the initial conditions, the residual cement constituents are evaluated at the end of the first step of chemical degradation, and subsequently employed to update the material properties. The weakened mechanical property potentially leads to consequent damage, which is converted into the reduction of elastic moduli and increment of transport properties as the initial conditions of the following step. The coupling procedure is ongoing in the rest of the simulation until the terminal point is achieved, which is depicted in figure 3.1.

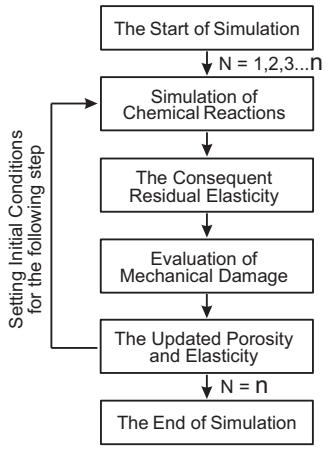

Figure 3.1: Schematic flow diagram of the coupling scheme for chemical and mechanical damage proposed in present work.

3.2.1 Chemical degradation modelling

Reactive transport modelling [27] is employed to evaluate the process of aggressive ion species transport and chemical reactions within the solid matrix. The detailed description of the model is available in the literature [33], therefore only the primary governing equations are outlined below to demonstrate the fundamental mechanisms involved.

3.2.1.1 Transport equations

The diffusion of aggressive ion species dominates the chemical degradation of cement-based materials [34]. Considering the discussion about the electrochemical potential effect on diffusion in available literatures [16, 23, 33], the Fickian diffusion equation is adopted and described as equation (3.1).

$$\frac{\partial \phi C_i}{\partial t} = D_e \frac{\partial^2 C_i}{\partial x^2} + q_i \tag{3.1}$$

$$D_e = \phi \tau_0 \tau D_0 \tag{3.2}$$

where for species i of interest, C_i, D_0 and q_i are the concentration, the diffusion coefficient in bulk water and the source/sink term individually. The effective diffusion coefficient D_e of species i is defined by the porosity of the material ϕ, tortuosity $\tau_0 \cdot \tau$ and D_0. The Millington and Quirk model [35] describes the tortuosity in equation (3.3) with the porosity dependant coefficient τ_0 and saturation S_l dependant parameter τ.

$$\tau_0 \tau = \phi^{1/3} S_l^{7/3} \tag{3.3}$$

3.2.1.2 Thermodynamic equilibrium

The reactions between the diffused ion species and solid phases in the material matrix are mainly considered as precipitation/dissolution of cement minerals, and governed by the mineral saturation Ω_m that is calculated as

$$\Omega_m = K_m^{-1} \prod_{j=1}^{N_c} C_j^{\nu_{mj}} \gamma_j^{\nu_{mj}} \quad m = 1, ..., N_p \tag{3.4}$$

where K_m represents the equilibrium constant of the mineral, C_j $(mol \cdot kg^{-1})$, ν_{mj} and γ_j are the molal concentration, stoichiometric coefficient and activity coefficient of the j-th primary species respectively. N_c represents the number of primary species and N_p represents that of minerals. The cement minerals start dissolving if $\Omega_m < 1$ and precipitating if $\Omega_m > 1$, and remain in equilibrium when $\Omega_m = 1$.

3.2.1.3 Kinetics

For chemical reactions under kinetic constraint, the reaction rate r_m is determined by Lasaga et al. [36]

$$r_m = \pm k_m A_m \mid 1 - \Omega_m^{\theta} \mid^{\eta} \quad m = 1, ..., N_p \tag{3.5}$$

where k_m $(mol \cdot m^{-2} \cdot s^{-1})$ and A_m $(m^2 \cdot g^{-1})$ are the rate constant and specific reactive surface area respectively. θ and η are model parameters calibrated by experiments, and frequently set to unity.

3.2.2 Mechanical damage modelling

The damage mechanics can represent the degrading process within materials, including the propagation of microcracks and reduction of mechanical properties, and quantitatively evaluate the damage phenomena with numerical modelling.

3.2.2.1 Damage evaluation modelling

The constitutive description of the progressive reduction of material stiffness induced by the propagation of microcracks is an extensively investigated topic. For the adopted isotropic damage model, a scalar damage parameter d is described by the exponential damage function representing the reduction of Young's modulus for the material, which is given in equation (3.6) and (3.7). The Poisson's ratio is assumed to be constant in the process of mechanical damage [37], and the residual stiffness tensor $\boldsymbol{C_r}$ is obtained by d and initial stiffness tensor $\boldsymbol{C_0}$ in equation (3.8).

$$d(\kappa) = 1 - \frac{\kappa^0}{\kappa}\left[1 - \alpha + \alpha \exp\left[\beta[\kappa^0 - \kappa]\right]\right] \tag{3.6}$$

$$E = (1 - d(\kappa))E_0 \tag{3.7}$$

where κ^0 is the elastic threshold; κ is the current damage threshold; E_0 and E are initial and residual Young's Modulus separately; α and β are model parameters related to the material.

$$\boldsymbol{C_r} = (1 - d(\kappa))\boldsymbol{C_0} \tag{3.8}$$

Based on the work of Simo and Ju [38], the damage criterion is described as

$$\Phi = \tilde{\varepsilon}(\varepsilon) - \kappa \leq 0 \tag{3.9}$$

where $\tilde{\varepsilon}$ is the equivalent strain function. The consistent loading/unloading conditions are formally described as

$$\dot{\kappa} \geq 0, \quad \Phi\dot{\kappa} = 0, \quad \dot{\Phi}\dot{\kappa} = 0 \tag{3.10}$$

In terms of a N_d-dimension domain of cement-based materials, the equivalent strain $\tilde{\varepsilon}$, which is determined by the principal strain ε_i [39], is suitable to describe the mechanical performance in constitutive model and defined as equation (3.11).

$$\tilde{\varepsilon} = \sqrt{\sum_{i=1}^{N_d} (< \varepsilon_i >)^2} \tag{3.11}$$

3.2.2.2 Displacement based non-local damage model

The typical damage model in section 3.2.2.1 exhibits the mesh dependency, and material non-locality is required to distribute state variables over the vicinity of the point of interest. In the non-local damage model, the non-local counterpart of a state variable is calculated by weighted averaging the "local" state variable in the vicinity of each point. The integral type non-local damage model [28] is based on the weighted average of strain-related state variables, and the strain averaging is relatively straightforward to facilitate the numerical implementation. In the displacement based non-local damage model [30, 31], the weighted state variable is displacement, and the non-local displacement $\overline{\boldsymbol{u}}$ is determined as the weighted average of local displacement $\boldsymbol{u}(z)$ described in equation (3.12), and introduced to the constitutive model for the evaluation of mechanical damage.

$$\overline{\boldsymbol{u}} = \int \overline{\alpha}(x, z)\boldsymbol{u}(z)dz \tag{3.12}$$

$$\overline{\alpha}(x,z) = \left[c_0(x) + \mathbf{z}^{\mathbf{T}} c_1(x)\right] \alpha(x-z) \tag{3.13}$$

where $\overline{\alpha}(x,z)$ is the weighting function and consists of a polynomial of order 1 and a bell shaped function described in equation (3.14). The point z is in the weighted averaging scope of the point x, and $\mathbf{z}$ is the vector between the two points. The Gaussian function $\alpha(x-z)$ consists of the characteristic length l_c and the distance between point x and z as defined in equation (3.14).

$$\alpha(x-z) = \exp\left[-\left(\frac{2(x-z)}{l_c}\right)^2\right] \tag{3.14}$$

A small system of linear equations is obtained by the combination of equations (3.12) and (3.13) to determine two coefficients $c_0(x)$ and $\boldsymbol{c}_1(x)$.

$$\begin{bmatrix} \int \alpha(x-z)dz & \int \mathbf{z}^{\mathbf{T}} \alpha(x-z)dz \\ \int \mathbf{z}\alpha(x-z)dz & \int \mathbf{z}\mathbf{z}^{\mathbf{T}} \alpha(x-z)dz \end{bmatrix} \begin{Bmatrix} c_0(x) \\ \boldsymbol{c}_1(x) \end{Bmatrix} = \begin{Bmatrix} 1 \\ x \end{Bmatrix} \tag{3.15}$$

The non-local strain is subsequently calculated as the symmetric gradient of the non-local displacement by equation (3.16).

$$\overline{\boldsymbol{\varepsilon}}(x) = \nabla^s \overline{\boldsymbol{u}}(x) \tag{3.16}$$

3.2.3 Constitutive laws of the coupled damage

The quantitative evaluation of chemical and mechanical damage on material properties is demonstrated in this section, and the coupling scheme is proposed to incorporate the two mechanisms appropriately. The porosity and elastic moduli of the cement-based material are updated individually after the evaluation of either the chemical or mechanical degradation, which has retroaction on the following simulation process.

The chemical reactions between cement material and the aggressive ion species are evaluated by the chemical model in section 3.2.1.1. The mineral dissolution and precipitation lead to the volume variation of solid phases in matrix, eventually resulting

in porosity change, calculated as

$$\phi_c = \sum_{s=1}^{N_s} \triangle f_s \tag{3.17}$$

where $\triangle f_s$ is the change of volume fraction of the solid phase and N_s is the number of solid phases in the material. The chemically induced porosity change ϕ_c influences the process of chemical degradation, which can be demonstrated by equations (3.1)-(3.5). As discussed in section 3.1, the porosity change due to chemical degradation is insufficient to describe the variation of the elastic moduli properly, and the microstructure of the material is required to be incorporated to define the mechanical properties for the different solubility of each solid phase. The Mori-Tanaka scheme [21] homogenizes the multiphase materials as the reference medium and inclusions, and evaluates the Young's modulus E_{hom} and Poisson's ratio ν_{hom} of the cement-based materials by equation (3.18) in this work.

$$E_{hom} = \frac{9\psi_{hom}\mu_{hom}}{3\psi_{hom} + \mu_{hom}}; \quad \nu_{hom} = \frac{3\psi_{hom} - 2\mu_{hom}}{6\psi_{hom} + 2\mu_{hom}} \tag{3.18}$$

The homogenized bulk modulus ψ_{hom} and shear modulus μ_{hom} of the material are calculated by equation (3.19) and (3.20).

$$\psi_{hom} = \sum f_i\psi_i\Big(1 + A^m\Big(\frac{\psi_i}{\psi_m} - 1\Big)\Big)^{-1} \times \Big[\sum f_i\Big(1 + A^m\Big(\frac{\psi_i}{\psi_m} - 1\Big)\Big)^{-1}\Big]^{-1} \tag{3.19}$$

$$\mu_{hom} = \sum f_i\mu_i\Big(1 + B^m\Big(\frac{\mu_i}{\mu_m} - 1\Big)\Big)^{-1} \times \Big[\sum f_i\Big(1 + B^m\Big(\frac{\mu_i}{\mu_m} - 1\Big)\Big)^{-1}\Big]^{-1} \tag{3.20}$$

$$A^m = \frac{3\psi_m}{3\psi_m + 4\mu_m}; \quad B^m = \frac{6(\psi_m + 2\mu_m)}{5(3\psi_m + 4\mu_m)} \tag{3.21}$$

where ψ_m and μ_m are the bulk and shear moduli of the reference medium, ψ_i and μ_i are those of inclusions, and f_i is the volume fraction of inclusions.

With the residual volume fractions after chemical degradation and intrinsic elastic properties of solid phases, the Young's modulus E_c and Poisson's ratio ν_c of the chemically degraded material are obtained by equation (3.22), and subsequently adopted to evaluate residual stiffness tensor $\boldsymbol{C_c}$ after chemical degradation in equation (3.23)

$$E_c = E_{hom}; \quad \nu_c = \nu_{hom} \tag{3.22}$$

$$\boldsymbol{C_c} = \boldsymbol{C_0}(E_c, \nu_c) \tag{3.23}$$

For cement-based materials subject to leaching, the reduction of the elastic modulus has been investigated by diverse approaches [40–42], and the significant increase of elastic strain threshold for the leached material has been measured as the corresponding consequence of stiffness loss [41]. The evolution of the damage threshold is difficult to confirm in laboratory tests, therefore the equivalency between the variation of elastic threshold due to mechanical damage and that due to chemical reactions is assumed in the present work. With this assumption, the curve of strain-stress relation is evaluated by equation (3.8), and accommodates the chemical and mechanical degradation as shown in figure 3.2.

With the residual Young's modulus E_c in equation (3.22) after chemical degradation, the current elastic threshold is increasing from the original value $\tilde{\varepsilon}_o$ to $\tilde{\varepsilon}_c$, depicted in figure 3.2. The strain redistribution is evaluated with stiffness tensor $\boldsymbol{C_c}$ after chemical degradation, and the potential mechanical damage is evaluated if the updated equivalent strain $\tilde{\varepsilon}$ exceeds the current elastic threshold $\tilde{\varepsilon}_c$. As described in equation (3.9), the value of equivalent strain becomes damage threshold when mechanical damage occurs, denoted as $\tilde{\varepsilon}_m$ in figure 3.2.

Specifically, for the strain $\tilde{\varepsilon}_m$, the damage parameter $d(\tilde{\varepsilon}_m)$ is determined by equation (3.6) representing the fraction of Young's modulus reduction, and consists of both chemical and mechanical damage parameters, described in equation (3.24). The variable d_c represents the chemically induced damage on Young's modulus, and defined by the residual Young's modulus E_c after chemical degradation and the original Young's modulus E_o in equation (3.25). The mechanical damage of leached materials d_m is subsequently calculated by equation (3.26). Therefore, by coupling the chemical and mechanical damage, Young's modulus of the material reduces from E_o to E_m, described in equation (3.27).

$$d(\tilde{\varepsilon}_m) = 1 - \frac{\tilde{\varepsilon}_0}{\tilde{\varepsilon}_m}\left[1 - \alpha + \alpha \exp\left[\beta[\tilde{\varepsilon}_0 - \tilde{\varepsilon}_m]\right]\right] = d_c + d_m \tag{3.24}$$

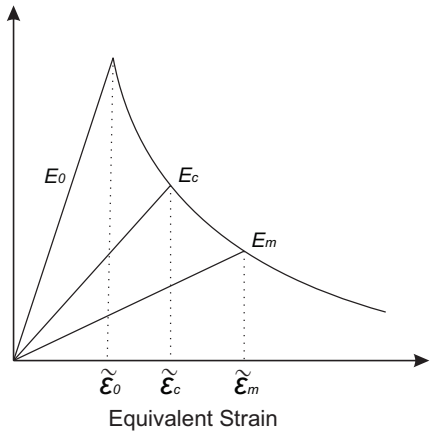

Figure 3.2: Schematic diagram of the evolution of Young's modulus and elastic threshold with chemical and mechanical damage.

$$d_c = 1 - E_c/E_o \tag{3.25}$$

$$d_m = d(\tilde{\varepsilon}_m) - d_c \tag{3.26}$$

$$E_m = (1 - d(\tilde{\varepsilon}_m))E_o = (1 - d_c - d_m)E_o \tag{3.27}$$

As described in section 3.2.2.1, Poisson's ratio remains constant in mechanical damage, and Young's modulus E_m is substituted into chemically degraded stiffness tensor $\boldsymbol{C_c}$ to update the stiffness tensor $\boldsymbol{C_m}$ of coupled degradation in equation (3.28).

$$\boldsymbol{C_m} = \boldsymbol{C_c}(E_m) \tag{3.28}$$

The microcracks due to mechanical damage within the cement skeleton can be interpreted as the equivalent pore space [43]. In the present work, the feedback of mechanical damage on the process of chemical degradation is achieved by relating the change of transport properties with the mechanically induced porosity ϕ_m for the consistence with the adopted reactive transport model. According to the residual stiffness obtained in the equation (3.27), the mechanical porosity ϕ_m is inversely calculated by the aforementioned Mori-Tanaka scheme. The porosity-based approach for the feedback on transport properties is consistent with the homogenized diffusion model described in equation (3.1), which is able to reflect the influence of damage on both sides of this governing equation in the reactive transport model. The overall porosity ϕ of the degraded material is updated by equation (3.29), and adopted together with the residual stiffness tensor $\boldsymbol{C_m}$ to represent the occurred chemical and mechanical degradation and also the initial conditions for the subsequent simulation.

$$\phi = \phi_o + \phi_c + \phi_m \tag{3.29}$$

In the present study, the quadrilateral four-node plane element is employed to achieve the coupled chemo-mechanical degradation on a mortar beam. The mechanical damage model in section 3.2.2 is applied on Gauss points of the element to evaluate the propagation of microcracks, which is subsequently converted into the homogenized change of transport properties as above described at the element level. The chemical degradation is performed with the same element size, and the impact of mechanical damage is correspondingly incorporated in the process of reactive transport. The numerical implementation of the coupled chemo-mechanical degradation is coded with MATLAB, and the coupling process in figure 3.1 is repeated until the proposed simulation loops are performed and achieve convergence.

3.3 The influence of leaching on the mechanical performance

The assessment of the influence of leaching is the crucial component in the fully coupled chemo-mechanical damage, due to the complexity of chemical deterioration process and the significance for precisely evaluating the residual mechanical properties. For cement-based materials, experimental studies have been performed to test the residual performance in tension/flexure [25, 44, 45] and compression [20, 46]. In this section, the leaching process on intact cement-based materials is simulated by the reactive transport modelling presented in section 3.2.1, and the residual elastic moduli of degraded material is subsequently evaluated by Mori-Tanaka scheme as demonstrated in section 3.2.3. Since the effect of chemical degradation on the mechanical properties is validated with existing experimental data on the material level, the partially leached mortar beam is submitted to three-point bending test to evaluate the flexural behaviour on the structural level with the mechanical damage model in section 3.2.2.

3.3.1 Chemical System

In the present work, the typical hydration products of Portland cement are employed for cement paste, including portlandite, C-S-H, ettingite, monosulphate, and the unhydrated clinker which is related with the degree of hydration. In terms of mortar, the sand aggregate is contained as an additional composition in the cement paste. It is assumed that the unhydrated clinker and sand are chemically nonreactive in the course of degradation.

The leaching process within the cement-based materials is dominated by the dissolution of portlandite and C-S-H [33, 47]. In Portland cement, portlandite is the first phase dissolved and depleted, due to the thermodynamic and kinetic properties [4, 33]. C-S-H is essentially amorphous and described as gels with an average Ca/Si ratio, while the incongruent solubility behaviour of C-S-H is related with the Ca/Si ratio [48]. As the leaching front moves into the interior of material matrix, the C-S-H with high Ca/Si ratio starts dissolving incongruently and forming C-S-H with low Ca/Si ratio, which is the decalcification of C-S-H. When the Ca/Si ratio decreases to approximately 0.8, C-S-H gel dissolves congruently [49]. In the present work, the intact and leached C-S-H is represented by gels with the Ca/Si ratio of 1.7 and 0.8 separately. The chemical system of the considered cement minerals is tabulated in table 3.1.

Table 3.1: The chemical formulae and thermodynamic data of the incorporated cement minerals in the chemical system

Cement mineral	Chemical formula	Log(K_m)	Reference
Portlandite	$Ca(OH)_2$	22.5444	[50]
C-S-H (Intact)	$Ca_{1.7}SiO_{6.317}H_{5.234}$	28.0022	[50]
C-S-H (Leached)	$Ca_{0.8}SiO_{4.34}H_{3.08}$	11.0503	[50]
Ettringite	$Ca_6Al_2(SO_4)_3(OH)_{12}{:}26H_2O$	56.8823	[50]
Monosulphate	$Ca_4Al_2(SO_4)(OH)_{12}{\cdot}6H_2O$	72.4704	[50]

3.3.2 Leaching induced reduction of elasticity

This section is dedicated to the elastic properties of cement-based material before and after leaching with the proposed methodology in section 3.2, which demonstrates the simulation of chemical reactions and evaluation of residual stiffness. Constantinides [40] and Heukamp et al. [41] performed diverse tests on both intact and leached cement-based materials, and investigated the impact of leaching on Young's modulus. The setup of the simulation is determined as cement-based material prepared with Portland cement subject to 6M ammonium nitrate (NH_4NO_3) solution according to the experiment. The compositions of cement paste in the work of Stora et al. [51] are employed, and extrapolated to obtain the volume fractions of compositions for mortar, as tabulated in table 3.2.

The model of a cuboid with a length of 20 mm and 5 $\times$ 5 mm cross section is employed for the simulation of leaching process as shown in figure 3.3. The mineral compositions of paste and mortar leached by 6M NH_4NO_3 solution for 15 days are

Table 3.2: The volume fractions (%) of compositions for cement paste and mortar adopted in simulations of section 3.3.2

Material Type	Portlandite	C-S-H (Intact)	Ettringite	Monosulphate	Unhydrated clinker	Sand	Porosity
Paste	10.8	49.7	2.3	0.4	18.4	N/A	18.4
Mortar	4.63	21.32	0.99	0.17	7.89	50	15

demonstrated in figure 3.4. Portlandite starts dissolving promptly once the chemical equilibrium between material matrix and pore solution is disturbed by NH_4NO_3 solution, almost depletes in elements near the interface. The leaching front is observed as the dissolution of portlandite for both cases, and subsequently the altered zone is determined as the portion between the leaching front and the interface, which shows accordance with the existing work [33, 52, 53]. It is captured that the decalcification of C-S-H initiates as the dissolution of portlandite slowing down. The intact C-S-H incongruently dissolves while releasing calcium ions into pore solution, and the leached C-S-H with low Ca/Si ratio is simultaneously formed.

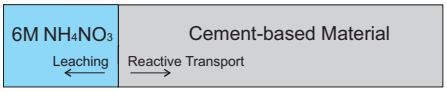

Figure 3.3: Schematic diagram of the one-dimensional model for cement-based material subject to 6M NH_4NO_3 leaching.

The significant variation of cement minerals in the altered zone has an enormous impact on the mechanical properties of the material. Constantinides and Ulm [54] demonstrated that the reduction of macroscopic elasticity for the leached cement paste arises from a coupled mechanism of the dissolution of portlandite and the decalcification of C-S-H. The loss of intrinsic elasticity resulted from the decalcification of C-S-H is suggested to be the primary source of the overall elastic stiffness reduction, dominating over the influence of portlandite depletion. The measured elastic moduli of the intact and leached C-S-H in nanoindentation tests are employed to evaluate the elastic stiffness, tabulated together with the corresponding data of other constituents in table 3.3.

The volume fraction of each constituent is incorporated in the Mori-Tanaka homogenization scheme to estimate the evolution of elastic moduli of the cement-based material. In figure 3.5, the reduction of elastic property exhibits a two-stage degradation process. In the vicinity of leaching front, the values of Young's modulus for both paste and mortar decrease from original values of 20.97 and 24.77 GPa to approximate

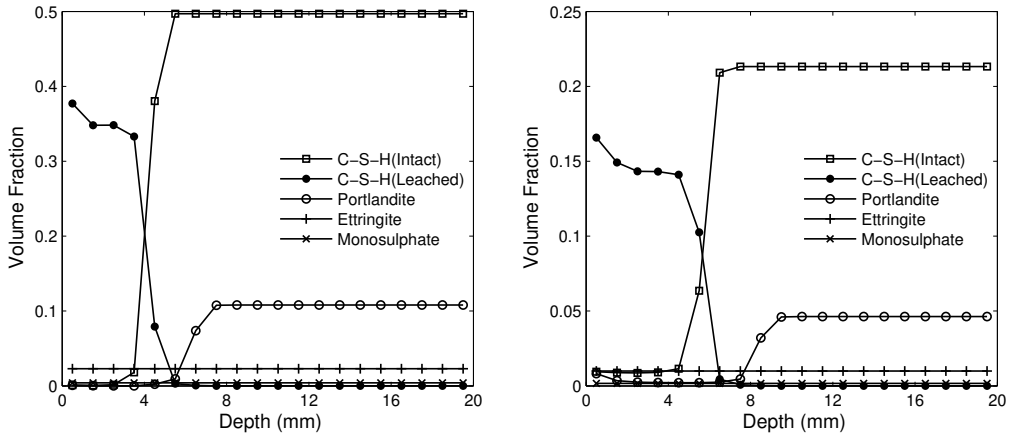

Figure 3.4: Profiles of minerals in volume fraction for (a) paste and (b) mortar exposed to 6M NH_4NO_3 solution for 15 days.

17 and 21 GPa separately, which can be attributed to the significant dissolution of portlandite since the incongruent dissolution of C-S-H is minor/negligible in the zone adjacent to leaching front as shown in figure 3.4. By contrast, the outer zones of paste and mortar both demonstrate a sharp diminution of elastic property dropping to 4.4 and 7.0 GPa approximately, while C-S-H with low Ca/Si ratio is the predominant constituent in this zone (figure 3.4) representing the extent of C-S-H decalcification in the leaching process.

Constantinides and Ulm [40] recorded the Young's modulus of cement paste and mortar decreasing from 21.65 and 25.14 GPa to 3.15 and 4.89 GPa respectively. Gallé et al. [42] measured the elastic modulus declining from 23 GPa to 7 GPa for cement paste subject to a thorough chemical degradation. The direct tensile tests of Heukamp et al. [41] demonstrated likewise the significant reduction of Young's modulus for the leached cement-based material. The proposed methodology in the present work is in accord with the above-mentioned experimental results, verifying the feasibility of evaluating the residual elastic property of leached cement-based materials.

3.3.3 The mechanical behaviour of a leached mortar beam

Le Bellégo [25] performed leaching and three-point bending test on mortar beam, which has been taken as a benchmark for the validation of chemo-mechanical simulation [17, 20]. Therefore, in this section, the residual linear elasticity is employed to evaluate the non-linear mechanical behaviour of leached structural component reproducing the experimental work of Le Bellégo in consistence with previous studies.

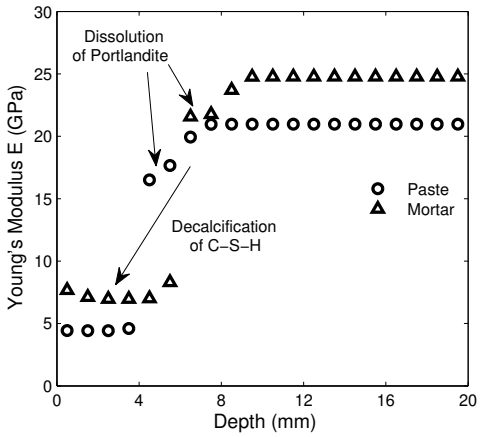

Figure 3.5: Profiles of Young's modulus for paste and mortar subject to 6M NH_4NO_3 solution leaching for 15 days.

Table 3.3: Intrinsic elastic properties of solid phases in cement-based material

Solid phase	E (GPa)	Poisson's ratio ν	Reference
Portlandite	42.3	0.324	[55]
C-S-H (Intact)	23.8	0.240	[54]
C-S-H (Leached)	4.3	0.240	[54]
Ettringite	22.4	0.250	[23]
Monosulphate	42.3	0.324	[23]
Unhydrated clinker	117.6	0.314	[56]
Sand	41.4-115.8	0.170	[57]

In the experiment, a mortar beam of 320 mm × 80 mm × 40 mm (length × height × width) was manufactured with a water/cement ratio of 0.5, and subject to leaching for 114 days. The 6M NH_4NO_3 solution was only imposed on the bottom surface of the beam, while the lateral surfaces and a 60 mm long section on both sides of bottom surface were covered by the coating of RTV epoxy. Therefore, the central portion of 200 mm × 40 mm on the bottom of the mortar beam was exposed to the 6M NH_4NO_3 solution. The depth of the altered zone is measured according to the dissolution front of portlandite, and the average depth of four leached beams is approximately 22 mm between the dissolution front of portlandite and bottom surface of the beam. The leached mortar beam was subsequently subject to displacement controlled three-point bending test. The displacement loading was applied on the center of the top surface of the beam, and the two supports on the bottom surface were 240 mm apart. The half symmetric configuration of Le Bellégo's experimental work is depicted in figure 3.6, and the element size is set to 2 mm. The element size is determined according to computational time and accuracy. The finer element size can benefit the capture of

detailed results of chemical degradation, but lead to prolonged computational time.

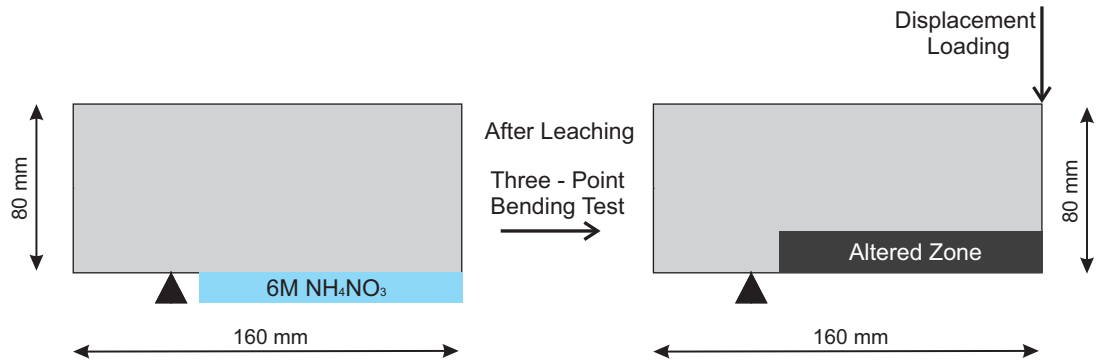

Figure 3.6: Schematic diagram of the model for the mortar beam subject to 6M NH_4NO_3 leaching and subsequently three-point bending test.

Table 3.4: The volume fractions (%) of compositions for mortar adopted in simulations of section 3.3.3

Portlandite	C-S-H (Intact)	Ettringite	Monosulphate	Unhydrated clinker	Sand	Porosity
6.45	18.6	0.94	0.06	3.95	50	20

The chemical degradation of the mortar beam leached by 6M NH_4NO_3 solution is reproduced by the reactive transport model prior to the evaluation of the residual mechanical behaviour. The paste of w/c = 0.5 [51] is extrapolated to determine the volume fractions of initial compositions for the mortar beam, as tabulated in table 3.4.

The dissolution front of portlandite is approximately 22 mm shown in figure 3.7c apart from the bottom surface of the mortar beam after for 114 days leaching, showing good agreement with the experimental results of Le Bellégo. The depth of C-S-H decalcification is slightly smaller than that of the altered zone (figure 3.7a and 3.7b), and the completely decalcified depth is 18 mm. The elastic proprieties of the intact mortar are E_o = 36.7 GPa and ν_o = 0.2, calculated by Mori-Tanaka scheme. The chemical degradation is reflected in the reduction of elastic properties of the material as discussed in section 3.3.2, which is demonstrated in figure 3.7d. The value of Young's modulus in the thoroughly leached zone plunges to approximate 6.4 GPa, representing the depletion of portlandite and complete decalcification of C-S-H. By contrast, the value is around 30 GPa in the outer contour of the leached zone, which is determined by the residual content of portladite and C-S-H (Intact). The length of

the altered zone is larger than that of the exposed zone due to the two-dimensional diffusion of aggressive ion species from NH_4NO_3 solution, and the leaching front subsequently disperses on the edge of exposed zone.

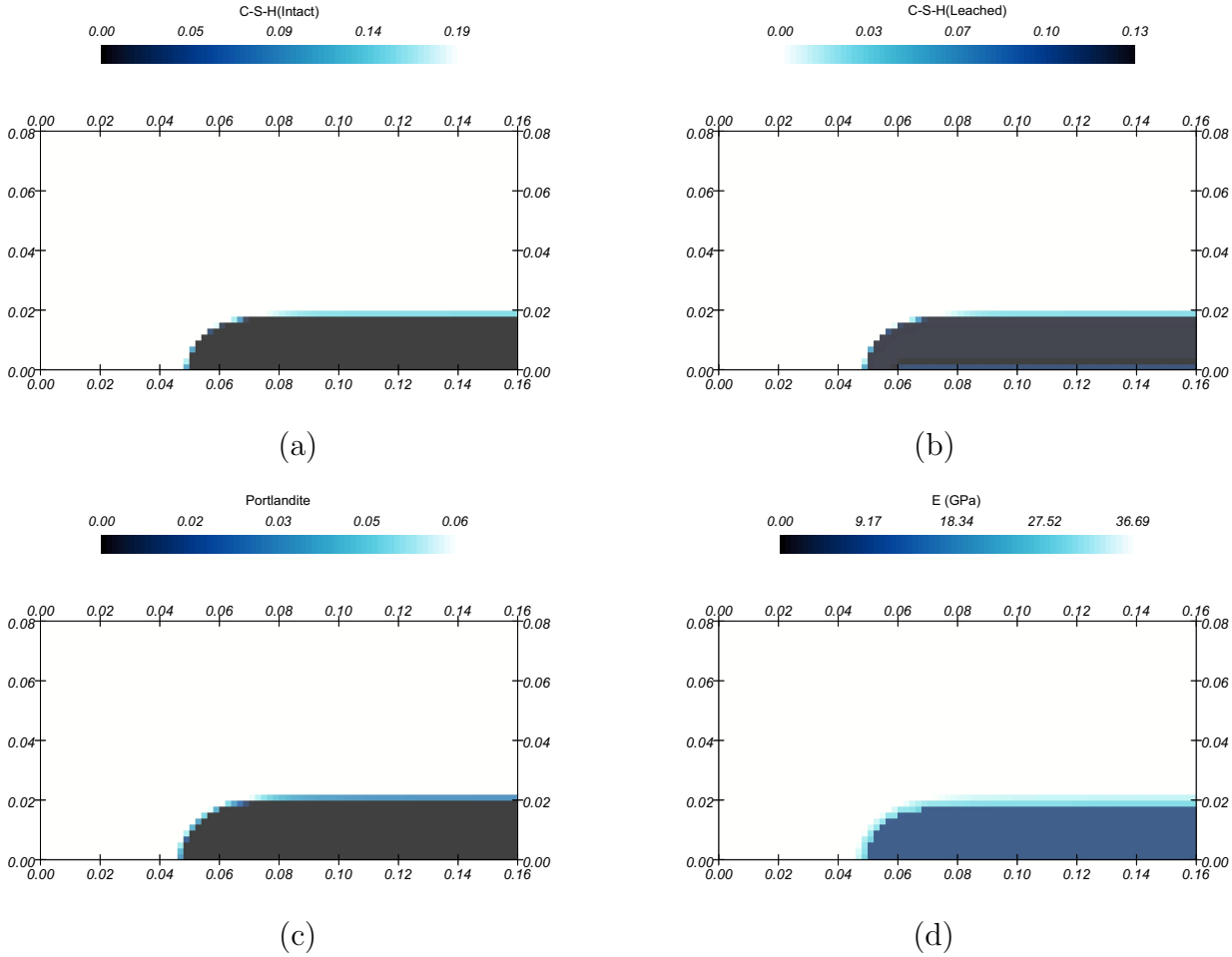

Figure 3.7: Profiles of (a) C-S-H(Intact), (b) C-S-H(Leached), (c) portlandite in volume fractions and (d) Young's modulus (GPa) for the mortar beam exposed to 6M NH_4NO_3 solution for 114 days.

The leaching with 6M NH_4NO_3 solution renders the mortar beam partially degraded as shown in figure 3.7, and the simulated outcome is employed to evaluate the three-point bending behaviour of the leached mortar beam. The elastic strain threshold of the mortar is evolving with both chemical and mechanical damage from the initial value of 1.15 $\times 10^{-4}$ as discussed in section 3.2.3. The three-point bending behaviour of the intact mortar beam is simulated and compared with Le Bellégo's experiment [25] for contrastive analysis of the leaching effect on the flexural performance.

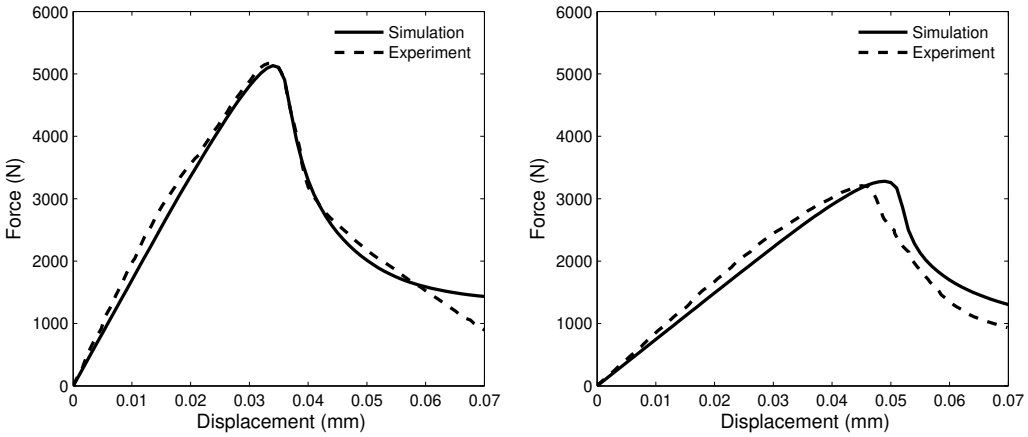

Figure 3.8: Comparison of force versus displacement curves between three-point bending simulation and experiment for (a) the intact mortar beam and (b) the one exposed to 6M NH_4NO_3 solution for 114 days.

The loading/unloading process is well simulated for the intact mortar beam (figure 3.8a), except for the slight deviation exhibited in the latter section of the unloading curve. The maximum load demonstrated in the simulation is in good agreement with the experimental result, representing that the overall stiffness of the mortar beam is evaluated precisely with the proposed method. For the mortar beam leached by 6M NH_4NO_3 solution for 114 days, the loading process of the simulation matches with the experimental curve properly (figure 3.8b), whilst the predicted maximum load is slightly overestimated leading to the similar trend in the unloading curve. This difference is considered mainly as the influence of the assumption of damage threshold evolution discussed in section 3.2.3, and the overall mechanical behaviour of the mortar beam predicted with the proposed methodology is satisfactory.

The smooth gradient of the unloading curve is attributed to the displacement-based non-local damage model, and subsequently verifies the necessity of incorporating non-local version of mechanical damage model in the simulation which is suggested by Stora et al. [17]. By contrast, a finer mesh is adopted in Stora's work, however the simulated post-peak behaviour is unsatisfactory for fitting poorly with Le Bellégo's experimental outcomes.

The study on the residual elastic properties of materials and mechanical behaviour of structural components in this section can gain insights into damage mechanisms of the leached cement-based material and build confidence to evaluate the fully coupled chemo-mechanical degradation.

3.4 The simulation of coupled chemical and mechanical degradation

The simultaneously mutual effect between chemical degradation and mechanical damage for cement-based materials exposed to the aggressive environmental conditions requires that the numerical modelling is capable of coupling the two mechanisms in the duration of the service life. The evaluation of leaching process and chemical degradation on mechanical performance in section 3.3 is incorporated as the core component in the fully coupled chemo-mechanical modelling, and performed in a staggered manner as demonstrated in figure 3.1. The present study is focusing on the coupling of chemical reactions and microcracks propagation, and the creep effect [12, 58] is not incorporated. In order to reduce the influence of creep, a small flexural displacement of 1.8 $\times 10^{-2}$ mm is adopted as suggested in the study of Stora et al. [17].

The simulation setup is to apply a prescribed displacement on the center of the top surface of the mortar beam while the central portion (200 mm $\times$ 40 mm) on the bottom surface is exposed to 6M NH_4NO_3 solution for 114 days, which is referred to as the coupled case hereinafter and demonstrated in figure 3.9. After the commencement of the coupled damage simulation, the proposed method evaluates the leaching degradation and subsequent mechanical equilibrium of the mortar beam in an eight-day cycle.

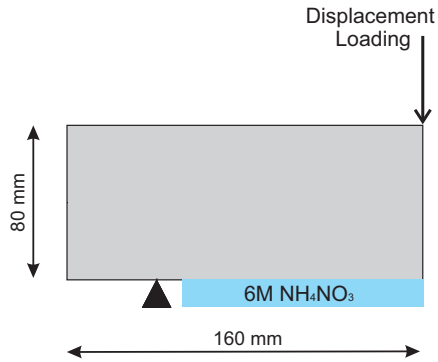

Figure 3.9: Schematic diagram of the model for the mortar beam subject to the displacement loading and 6M NH_4NO_3 leaching.

3.4.1 The coupled chemo-mechanical degradation on leached mortar beam

As the leaching process reduces the elastic properties of the beam, the static equilibrium is perturbed and causes deformation. The potential mechanical damage is subsequently evaluated by the proposed model until achieving convergence, and considered as microcracks instantaneously filling with pore solution. The propagation of microcracks occurs in mortar beam during the leaching process, and subsequently promotes chemical reactions to generate the greater degradation compared with the leaching results (figure 3.7) of the beam without displacement loading. The general patterns of the degradation for the two cases are similar, however the simulation outcomes in figure 3.10 demonstrate the effect of the coupled chemo-mechanical damage on the compositions and elastic stiffness of the material.

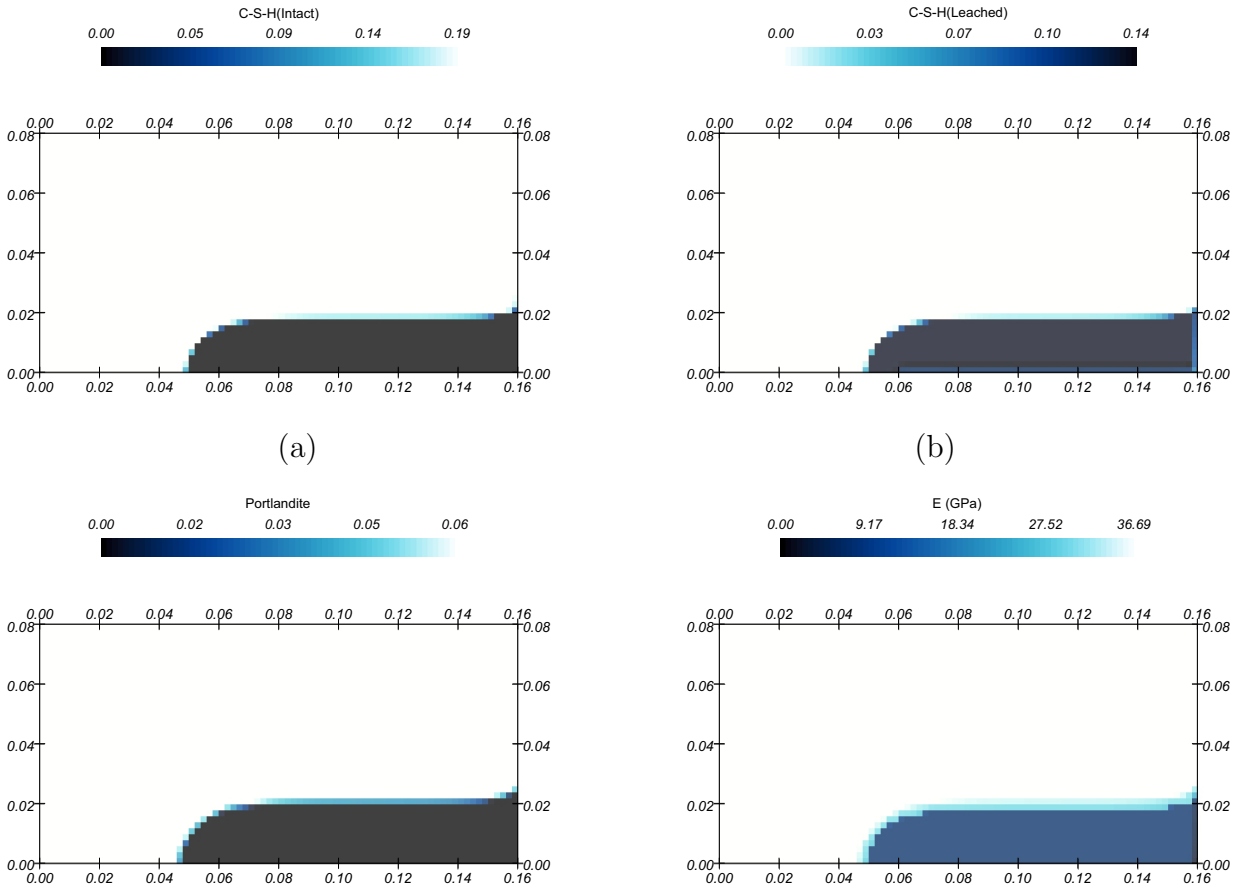

Figure 3.10: Profiles of (a) C-S-H(Intact), (b) C-S-H(Leached), (c) portlandite in volume fractions and (d) Young's modulus (GPa) of the mortar beam simultaneously subject to the imposed displacement of 1.8×10^{-2} mm and 6M NH_4NO_3 solution for 114 days.

The leaching front reaches the depth of 26 mm in figure 3.10c at the central cross section, and the corresponding depth for the depletion of portlandite is approximately 24 mm. The depth of complete C-S-H decalcification in figure 3.10a and 3.10b is 22 mm, which too occurs at the central cross section. In figure 3.10d, the residual Young's modulus reflects the same trend as the volume fractions of portlandite and C-S-H, and the profile exhibits the convex shape in the middle of the interface between the intact and degraded zone, of which the influence is discussed in section 3.4.2. In general, the degradation of the coupled case presents the localized pattern and greater damage in the vicinity of the central cross section in contrast to the chemical degradation of leaching, and the differences between the two cases are attributed to the imposed displacement which can cause mechanical damage during the leaching process.

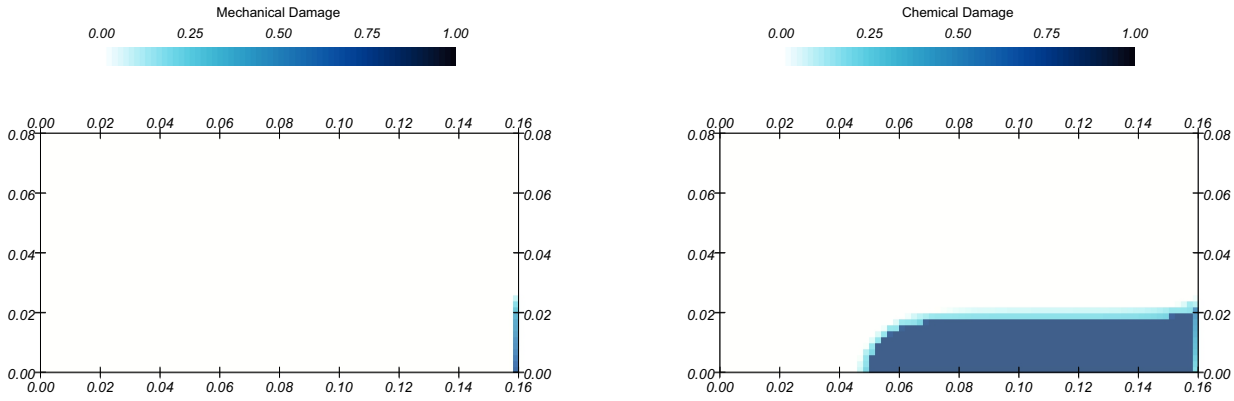

(a) (b)

Figure 3.11: Profiles of the (a) mechanical and (b) chemical damage parameters for the mortar beam simultaneously subject to the imposed displacement of 1.8×10^{-2} mm and 6M NH_4NO_3 solution for 114 days.

The damage parameter of coupled chemo-mechanical degradation is defined as the fraction of Young's modulus reduction in equation (3.27), and consists of two parameters with regard to chemical (d_c) and mechanical (d_m) damage respectively. For a beam subject to three-point bending test, the tensile strain concentrates in the lower central cross section. The leaching front propagates upwards from the bottom surface progressively weakening the elastic stiffness of the beam, and consequently exacerbates the tensile deformation. Therefore, the mechanical damage of the coupled case is accumulating at the centre of the bottom surface towards the interior as shown in figure 3.11a, and aggravates the penetration of the leaching front to generate deeper altered zone compared with the chemical degradation of leaching in figure 3.7. Since the leaching process at the central cross section is promoted by the mechanical

damage, the ion species of NH_4NO_3 solution are migrating and consumed rapidly generating the concentration gradient between the surrounding degraded zone and central cross section, which drives the leaching process towards the central portion and forms the localized pattern of degradation. In the zone of mechanical damage in figure 3.11a, the chemical degradation shown in figure 3.11b is moderated due to the mechanical damage and the consequent promotion of ion transport process, and the overall damage degree is greater than that of the surrounding zone demonstrated in figure 3.10d.

The width of damage zone in figure 3.11a is equal to the element size, since the damage just occurs in elements of the lower central cross section due to the small displacement loading. The non-local damage model can negate mesh dependence during the development of damage zone, if further displacement is applied.

In the course of the coupled chemical and mechanical damage, the front of localized degradation is progressing upwards along the central cross section causing the reduction of Young's modulus and subsequent redistribution of deformation in the area. The lower half of the middle portion of the mortar beam is zoomed in to demonstrate the variation of equivalent strain in figure 3.12a-c with time. By 40 days leaching of the coupled case in figure 3.12a, the equivalent strain of the bottom central cross section is distinctly greater than that of the neighborhood. As the leaching front progresses inwards by 80 days, the interior of the beam is undergoing stiffness reduction, and the equivalent strain subsequently spreads through the inner portion of the central cross section as shown in figure 3.12b. By the end of 114 days leaching in the coupled case, the equivalent strain of the bottom central cross section is not further decreasing significantly demonstrated in figure 3.12c, and the value is increasing steadily in the middle of the central cross section representing the continuous stiffness reduction due to the coupled chemo-mechanical damage. The comparison of the equivalent strain in the lower central cross section is demonstrated in figure 3.12e.

The corrosion depth of the surrounding zone increases with the propagation of leaching front, and the corresponding reduction of stiffness has a similar impact on the distribution of equivalent strain. After 40 days leaching in figure 3.12a, the equivalent strain is concentrated around the lower centre of the beam, as the leached zone is developing in the vicinity of bottom surface. The overall area of the leached zone is expanding with the leaching process, which means that the stiffness-degraded zone is growing and therefore the equivalent strain is increasing. In figure 3.12a-c, the equivalent strain around the lower centre of the beam is spreading gradually with

the proceeding of the coupled degradation, and radiating outward as a result of the extension of the stiffness-degraded zone along with time.

The chemical degradation of 114 days leaching on the mortar beam is demonstrated in figure 3.7, and a subsequent displacement of 1.8×10^{-2} mm is imposed on the leached beam, which is referred to as the non-coupled case hereinafter, to demonstrate the differences with the coupled case. The mechanical damage is not occurring during the displacement loading process, since the elastic strain threshold in the altered zone has increased remarkably with the significant reduction of Young's modulus by the end of 114 days leaching. Therefore, the profile of the residual stiffness in the non-coupled case is identical to that depicted in figure 3.7d, demonstrating a more uniform distribution than that of the coupled case in figure 3.10d. The deformation due to the subsequent displacement exhibits the same feature as well. In figure 3.12d, the maximum of equivalent strain in the non-coupled case occurs in the lower central cross section, and is approximately half that of the coupled case in figure 3.12c, which is attributed to the absence of mechanical damage and thus the greater residual stiffness. Correspondingly, the greater equivalent strain is observed over the neighborhood of central cross section in non-coupled case as a consequence of the uniform distribution of Young's modulus, and the overall distribution of the equivalent strain also exhibits the outgoing radiational pattern.

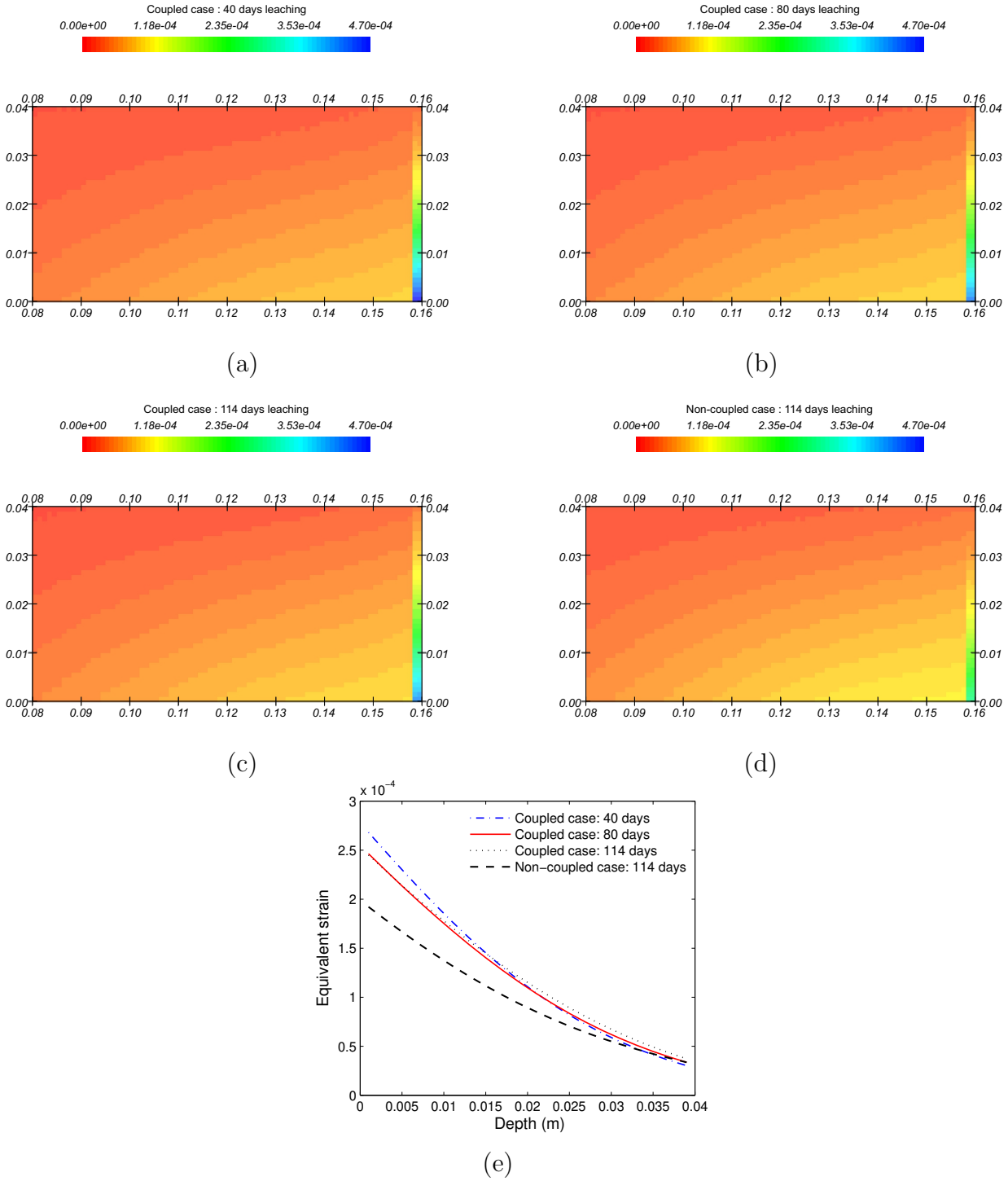

Figure 3.12: Profiles of equivalent strain of the mortar beam subject to the imposed displacement of 1.8×10^{-2} mm and 6M NH_4NO_3 solution for the coupled damage simulation of (a) 40, (b) 80, (c) 114 days and (d) non-coupled damage simulation after 114 days leaching; (e) the comparison of equivalent strain in the lower central cross section between cases.

3.4.2 The residual mechanical behaviour of mortar beams with coupled and non-coupled degradation

The mortar beam undergoing 114 days leaching was sequentially subject to an imposed displacement of 1.8 $\times 10^{-2}$ mm (non-coupled case) in section 3.4.1, which was subsequently contrasted with the beam on which the same leaching duration and imposed displacement were applied simultaneously (coupled case). The outcomes of the two cases are adopted as the starting points to evaluate the mechanical behaviour of the degraded beams with the further imposed displacement in this section. The current mechanical damage of the coupled case is shown in figure 3.11a, while no mechanical damage occurred in the non-coupled case. The subsequent propagation of damage due to the further imposed displacement is demonstrated in figure 3.13.

Based on the coupled damage of the beam in figure 3.11, the consequent mechanical damage accumulates between 20 mm and 40 mm height of the central cross section in figure 3.13a as the imposed displacement is increased to 3.5×10^{-2} mm. The mechanical damage is increased in the central cross section and extending upwards while the displacement loading reaches 4.5×10^{-2} mm in figure 3.13b, and the longitudinal propagation of damage is observed with the scope of approximate 20 mm at the height of 24 mm.

In the non-coupled case, the damage pattern is similar with that of the coupled case when the displacement of 3.5×10^{-2} mm is loaded in figure 3.13c, except for the slightly longitudinal propagation of damage at the height of around 22 mm. Subsequently, the mortar beam subject to the displacement of 4.5×10^{-2} in figure 3.13d exhibits the significant propagation of mechanical damage in both vertical and longitudinal orientation.

The convex area of the residual stiffness profile in figure 3.10d demonstrates a larger depth and greater degradation in the vicinity of central cross section compared with that of non-coupled case in figure 3.7d. Consequently, the elastic strain threshold of the convex area in the coupled case increases with the stiffness reduction, which retards the damage propagation in the test of residual mechanical behaviour. For the same reason, no further mechanical damage is formed in the lower central cross section (figure 3.13a and b) during the displacement loading process since the strain threshold increases due to the coupled damage in figure 3.11. By contrast, the interface between the intact and altered zone is flat in non-coupled case (figure 3.7), and the profile of residual Young's modulus is generally uniform. In this context, the centre of the interface has the same elastic strain threshold as the neighborhood and is subject to

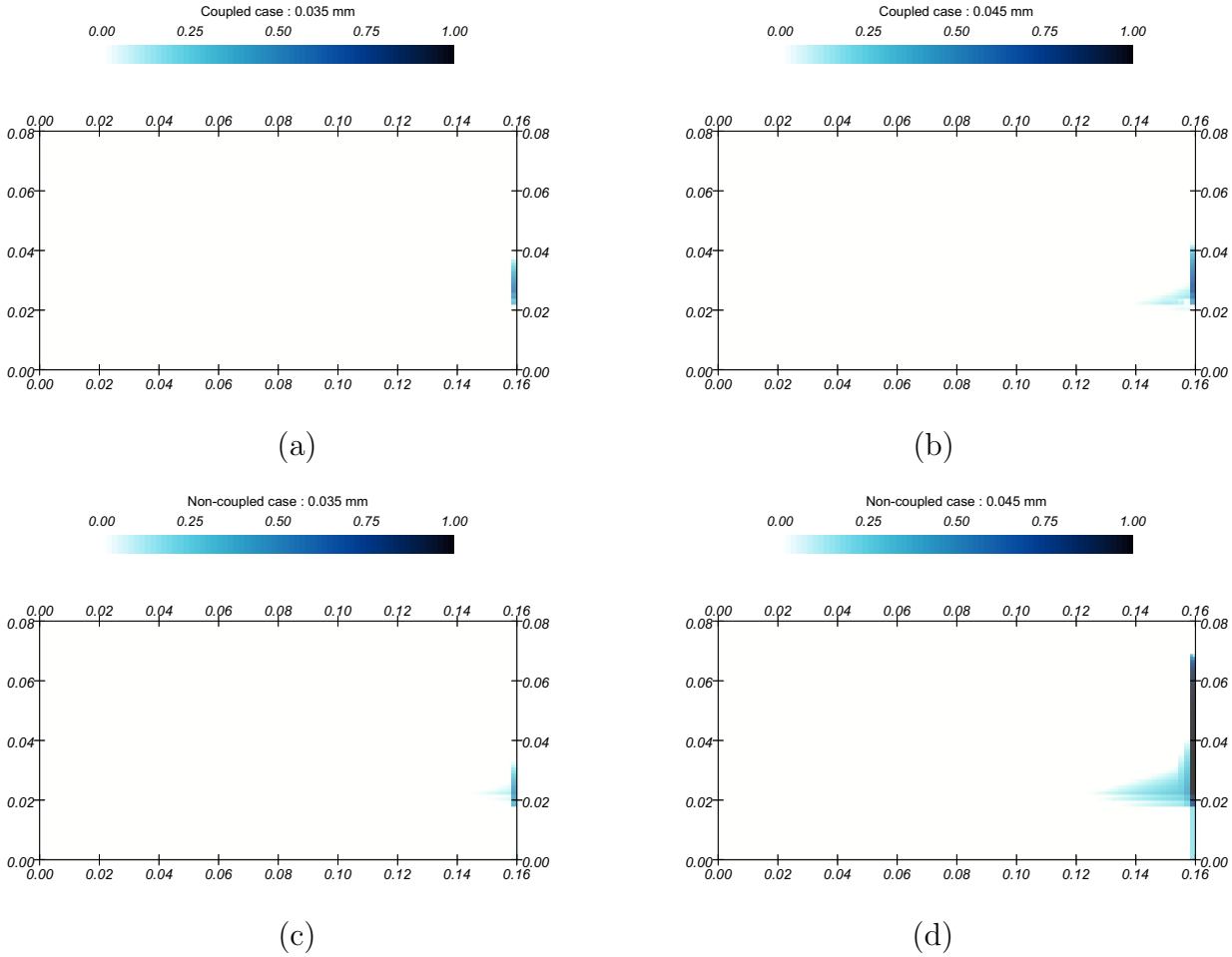

Figure 3.13: Profiles of damage parameters of the mortar beam subject to the total imposed displacement of (a) 3.5×10^{-2} mm and (b) 4.5×10^{-2} mm after the coupled degradation of a displacement of 1.8×10^{-2} mm and 6M NH_4NO_3 solution leaching for 114 days; and profiles of damage parameters of the mortar beam subject to the imposed displacement of (c) 3.5×10^{-2} mm and (d) 4.5×10^{-2} mm after 114 days leaching of 6M NH_4NO_3 solution.

larger tensile strain in the three-point bending test, which subsequently explains the prompt propagation of mechanical damage in non-coupled case in figure 3.13c and d.

According to the results above, the overall development of microcracks in the coupled case differs from that in non-coupled case. It is noteworthy that the greater degradation occurred in the convex area in the simulation of coupled chemo-mechanical degradation, and can restrain the damage propagation in reloading stage in contrast to the non-coupled case. In the work of Stora [17], the accumulation of microcracks in fully coupled degradation is captured at central cross section, however the profile of residual constituents (e.g. portlandite) is approximately the same as that in non-coupled degradation representing the incompleteness of promoting chemical degradation, which subsequently leads to the absence of damage alleviation in reloading

test.

3.5 Conclusions

In the present work, the coupled chemo-mechanical degradation model is proposed for cement-based materials submitted to aggressive aqueous solution and external loads. The accommodation of the reactive transport model and displacement based non-local damage model enables the proposed method to simulate the process of aquatic chemistry and propagation of microcracks separately. The coupling scheme is developed with regard to porosity and elastic moduli based on the principles of the two models.

The reactive transport model is able to evaluate the complex chemical degradation, such as portlandite dissolution and C-S-H decalcification, which are recognized as the main sources of the stiffness reduction for cement-based material. The volume fractions of solid phases are subsequently updated after the chemical reactions, and the residual elastic moduli are evaluated in homogenization approach based on the Mori-Tanaka scheme. The chemically induced stiffness reduction is moderate due to the prompt dissolution of portlandite until depletion, and subsequently the decalcification of C-S-H leads to a plunge of Young's modulus. The validation of existing experimental data demonstrates that the proposed method is able to capture the impacts of chemical degradation on the mechanical properties of cement-based materials.

The three-point bending simulations are performed on mortar beam subject to 6M NH_4NO_3 solution for 114 days in coupled and non-coupled cases. By contrast to previous study of Stora et al. [17], the incorporation of non-local damage model is indispensable to capture the post-peak behaviour and coupled degradation of the beam. In the coupled case, the degradation profiles exhibit the localized pattern as a result of mechanical damage at the central cross section of the beam, which demonstrates that the proposed method is feasible to feed back the mechanical damage to the process of chemical degradation. The profiles of the equivalent strain in coupled case demonstrate the detailed evolution with time and features missed in non-coupled case. The residual flexural behaviour of the beam is further tested, and the pattern of damage propagation exhibits significant differences. The mechanical damage occurred during the coupled degradation process can aggravate the penetration of the leaching front and cause additional damage by contrast with the non-couple case, which

consequently softens the damage prone area and retards mechanical degradation for the subsequent displacement loading.

The differences between the coupled and non-coupled case are remarkable under the same chemical and mechanical boundary conditions, and suggest the significance of coupling chemical and mechanical degradation for investigating the durability of cement-based materials. The proposed coupled chemo-mechanical degradation modelling accommodates the variation and effect of the material constituents on microscale and the structural behaviour on macroscale, and is a practical technique for assessment of the chemo-mechanical degradation related infrastructures in the framework of service reliable and durable engineering materials.

References

[1] Marcin Koniorczyk, Dariusz Gawin, and Bernhard A. Schrefler. Multiphysics model for spalling prediction of brick due to in-pore salt crystallization. *Computers & Structures*, 196:233 – 245, 2018.

[2] S.T. Yang, K.F. Li, and C.Q. Li. Numerical determination of concrete crack width for corrosion-affected concrete structures. *Computers & Structures*, 207:75 – 82, 2018.

[3] S. Biswal, D.H. Reddy, and A. Ramaswamy. Reducing uncertainties in estimating long-time prestress losses in concrete structures using a hygro-thermo-chemo-mechanical model for concrete. *Computers & Structures*, 211:1 – 13, 2019.

[4] H. F. W. Taylor. *Cement chemistry.* Thomas Telford, London, second edition, 1997.

[5] B. Gérard. Contribution des couplages mécanique-chimie-transfert dans la tenue a long terme des ouvrages de stockage de déchets radioactifs. *PhD Thesis, Laboratoire de Méchanique et Technologie, E.N.S. de Cachan, in French*, 1996.

[6] A. Delagrave, B. Gérard, and J. Marchand. *Modelling the calcium leaching mechanisms in hydrated cement pastes.* In: K. Scrivener, J. Young (Eds.), Mechanics of Chemical Degradation of Cement-Based Systems. Chapman & Hall, London, pp. 30—37, 1997.

[7] G. Pijaudier-Cabot, B. Gérard, and L. Molez. *Damage mechanics of concrete structures subjected to mechanical and environmental actions.* In: R. de Borst, N. Bićanić, H. Mang, G. Meschke (Eds.), Computational Modelling of Concrete Structures. Balkema, Rotterdam, pp. 559-–566, 1998a.

[8] G. Pijaudier-Cabot, B. Gérard, N. Burlion, and L. Molez. *Localisation of damage in quasi-brittle materials and influence of chemically activated damage.* In: R. de Borst, E. van der Giessen (Eds.), Material Instabilities in Solids. John Wiley & Sons, Chicester, pp. 441-–456, 1998b.

[9] Caroline Le Bellégo, B. Gérard, and G. Pijaudier-Cabot. Chemo-mechanical effects in mortar beams subjected to water hydrolysis. *Journal of Engineering Mechanics*, 126(3):266–272, 2000.

[10] V.H. Nguyen, B. Nedjar, and J.M. Torrenti. Chemo-mechanical coupling behaviour of leached concrete: Part ii: Modelling. *Nuclear Engineering and Design*, 237(20):2090 – 2097, 2007.

[11] Detlef Kuhl, Falko Bangert, and Günther Meschke. Coupled chemo-mechanical deterioration of cementitious materials. part I: Modeling. *International Journal of Solids and Structures*, 41(1):15–40, 2004.

[12] Dawei Hu, Hui Zhou, Fan Zhang, and Jianfu Shao. Modeling of short- and long-term chemomechanical coupling behavior of cement-based materials. *Journal of Engineering Mechanics*, 140(1):206 – 218, 2014.

[13] Rossella Pignatelli, Claudia Comi, and Paulo J.M. Monteiro. A coupled mechanical and chemical damage model for concrete affected by alkali–silica reaction. *Cement and Concrete Research*, 53:196 – 210, 2013.

[14] Nicola Cefis and Claudia Comi. Chemo-mechanical modelling of the external sulfate attack in concrete. *Cement and Concrete Research*, 93:57 – 70, 2017.

[15] William M. White. *Geochemistry*. John Wiley & Sons, Ltd., 2013.

[16] Bruno M. Huet, Jean H. Prévost, and George W. Scherer. Quantitative reactive transport modeling of portland cement in CO_2-saturated water. *International Journal of Greenhouse Gas Control*, 4(3):561 – 574, 2010.

[17] E. Stora, B. Bary, Q.-C. He, E. Deville, and P. Montarnal. Modelling and simulations of the chemo-mechanical behaviour of leached cement-based materials: Interactions between damage and leaching. *Cement and Concrete Research*, 40(8):1226 – 1236, 2010.

[18] Anthony Soive and Van Quan Tran. External sulfate attack of cementitious materials: New insights gained through numerical modeling including dissolution/precipitation kinetics and surface complexation. *Cement and Concrete Composites*, 83:263 – 272, 2017.

[19] Fabien Georget, Jean H. Prévost, and Bruno Huet. Reactive transport modelling of cement paste leaching in brines. *Cement and Concrete Research*, 111:183 – 196, 2018.

[20] Franz H. Heukamp. *Chemomechanics of Calcium Leaching of Cement-Based Materials at Different Scales: The Role of CH-Dissolution and C-S-H-Degradation*

on Strength and Durability Performance of Materials and Structures. PhD Thesis, MIT, 2002.

[21] T Mori and K Tanaka. Average stress in matrix and average elastic energy of materials with misfitting inclusions. *Acta Metallurgica*, 21(5):571 – 574, 1973.

[22] Eveline Herve and Andre Zaoui. n-Layered inclusion-based micromechanical modelling. *International Journal of Engineering Science*, 31(1):1 – 10, 1993.

[23] E. Stora, B. Bary, Q.-C. He, E. Deville, and P. Montarnal. Modelling and simulations of the chemo–mechanical behaviour of leached cement-based materials: Leaching process and induced loss of stiffness. *Cement and Concrete Research*, 39(9):763 – 772, 2009.

[24] Q.-S. Zheng and D.-X. Du. An explicit and universally applicable estimate for the effective properties of multiphase composites which accounts for inclusion distribution. *Journal of the Mechanics and Physics of Solids*, 49(11):2765 – 2788, 2001.

[25] Caroline Le Bellégo. *Couplages chimie - mécanique dans les structures en béton attaquées par l'eau: Estude expérimentale et analyse numérique*. PhD Thesis, ENS Cachan, France, 2001 (in French).

[26] Caroline Le Bellégo, B. Gérard, and G. Pijaudier-Cabot. Coupled mechanical and chemical damage in calcium leached cementitious structures. *Journal of Engineering Mechanics*, 129(3):333 – 341, 2003.

[27] Tianfu Xu, Eric Sonnenthal, Nicolas Spycher, and Karsten Pruess. *TOUGHREACT: A new code of the TOUGH family of nonisothermal multiphase reactive geochemical transport in variably saturated geologic media*. Lawrence Berkeley National Laboratory, Berkeley, California, 2003.

[28] Gilles Pijaudier-Cabot and Zdeněk P. Bažant. Nonlocal damage theory. *Journal of Engineering Mechanics*, 113(10):1512–1533, 1987.

[29] R. H. J. Peerlings, R. De Borst, W. A. M. Brekelmans, and J. H. P. De Vree. Gradient enhanced damage for quasi-brittle materials. *International Journal for Numerical Methods in Engineering*, 39(19):3391–3403, 1996.

[30] Antonio Rodríguez-Ferran, Irene Morata, and Antonio Huerta. A new damage model based on non-local displacements. *International Journal for Numerical and Analytical Methods in Geomechanics*, 29(5):473–493, 2005.

[31] M. Jirásek and S. Marfia. Non-local damage model based on displacement averaging. *International Journal for Numerical Methods in Engineering*, 63(1):77–102, 2005.

[32] Terry Bennett and Sivakumar Kulasegaram. On the use of a damage model based on non-local displacements in the element-free galerkin method. In C. A. Motasoares, J. A. C. Martins, H. C. Rodrigues, Jorge A. C. Ambrósio, C. A. B. Pina, C. M. Motasoares, E. B. R. Pereira, and J. Folgado, editors, *III European Conference on Computational Mechanics*, page 362. Springer Netherlands, 2006.

[33] Zhongcun Zuo and Terry Bennett. Simulation of the degradation of oilwell cement for the prediction of long-term performance. *Construction and Building Materials*, 202:669 – 680, 2019.

[34] Edward N. Matteo and George W. Scherer. Experimental study of the diffusion-controlled acid degradation of Class H Portland cement. *International Journal of Greenhouse Gas Control*, 7:181 – 191, 2012.

[35] R. J. Millington and J. P. Quirk. Permeability of porous solids. *Transactions of the Faraday Society*, 57:1200 – 1207, 1961.

[36] Antonio C. Lasaga, Josep M. Soler, Jiwchar Ganor, Timothy E. Burch, and Kathryn L. Nagy. Chemical weathering rate laws and global geochemical cycles. *Geochimica et Cosmochimica Acta*, 58(10):2361 – 2386, 1994.

[37] René de Borst, Mike A. Crisfield, Joris J. C. Remmers, and Clemens V. Verhoosel. *Non-Linear Finite Element Analysis of Solids and Structures*. John Wiley & Sons, Ltd, 2012.

[38] J.C. Simo and J.W. Ju. Strain- and stress-based continuum damage models. *International Journal of Solids and Structures*, 23(7):821 – 869, 1987.

[39] J. Mazars and G. Pijaudier-Cabot. Continuum damage theory - application to concrete. *ASCE Journal of Engineering Mechanics*, 115:345–365, 1989.

[40] Georgios Constantinides. *The elastic properties of calcium leached cement pastes and mortars: A multi-scale investigation*. MSc Thesis, MIT, 2002.

[41] F. H. Heukamp, F.-J. Ulm, and J. T. Germaine. Does calcium leaching increase ductility of cementitious materials? Evidence from direct tensile tests. *Journal of Materials in Civil Engineering*, 17(3):307–312, 2005.

[42] C. Gallé, H. Peycelon, and P. Le Bescop. Effect of an accelerated chemical degradation on water permeability and pore structure of cementbased materials. *Advances in Cement Research*, 16(3):105–114, 2004.

[43] Lazar M. Kachanov. Rupture time under creep conditions. *International Journal of Fracture*, 97(1):11–18, Apr 1999.

[44] U. Schneider and S.-W. Chen. The chemomechanical effect and the mechanochemical effect on high-performance concrete subjected to stress corrosion. *Cement and Concrete Research*, 28(4):509 – 522, 1998.

[45] U. Schneider and S.-W. Chen. Deterioration of high-performance concrete subjected to attack by the combination of ammonium nitrate solution and flexure stress. *Cement and Concrete Research*, 35(9):1705 – 1713, 2005.

[46] F. Agostini, Z. Lafhaj, F. Skoczylas, and H. Loodsveldt. Experimental study of accelerated leaching on hollow cylinders of mortar. *Cement and Concrete Research*, 37(1):71 – 78, 2007.

[47] A.W Harris, M.C Manning, W.M Tearle, and C.J Tweed. Testing of models of the dissolution of cements—leaching of synthetic CSH gels. *Cement and Concrete Research*, 32(5):731 – 746, 2002.

[48] U.R. Berner. Modelling the incongruent dissolution of hydrated cement minerals. *Radiochimica Acta*, 44(45):387 – 393, 1988.

[49] Ana Trapote-Barrreira. *Dissolution kinetics of C-S-H gel and durability of mortar*. PhD Thesis, Universitat Politècnica de Catalunya (UPC), Spain, 2015.

[50] Thomas J. Wolery. EQ3/6, A software package for geochemical modeling of aqueous systems: package overview and installation guide. *Lawrence Livermoer Laboratory, Berkeley, California*, 1992.

[51] E. Stora, Q.-C. He, and B. Bary. Influence of inclusion shapes on the effective linear elastic properties of hardened cement pastes. *Cement and Concrete Research*, 36(7):1330 – 1344, 2006.

[52] F. Adenot and M. Buil. Modelling of the corrosion of the cement paste by deionized water. *Cement and Concrete Research*, 22(2):489 – 496, 1992.

[53] Marc Mainguy, Claire Tognazzi, Jean Michel Torrenti, and Frédéric Adenot. Modelling of leaching in pure cement paste and mortar. *Cement and Concrete Research*, 30(1):83 – 90, 2000.

[54] Georgios Constantinides and Franz-Josef Ulm. The effect of two types of C-S-H on the elasticity of cement-based materials: Results from nanoindentation and micromechanical modeling. *Cement and Concrete Research*, 34(1):67 – 80, 2004.

[55] Paulo J.M. Monteiro and C.T. Chang. The elastic moduli of calcium hydroxide. *Cement and Concrete Research*, 25(8):1605 – 1609, 1995.

[56] A. Boumiz, D. Sorrentino, C. Vernet, and F. Cohen Tenoudji. *Modelling the development of the elastic moduli as a function of the degree of hydration of cement pastes and mortars.* In: A. Nonat (Ed.), Proceedings 13 of The 2nd RILEM Workshop on Hydration and Setting, Dijon, France, 1997.

[57] N. P. Daphalapurkar, F. Wang, B. Fu, H. Lu, and R. Komanduri. Determination of mechanical properties of sand grains by nanoindentation. *Experimental Mechanics*, 51(5):719–728, Jun 2011.

[58] Thomas de Larrard, Farid Benboudjema, Jean-Baptiste Colliat, Jean-Michel Torrenti, and Frédéric Deleruyelle. Uncertainty propagation on damage evolution of a concrete structure subjected to coupled leaching and creep. *European Journal of Environmental and Civil Engineering*, 14(6-7):891–921, 2010.

Chapter 4

The chemo-mechanical effect of carbonation

In this chapter, the study of chemo-mechanical effect of carbonation is presented as a manuscript which is

Zhongcun Zuo and Terry Bennett : The chemo-mechanical effect of calcium carbonate precipitation for cement-based materials exposed to carbonated brine, *Cement and Concrete Research* (ready for submission).

Statement of Authorship

Title of Paper	The chemo-mechanical effect of calcium carbonate precipitation for cement-based materials exposed to carbonated brine
Publication Status	☐ Published ☐ Accepted for Publication ☐ Submitted for Publication ☑ Unpublished and Unsubmitted work written in manuscript style
Publication Details	Zhongcun Zuo & Terry Bennett (2020). The chemo-mechanical effect of calcium carbonate precipitation for cement-based materials exposed to carbonated brine, Cement and Concrete Research (ready for submission).

Principal Author

Name of Principal Author (Candidate)	Zhongcun Zuo
Contribution to the Paper	Undertook literature review, determined research theme, developed the theoretical proof for numerical modelling, performed simulations and interpretation of results, and wrote the manuscript.
Overall percentage (%)	75%
Certification:	This paper reports on original research I conducted during the period of my Higher Degree by Research candidature and is not subject to any obligations or contractual agreements with a third party that would constrain its inclusion in this thesis. I am the primary author of this paper.
Signature	Date 20/1/2020

Co-Author Contributions

By signing the Statement of Authorship, each author certifies that:

i. the candidate's stated contribution to the publication is accurate (as detailed above);

ii. permission is granted for the candidate in include the publication in the thesis; and

iii. the sum of all co-author contributions is equal to 100% less the candidate's stated contribution.

Name of Co-Author	Terry Bennett
Contribution to the Paper	Supervised the selection of research theme, helped with data analysis, and revised the manuscript.
Signature	Date 20/1/2020

The chemo-mechanical effect of calcium carbonate precipitation for cement-based materials exposed to carbonated brine

Abstract

Cement-based material is significantly transformed with exposure to carbonated brine, and calcium carbonate is the product exerting chemical and mechanical influences on the material. The presence of magnesium in cement leaching system is demonstrated to be crucial in the process of chemical reactions with existing experimental outcomes and numerical simulation, which protects cement from degradation by sealing the surface. In absence of magnesium, the concentration of dissolved CO_2 dominates the degradation rate by the pore-clogging effect of the calcium carbonate layer. The interplay of pH and CO_2 concentration leads to the shifting calcium carbonate layer due to mechanisms of dissolution and re-precipitation. Based on a micromechanical model, the precipitated calcium carbonate is incorporated with leached cement paste to evaluate the residual elastic moduli. Numerical analyses of cement paste beam exposed to carbonate brine exhibit that the shifting carbonate layer indicates the completely decalcified zone which influences the overall flexural behaviour.

Keywords : $CaCO_3$; Degradation; Durability; Elastic Moduli; Microstructure.

4.1 Introduction

The precipitation of calcium carbonate ($CaCO_3$) is observed in cement-based materials in contact with solutions rich in carbonate ions [1]. In terms of industrial applications, the presence of $CaCO_3$ plays an influential role in infrastructures as a beneficial mechanism for carbon capture and storage [2, 3], geological disposal facility [4] and remediation of cement and concrete [5–7]. Therefore, the understanding of fundamental mechanisms of calcium carbonate precipitation (CCP) and subsequent chemo-mechanical effects on cement-based materials is crucial to gain insights into the serviceability of the aforementioned applications.

The process of CCP is complex and volatile due to the influence of ion species in the reactive environment, therefore the stable polymorph of $CaCO_3$ is not straightforwardly achieved. It has been recognized that magnesium ions can have an stabilizing effect on CCP in chemical mechanisms, which is discussed detailedly in the following section. However, the effect of Mg ions has not been thoroughly highlighted in carbonation related studies of cement-based materials, and subsequently the interpretation of experimental outcomes is insufficient to cover involved mechanisms, which can lead to the difficulty in reproducing conclusions of existing studies. In addition, the pore-clogging effect of CCP is a crucial feature in carbonation of cement-based materials, and the formation of $CaCO_3$ in the matrix can serve as both a barrier protecting the interior intact and a reinforcement strengthening the degraded cement materials in terms of elastic moduli. The chemical and mechanical effects of CCP on the overall performance of cement-based materials remain to be further investigated, and the integrated methodology of reactive transport, micromechanics and non-local damage model is presented in this study.

4.1.1 Mechanisms of CCP

The crystallization pathway of $CaCO_3$ is not straightforward, and differs significantly determined by the compositions of the reactive solution.

The amorphous calcium carbonate (ACC), transforming to the crystalline $CaCO_3$ as a precursor [8–10], occurs in modern precipitation environments with the chemical formula documented as $CaCO_3{\cdot}nH_2O$ (n = 1:1.6) [11], and its formation can be described with the chemical formula [12]

$$CaCO_3 \cdot nH_2O = Ca^{2+} + CO_3^{2-} + nH_2O \tag{4.1}$$

Rodriguez-Blanco et al. [13] demonstrated that the transformation of ACC into crystalline $CaCO_3$ is affected by the initial pH of the aqueous solution. Specifically, calcite was observed as a result of the direct transformation of ACC in a neutral solution. By contrast to the case of a high pH solution, the crystallization pathway involves two mechanisms [14]: i) ACC dehydrates to form crystalline vaterite rapidly; ii) the vaterite dissolves and reprecipitates to form calcite. The reaction rate of the latter mechanism is dominated by the reactive surface area of calcite, and approximately one magnitude less than that of the former one. Purgstaller et al. [15] carried out experiment with a magnesium free solution, and likewise demonstrated that ACC transformed into calcite via a precursor – vaterite.

For the aqueous solution carrying Mg ions, Loste et al. [8] demonstrated that ACC is the first phase precipitated in all experimental cases. The experiment with the presence of magnesium ions (Mg/Ca ratio = 1:9) in the reactive solution [13] demonstrated that Mg^{2+} improved the stability of ACC, and subsequently increased the induction time of ACC crystallization by one order of magnitude without the formation of vaterite in contrast with the magnesium free system. The high dehydration energy of Mg^{2+} compared to Ca^{2+} kinetically inhibits crystallizing process [16, 17], which subsequently stabilizes ACC and reduces its solubility. The growth of calcite is favored and the crystallization of vaterite is limited, due to stabilized ACC decreasing the supersaturation level of the reactive solution [13].

In the subsequent experimental studies [18–20] focusing on the fundamental mechanism of the interaction between Mg and ACC, the incorporation of Mg in ACC is reported, which results in the formation of amorphous calcium magnesium carbonate (ACMC) and its transformation to crystalline Mg enriched calcite (Mg-calcite). Purgstaller et al. [15] performed experiments with reactive solutions of different Mg/Ca ratios, and revealed two distinctive pathways for the formation of crystalline $CaCO_3$. In the case of reactive solution with an initial Mg/Ca ratio of 1:8, the formation of crystalline Mg-calcite, which contains approximate 8 mol% Mg, occurred from reactive solution directly without the ACMC precursor phase. In the cases of solutions with initial Mg/Ca molar ratios (1:4, 1:5 and 1:6), ACMC precipitated and served as a precursor for the transformation to Mg-calcite with up to 20 mol% Mg, while the stabiltiy of ACMC is improved with the increasing Mg/Ca ratio. In the solution with Mg/Ca ratio ≥ 4 [21–23], the high-magnesium calcite was formed via a precursor amorphous phase. Meanwhile, the precipitation of aragonite from the high Mg/Ca ratio solution was observed [21], which is attribute to the denser structure

of aragonite avoiding the incorporation of partially dehydrated Mg^{2+} and consequent inhibition of aragonite growth.

Therefore, the formation of ACMC occurs in the solution with Mg/Ca ratio $\geq$ 1:8 according to the existing experimental outcomes, and its chemical formula is described as [12]

$$Ca_{1-x}Mg_xCO_3 \cdot nH_2O = (1-x)Ca^{2+} + xMg^{2+} + CO_3^{2-} + nH_2O \tag{4.2}$$

where x can be larger than 0.88 and n is variable. In this context, ACMC acts as an energetically favorable pathway for the crystallization of Mg-calcite, and its formation is of particular interest for the study of the precipitation of $CaCO_3$-like phases. The stability of ACMC is improved by the strong bond between magnesium ions and structural water which enhances the activation energy relevant to dehydration [24]. Purgstaller et al. [25] consequently investigated the solubility product of the synthesized ACMC, and gained an insight into the governing factors of ACMC solubility.

ACMC is a special morphology product of CCP with the presence of Mg^{2+} in the reactive solution, of which the effect is discussed in section 4.2.

4.1.2 The chemo-mechanical effect of CCP on cement-based materials

For a Portland cement-based system, CCP occurs with other chemical reactions, since the presence of water is necessary and can subsequently initiate the complex process of chemical degradation. The leaching on the material by the percolating solution causes a series of chemical reactions, and portlandite is the first dissolved phase in the material [1]. Calcium silicate hydrate (C-S-H) in Portland cement-based materials, serving as the primary bonding phase, is amorphous and nonstoichiometric colloidal, and described as the gel with an average Ca/Si molar ratio in the scope of approximate 0.8 to 1.75 [26, 27]. Berner [28] formulated a model accommodating the incongruent dissolution based on thermodynamic considerations, and related the incongruent solubility with the Ca/Si molar ratio of C-S-H gels. After the dissolution of portlandite, C-S-H starts to dissolve incongruently presenting the release of calcium ions and formation of C-S-H with lower Ca/Si ratio, which is referred to as the decalcification of C-S-H.

The portlandite dissolution and C-S-H decalcification can create voids and destruct the microstructure of the porous cement matrix, which subsequently results

in changes in the shielding capacity of the material [29, 30]. The significant loss of mechanical properties for cement-based materials undergoing chemical degradation has been long recognized [31, 32], and the decalcification of C-S-H is demonstrated as the primary cause of the macroscopic elasticity reduction [33].

The carbonation of cement-based materials exposed to CO_2 saturated solution have been conducted with the same setup in experiments [34–36]. The microstructure of carbonated materials, which is related to mechanical properties, is concluded as the mixture of $CaCO_3$ and decalcified C-S-H without evident order [34]. The Young's modulus of carbonated specimens is reported to be approximately that of intact material in the experiment [36], which differs from experimental outcomes [31, 32]. Therefore, CCP in these experiments demonstrates the enhancement effect in elastic properties of cement-based materials that undergo portlandite dissolution and C-S-H decalcification. The presence of $CaCO_3$ likewise strengthens specimens of the atmospheric carbonation case in experiments [36, 37].

4.1.3 Scope and aim

The precipitation of $CaCO_3$ in the interior of cement-based materials can result in reducing or even blocking the pore space [38], and the formation of $CaCO_3$ layer is suggested to significantly retard the chemical degradation by sealing cement matrix [39, 40]. Rimmelé et al. [41] report that $CaCO_3$ precipitates at the vicinity of reaction front and subsequently dissolves, which leads to remarkable variation of porosity especially for cement exposed to CO_2 saturated solution. The $CaCO_3$ layer occurs adjacent to the reaction front, and the dissolution of $CaCO_3$ layer dominates the rate of cement degradation in the experiment [42]. The laboratory experiments [43, 44] demonstrate that the formation of a $CaCO_3$ layer within cement matrix can reduce the porosity and is subsequently related to the alleviation of the chemical degradation.

Dow and Glasser [45] investigated a surface layer of $CaCO_3$ on the interface of carbonate rich solution and cement-based materials. Schwotzer et al. [46] proposed that the $CaCO_3$ layer, which is deposited on the surface of cement materials in contact with carbonated hard water, prevents the cement matrix from leaching process. In this case, the reactants (calcium and carbonate ions) are provided by the water rather than the pore solution, so that the formation of $CaCO_3$ cannot really affect the chemical equilibrium in pore solution and cause subsequent reactions within cement matrix. Matteo et al. [3] performed flow-through experiments of cement paste with solution carrying both calcium and carbonate ions, and demonstrated the sealing

effect of $CaCO_3$ layer on cement paste. However, the $CaCO_3$ layer formed in the interior of cement matrix rather than the water/cement interface, and the reaction zone of cement paste in the experiment was recorded, which seems to contradict the conclusion of Schwotzer et al. and implies two different mechanisms of $CaCO_3$ layer occurring in the two experimental studies separately.

In the present work, the formation of $CaCO_3$ layer for cement-based materials exposed to solutions with different compositions is investigated based on fundamental mechanisms of CCP, and the interpretation of divergences presented in the aforementioned experimental observations [3, 46] is subsequently attempted to demonstrate the influence of Mg on the precipitation of $CaCO_3$-like phases. The simultaneous dissolution and precipitation of solid phases in cement-based materials are evaluated by reactive transport model [47] to reproduce the complex chemical reactions in contact with carbonated brine, and the volume fractions of cement constituents are subsequently obtained to calculate the elastic moduli of the material by the Mori-Tanaka micromechanical model [48] for the assessment of the residual mechanical properties. The chemo-mechanical evaluation of cement-based materials subject to carbonated brine is further applied on a cement beam, and the four-point bending test is simulated to evaluate the impact of dissolution/precipitation on the flexural behaviour of the beam.

The sealing layer on the interface between cement paste and Mg rich solution is investigated according to the latest experimental data of ACMC solubility in section 4.2, which is verified with the experiment [46]. The $CaCO_3$ layer formed in cement is simulated with carbonated brine of different concentrations and validated with the experiment [3] in section 4.3, and the subsequent impact on elastic moduli is evaluated by Mori-Tanaka scheme. Based on the residual stiffness after chemical reactions, the flexural behaviour of a cement paste beam subject to carbonated brine is demonstrated with numerical modelling in section 4.4.

4.2 The formation of ACMC in cement-based materials

The incorporation of Mg into ACC is recognized to play a crucial role in the stabilization of the amorphous phase by preventing the dehydration of ACC (section 4.1.1). The solubility of ACMC is related with the energetically favorable pathway

of the crystalline minerals, such as Mg-calcite and disordered dolomite, and the solubility product of ACMC is studied as a function of the Mg content in the amorphous phase [25]. In this section, the formation of ACMC in contact with Mg rich leaching solution is discussed on the basis of existing experimental phenomena, and investigated by numerical modelling with the latest experimental data, which sheds light on a crucial mechanism related to the carbonation of cement-based materials.

4.2.1 The interpretation of experiments

In the study of Schwotzer et al. [46], the hard tap water was adopted as leaching solution for the carbonation experiments of cement paste. The experimental system was open to atmosphere allowing the uptake of CO_2, and two exposure conditions were performed to present the different availability of carbonate ions on the interface between cement paste and leaching solution.

Following a two-day exposure to hard tap water in the experiment, a dense layer of carbonate was recorded on the surface of cement paste, and the solid phases and total porosity of cement paste did not change significantly up to ten-day exposure under both conditions. In order to demonstrate the effect of chemical compositions in leaching solution, the same experimental methods and procedures were performed with demineralized water in contrast tests, which demonstrated the dissolution of portlandite and precipitation of $CaCO_3$ within the material. The chemical compositions of the two types of water are tabulated in table 4.1.

Table 4.1: The chemical compositions of aqueous solutions in experiments [46].

Type of water	Ca	Mg	Na	K	Cl	N	S	pH
	mg/L	mg/L	mg/L	mg/L	mg/L	mg/L	mg/L	-
Hard tap water	89.1	10.8	17	3.2	30	1.8	56.7	7.5
Demineralized water	<0.01	<0.01	<0.01	<0.01	<0.01	<0.01	<0.03	6.0

In the case of hard tap water, the surface layer and approximately intact cement matrix imply that hard tap water can supply the reactants of the carbonate product, which exhibits a thoroughly sealing and protective effect for cement-based materials. By contrast, the demineralized water, which carries HCO_3^- by achieving the equilibrium with atmospheric CO_2 (equation (4.3)), causes chemical reactions within cement matrix, and the subsequently released Ca^{2+} reacts with the diffused HCO_3^- precipitating $CaCO_3$ (equation (4.4)) in the interior of the material.

$$CO_2(g) + H_2O \rightleftharpoons H_2CO_3 \rightleftharpoons HCO_3^- + H^+ \tag{4.3}$$

$$Ca^{2+} + HCO_3^- \rightleftharpoons CaCO_3 + H^+ \tag{4.4}$$

Matteo et al. [3] performed flow-through experiments of carbonated brine with different concentrations on cement paste. In the test with CB-I solution in table 4.4, Ca^{2+} and HCO_3^-, which are dominant reactants of the precipitation of $CaCO_3$ in equation (4.4), were carried in the leaching solution in order to realize the formation of carbonate layer on the water/cement interface as that in the study of Schwotzer [46]. However, the sealing layer did not occur on the surface of cement paste, and a Ca-rich layer was observed in the interior of the material exhibiting a pore-clogging behaviour.

The aforementioned cases of Matteo's experiment and demineralized water both contain HCO_3^- in leaching solutions with or without Ca^{2+}, and neither can reproduce the formation of carbonate layer on the water/cement interface. The contradictory experimental phenomena require a mechanism other than the precipitation of $CaCO_3$ in equation (4.4) to expound the protective effect of the surface sealing layer.

It is noteworthy that the presence of Mg in the hard tap water with the approximate Mg/Ca molar ratio of 1:5 as shown in table 4.1. According to the discussion in section 4.1.1, the incorporation of Mg in ACC occurs and subsequently forms ACMC as the precursor of Mg-calcite, which is demonstrated in the experiment [15]. Therefore, it is plausible that the surface carbonate layer in the experiment with hard tap water is composed of ACMC, of which the formation immediately seals and protects the cement paste. The transformation behaviour of ACMC into crystalline phase is still not thoroughly illuminated [25], nevertheless the crystallization process is not assumed to compromise the self-sealing effect of the carbonate layer on the water/cement interface.

4.2.2 The numerical simulation of the surface ACMC layer

The numerical study of ACMC in the cement-based system can promote better understanding of the experimental outcomes, and benefit the extended research on cement carbonation related studies. The chemical equilibrium of the considered system is assumed at the beginning of simulation, and disturbed by the diffused ion species from the leaching solution, which is simulated by the reactive transport model [47]. The subsequent dissolution/precipitation of solid phases is determined by the saturation ratio Ω that is defined as

$$\Omega = \frac{IAP}{K} \tag{4.5}$$

$$IAP = \prod_{j=1}^{N_p} C_j^{\nu_{nj}} \gamma_j^{\nu_{nj}}, \quad n = 1, 2, 3..., N_m \tag{4.6}$$

where K is the solubility product, and IAP stands for ion activity product. In equation (4.6), IAP is calculated by the concentration C_j, activity coefficient γ_j and stoichiometric coefficient ν_{nj} of the j-th primary species, while N_p and N_m are the number of primary species and minerals respectively. The saturation index of a solid phase is described as

$$SI = log(\Omega) \tag{4.7}$$

The solid phase dissolves when $SI < 0$ and precipitates when $SI > 0$, and is at equilibrium when $SI = 0$.

In the present study, the Ca/Si ratio of intact C-S-H is considered as 1.7, while that of leached C-S-H is 0.8. The cement paste prepared at a water/cement ratio of 0.4 in the work of Stora et al. [49] is adopted to numerically simulate the experiments of Schwotzer et al. [46], and the volume fractions of solid phases in the paste are tabulated in table 4.2.

Table 4.2: The volume fractions (%) of solid phases for cement paste adopted in simulations.

Portlandite	C-S-H (Intact)	Ettringite	Monosulphate	Unhydrated clinker	Porosity
10.8	49.7	2.3	0.4	18.4	18.4

The chemical constitution and thermodynamic data of ACMC have been increasingly highlighted in latest works. The Mg/Ca molar ratio of the synthetic ACMC is proposed to be 0.15:0.85 [50], which is related to the concentration of reactants in the aqueous solution. ACMC with Mg content varying between 0 and 100 mol%, including the case of Mg:Ca = 0.15:0.85, was synthesised in experiments [25], and solubility product was studied based on the Mg content. The detailed information of cement minerals and ACMC adopted in simulations is tabulated in table 4.3.

The configuration of one-dimensional simulations is demonstrated in figure 4.1, in which a surface element is set up on the interface between cement paste and leaching solution to capture the formation and subsequent effect of the carbonate layer. In the experiments, the observation scale is between 0.01 and 100 μm. The element size of cement paste is set up to 100 μm in simulations, while the size of surface element is

Table 4.3: The chemical input data of the considered solid phases in simulations.

Solid phase	Chemical formula	Log(K)	Reference
Portlandite	$Ca(OH)_2$	22.5444	[51]
C-S-H (Intact)	$Ca_{1.7}SiO_{6.317}H_{5.234}$	28.0022	[51]
C-S-H (Leached)	$Ca_{0.8}SiO_{4.34}H_{3.08}$	11.0503	[51]
Ettringite	$Ca_6Al_2(SO_4)_3(OH)_{12}{\cdot}26H_2O$	56.8823	[51]
Monosulphate	$Ca_4Al_2(SO_4)(OH)_{12}{\cdot}6H_2O$	72.4704	[51]
Calcite	$CaCO_3$	1.8487	[51]
ACMC	$Ca_{0.85}Mg_{0.15}CO_3{\cdot}0.51H_2O$	-6.04	[25]

10 μm. The solubility of CO_2 in the leaching solution at atmospheric partial pressure is measured as 0.18 mM [45], which is adopted in simulations.

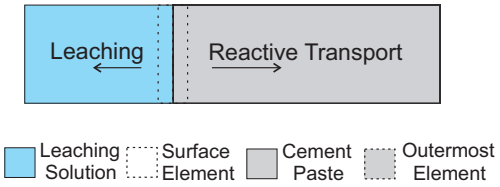

Figure 4.1: Schematic flow diagram of the one-dimensional domain of cement paste subject to leaching solution.

The chemical process of cement paste exposed to hard tap water in table 4.1 is reproduced with numerical modelling to explore the mechanism of the surface carbonate layer in the experiment [46]. The variation of solid phase in the surface element is demonstrated in figure 4.2. The volume fraction of ACMC in the surface element is increasing rapidly as observed in the experiment, and subsequently the porosity decreases representing the clogging of pore space due to the formation of ACMC. By contrast, the constituents of cement paste in the outermost element remain approximately constant in the course of ACMC formation as shown in figure 4.2, which demonstrates the sealing effect of the ACMC layer and the subsequent protection on the cement paste.

In order to numerically reproduce the experimental outcomes, $CaCO_3$ is represented with calcite in table 4.3 by the reactive transport modelling. The outcome of cement paste leached by demineralized water is depicted in figure 4.3. ACMC is not observed in the surface element, which is attributed to the absence of the essential reactants - Mg^{2+} in the system. The dissolution of portlandite is exhibited by the decreased volume fraction with time, and decalcification of C-S-H is represented by

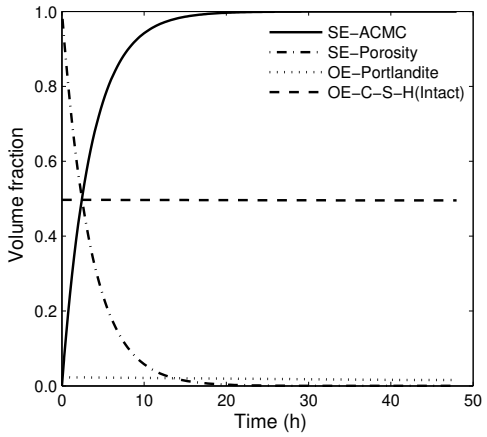

Figure 4.2: Profiles of the surface element (SE) and the outermost element (OE) of cement paste for the system in figure 4.1 subject to the hard tap water in table 4.1 for 2 days, including the content of ACMC and porosity of SE, and portlandite and C-S-H(Intact) of OE.

the increased C-S-H(Leached), which can release Ca^{2+} into pore solution. As the concentration of Ca^{2+} grows, the precipitation of calcite occurs due to chemical reactions between dissolved CO_2 and Ca^{2+} as described in equation (4.3) and (4.4).

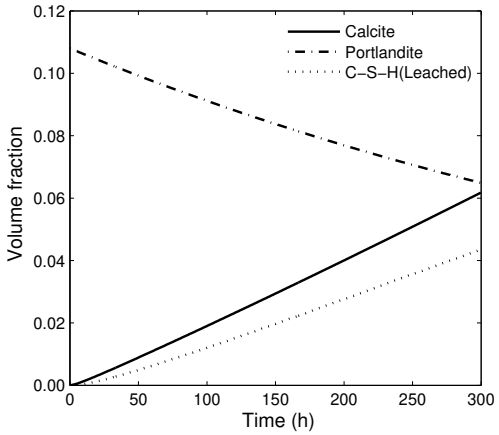

Figure 4.3: Profiles of calcite, portlandite and C-S-H(Leached) in the outermost element of cement paste subject to the demineralized water in table 4.1 for 300 hours.

4.2.3 General discussion

The carbonate layer on the interface between cement paste and leaching solution plays an important role in the process of chemical degradation, which is observed in the experiment [46] and numerically reproduced in the present work.

The water/cement interface serves as a nucleation site [52] of the deposition in the process of chemical reactions, which accounts for the location of carbonate layer. The constituent of the carbonate layer is suggested to be ACMC in the present work based on extensive experimental conclusions and data in section 4.1.1. The solubility and chemical formula of ACMC are investigated in the latest experiments [25], which effectively supports the numerical simulation of ACMC layer in the present section.

The rapid formation of the surface layer consumes aggressive ion species, for example HCO_3^- from dissolved CO_2, preventing cement paste from chemical degradation. The subsequently formed ACMC layer seals the interface of cement paste and obstructs the reactive transport between the external and pore solution, which can completely arrest the subsequent chemical reactions, such as the dissolution of portlandite and decalcification of C-S-H.

In the case of the demineralized water, the formation of ACMC layer is negated due to the absence of Mg^{2+}, nevertheless the precipitation of calcite occurs in the interior of cement matrix despite the fact that the demineralized water is unable to provide Ca^{2+} as reactant. Without the sealing effect of ACMC layer, the chemical equilibrium between pore solution and cement paste is affected, and Ca^{2+} is released into pore solution as a result of the dissolution of portlandite and decalcification of C-S-H. Therefore, the diffused HCO_3^- can react with Ca^{2+} precipitating calcite in pore space of cement matrix. The pore-clogging of calcite precipitation is reported in literature [53, 54], and acts as a protective behaviour for the material by retarding the process of reactive transport. By contrast to the completely ceased chemical degradation by ACMC layer, the precipitation of calcite can establish a protective mechanism to the material, which is however based on the premise of the already happened chemical degradation within cement matrix.

In this section, the case of leaching by hard tap water demonstrates that reactants (Mg^{2+}, Ca^{2+} and HCO_3^-) provided by external solution can result in the formation of surface layer. While in the case of leaching by demineralized water, Mg^{2+} and Ca^{2+} are both removed from external solution, and calcite forms in the interior of cement paste. According to the mechanism of ACMC formation on the water/cement interface, Matteo et al. [3] investigated whether a surface layer of calcite can form on the interface when the leaching solution is carrying Ca^{2+} and HCO_3^-, and the effect of CCP in the duration of chemical degradation with different ion concentrations, which is demonstrated in section 4.3.

4.3 The pore-clogging behaviour of CCP in cement-based materials

The pore-clogging effect of CCP is determined by the compositions of the leaching solution, especially the concentration of dissolved CO_2, which is the essential reactant of CCP and scarcely possible to abundantly consist in hydrated cement-based materials. Matteo et al. [3] performed a series of leaching experiments with different aqueous concentrations, and exhibited the mechanisms of cement degradation related to carbonation. In this section, the numerical simulation of Matteo's experimental process is preformed with the same methodology and setup as those described in section 4.2.

In the experiment, three batches of carbonated brine were adopted to represent different situations of dissolved CO_2, and the cement pasted was prepared with a water/cement ratio of 0.4. The sodium bicarbonate and hydrochloric acid were employed to achieve the specified concentration of dissolved CO_2 in leaching solution, and calcium chloride was added in one of the brine to compare with the experiment of Schwotzer et al. [46], as tabulated in table 4.4.

Table 4.4: The concentrations of dissolved CO_2 in leaching solutions in experiments [3].

Carbonated brine	$CO_{2(aq)}$	Ca	pH
	mM	mM	-
CB-I	30	5.3	5.6
CB-II	10	-	5.6
CB-III	0.01	-	5.6

During the leaching process, the Ca content of cement matrix decreases due to the dissolution of portlandite and decalcification of C-S-H, while the Ca concentration of pore solution subsequently increases. The bicarbonate ions diffused into pore space react with calcium ions in pore solution to precipitate $CaCO_3$ as equation (4.4), which can counteract the Ca loss and further increase Ca content by contrast with the intact material. The dissolution/precipitation of solid phases is related to the porosity of cement matrix, described as

$$\Delta\phi = -\sum_{i=1}^{N_i} \Delta fr_i \tag{4.8}$$

$$\phi = \phi_o + \Delta\phi \tag{4.9}$$

where $\Delta\phi$ is the change of porosity, and Δfr_i is the change of volume fraction for solid phase i in the material. N_i is the number of solid phases undergoing chemical reactions. ϕ and ϕ_o are the total and initial porosity respectively. If $\Delta fr_i > 0$, the solid phase i precipitates in the matrix, and the total porosity ϕ decreases for $\Delta\phi < 0$, vice versa. When the precipitation of solid phases, for example $CaCO_3$, dominates the porosity change $\Delta\phi$, the pore space is reducing gradually due to CCP until $\phi = 0$.

According to the experimental observation, the calcite layer formed between the leached zone and dissolution front of portlandite, which is referred to as the reaction front and identifies the nominal "reaction zone". The depth of reaction zone d_r is the distance between the reaction front and exposed surface, and adopted to determine the normalized depth d_n with the actual depth d_a as defined in equation (4.10).

$$d_n = \frac{d_a}{d_r} \tag{4.10}$$

The calcite layer is demonstrated by means of the Ca/Si ratio in cement matrix versus normalized depth in the experiment. In figure 4.4, the Ca/Si ratio measured in the leaching test with carbonate brine CB-I in table 4.4 is demonstrated against normalized depth d_n, which exhibits the formation of calcite layer. Ca^{2+} is incorporated in the test together with the 30 mM dissolved CO_2 to verify whether calcite can precipitate on the water/cement interface and protect cement paste as discussed in section 4.2.3. However, the peak value of Ca/Si ratio is observed at the normalized depth of approximate 1, implying that the formation of calcite layer occurs in the interior of cement matrix rather than on the surface of cement paste.

The chemical degradation happens in the reaction zone ($0 \leq d_n \leq 1$) in spite of the formation of calcite layer, which is captured in the numerical simulation as shown in figure 4.4. The profile of Ca/Si ratio exhibits similar pattern with the experimental outcome, despite the values present significant differences which is attributed to the different chemical systems in the experiment and simulation. The precipitation of calcite is simulated to investigate the variation of Ca/Si ratio along normalized depth. The coincident location of the both peak values demonstrates that the calcite layer is formed in the course of leaching process, and dominants the Ca/Si ratio of the material, which shows good agreements with the experimental results.

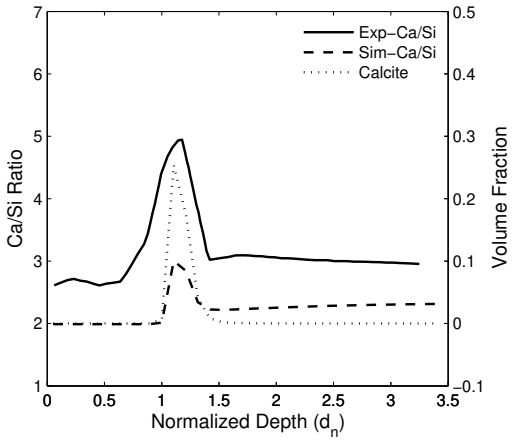

Figure 4.4: Profiles of Ca/Si ratio and calcite in simulation by 45 days, and Ca/Si ratio measured in experiment in the case of 30 mM dissolved CO_2.

To investigate the formation of calcite layer with the moderate concentration of dissolved CO_2, the carbonate brine CB-II in table 4.4 is adopted in the experiment, and the profile of Ca/Si ratio exhibits similar pattern with the case of CB-I. The peak value of Ca/Si ratio occurs in the vicinity of the reaction front as shown in figure 4.5, demonstrating the formation of reaction zone and the calcite layer. It is noteworthy that a second peak occurs in the neighbourhood of the water/cement interface, and Matteo et al. propose that a different mechanism may work in this case. The calcite layer is formed at the reaction front in the simulation, resulting in the peak value of Ca/Si ratio in the same depth in figure 4.5. However, the "second peak" is not captured in the outer reaction zone.

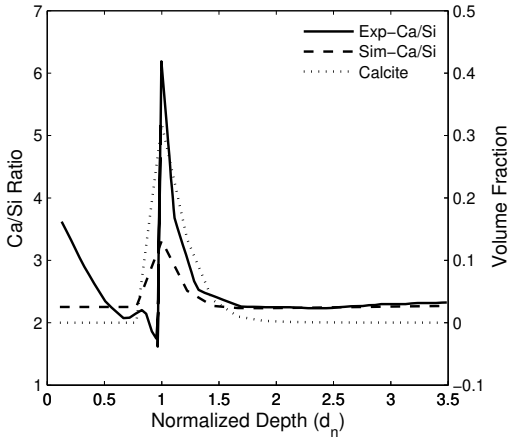

Figure 4.5: Profiles of Ca/Si ratio and calcite in simulation by 20 days, and Ca/Si ratio measured in experiment in the case of 10 mM dissolved CO_2.

In the case of low concentration of dissolved CO_2 with the carbonate brine CB-III in table 4.4, the profile of Ca/Si ratio in the experiment is generally increasing from the water/cement interface to the interior of cement matrix in figure 4.6, and demonstrates the absence of the peak of Ca/Si ratio. By contrast to the cases of CB-I and CB-II, it is plausible that the formation of calcite layer cannot occur in the condition of 0.01 mM dissolved CO_2. The slope of Ca/Si ratio represents the loss of Ca content by the dissolution of portlandite and decalcification of C-S-H, which is verified by the simulated outcomes in figure 4.6. The volume fraction of calcite is approximately zero throughout the model of simulation, and the the Ca/Si ratio exhibits the similar pattern with the experimental results.

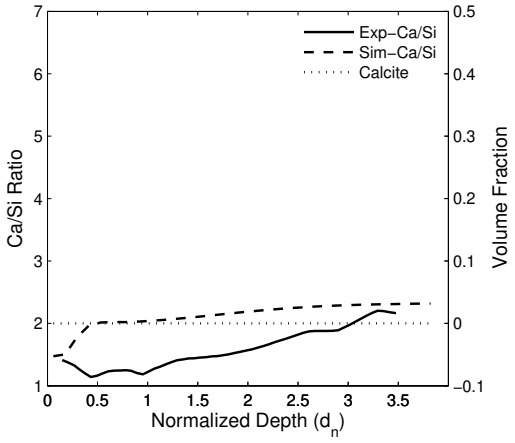

Figure 4.6: Profiles of Ca/Si ratio and calcite in simulation by 45 days, and Ca/Si ratio measured in experiment in the case of 0.01 mM dissolved CO_2.

The pore-clogging effect of calcite layer is demonstrated by the formation rate of reaction zone in figure 4.7. The dissolution of CO_2 into aqueous solution can produce carbonic acid, and H^+ is released into pore solution during the process of carbonation (equation (4.3) and (4.4)). Therefore, the solution CB-I with 30 mM dissolved CO_2 is the most acidic of the three cases, and subsequently results in the largest formation rate of reaction zone with a trend of diminishing gradually. By contrast, the formation rate is significantly reduced in the case of CB-II, and the development of the reaction zone comes to a halt rapidly. The depth of reaction zone is generally proportional to the square root of time in the case of CB-III, which is the typical feature of diffusion-controlled process [55]. According to the results in figure 4.4-4.6, the formation of calcite layer in the cases of CB-I and CB-II blocks the pathway of ion transport within the cement matrix, and subsequently slows down the process of chemical degradation, which can eventually cease the development of reaction zone.

Based on the comparison of CB-I and CB-II in figure 4.7, the depth of reaction zone is increasing with time in the condition of 30 mM dissolved CO_2, while the depth in the case of 10 mM remains at constant soon after the commencement of experiment. The reaction zone is developing in spite of the formation of calcite layer in presence of higher concentration (30 mM) of dissolved CO_2. The calcite layer occurs at the normalized depth of reaction zone $d_n = 1$ as shown in figure 4.4, therefore it is suggested that the calcite layer is moving inwards with the development of the reaction zone representing the precipitation and subsequent dissolution of calcite in the reaction front.

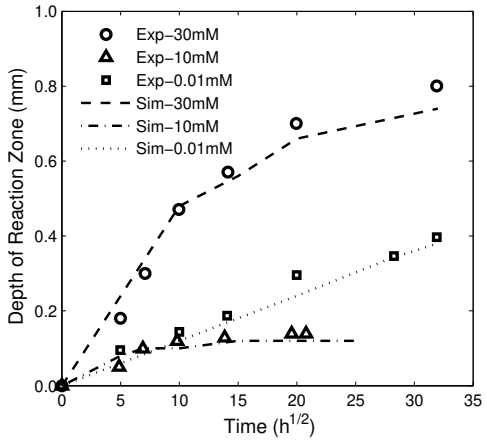

Figure 4.7: The depth of reaction zone versus the square root of time for 30 mM, 10 mM and 0.01 mM dissolved CO_2 in experiments and simulations.

In the present section, the formation of calcite layer is discussed on the basis of experimental outcomes and numerical simulations. In the experiment with CB-I, the reaction zone is firstly developed, while the calcite layer is formed and moving towards the interior until thoroughly clogging the pore space. It verifies that the surface layer cannot occur with the presence of both Ca^{2+} and dissolved CO_2 in the leaching solution, and is rational to attribute the sealing effect of surface layer [46] to the presence of Mg and the subsequent formation of ACMC as discussed in section 4.2. The calcite precipitation can retain Ca content within the cement matrix, and subsequently rise up the Ca/Si ratio, which seems unable to explain the second peak of Ca/Si ratio in the CB-II case. The high Ca/Si ratio is attributed to either the increasing Ca content or decreasing Si content, and the mechanism determining the difference between experimental and simulated outcomes requires further investigation.

4.4 The effect of CCP on mechanical behaviour

The evolution of CCP in cement-based materials is dominated by pH, the concentration of dissolved CO_2 [56], and the configuration of pH and CO_2 determines the process of chemical degradation. Specifically, the acid attack causes the dissolution of portlandite and decalcification of C-S-H when pH predominates the chemical reactions. By contrast, calcite precipitates and clogs the pore space of the material when CO_2 plays a leading role, and undergoes precipitation/dissolution cycle in the condition of high CO_2 concentration during the chemical degradation process.

The calcite layer is observed to precipitate and dissolve in the experiment [3], which presents that calcite layer is moving towards the interior of cement paste progressively. In this sense, the reaction zone is developing in the material matrix weakening the mechanical properties of the cement paste, while the formation of the calcite layer can strengthen the material as discussed in section 4.1.2. In this section, the movement of the calcite layer in a structural component subject to the carbonated brine is demonstrated by numerical simulations according to Matteo et al. experiment. The elastic moduli of the partially degraded component is evaluated by Mori-Tanaka scheme [48] incorporating both weakening (dissolution of portlandite and decalcification of C-S-H) and strengthening (calcite precipitation) effect of chemical reactions, and the overall mechanical behaviour is investigated by the four-point bending simulation.

4.4.1 The precipitation/dissolution of calcite layer in cement-based material

Matteo et al. [3] adopted carbonated brine of pH = 3.7 and 30 mM dissolved CO_2 in the leaching test, and captured that the calcite layer is shifting laterally in a duration of 73 days. The precipitation of calcite decreases the pH value of the pore solution [56] as described by equation (4.4), which can result in an acidic environment before clogging the pore space and the subsequent dissolution of calcite. Meanwhile, the reactants of carbonation are continuously transported by diffusion, and precipitate calcite in the deeper portion of the material, which accounts for the shifting calcite layer.

The formation and movement of the calcite layer are reproduced numerically by a cement paste beam of 0.16 m × 0.05 m × 0.03 m (length × height × width) subject to leaching solution of pH=3.7 and 30 mM dissolved CO_2, of which the half symmetric

setup is demonstrated in figure 4.8. The element size of the model is 1 mm, and the cement paste adopted in this section is the same as the material in section 4.2.

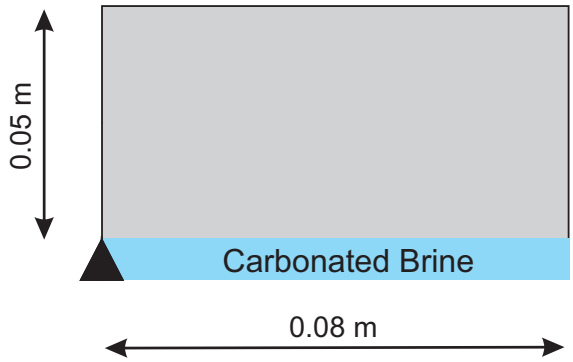

Figure 4.8: Schematic diagram of the simulation for cement paste beam leached by carbonated brine (pH=3.7 and 30 mM dissolved CO_2) .

The formation of a calcite layer with time in the beam is demonstrated in figure 4.9. After 150 days, calcite is formed in the outermost element layer on the bottom of the beam as depicted in figure 4.9a, while the moderate content of calcite appears in the elements adjacent to the bottom layer. By 500 days, calcite completely dissolves in the outermost element layer, and simultaneously precipitates in the depth between 1 mm and 3 mm shown in figure 4.9b, which presents the shifting calcite layer. The dissolution and precipitation of calcite proceed and subsequently develop a uniformly distributed calcite layer by 900 days in figure 4.9c. By 1400 days, the calcite layer spreads inwards, and generally appears in the depth of 2 mm to 3 mm as demonstrated in figure 4.9d.

The shifting calcite layer in the material matrix exhibits the varying amount and width in the process of chemical degradation, which can lead to the different impacts on the residual properties of the material. Therefore, the mechanical behaviour of cement paste undergoing calcite precipitation is proposed to be investigated in the present work based on the distribution of calcite during the leaching process.

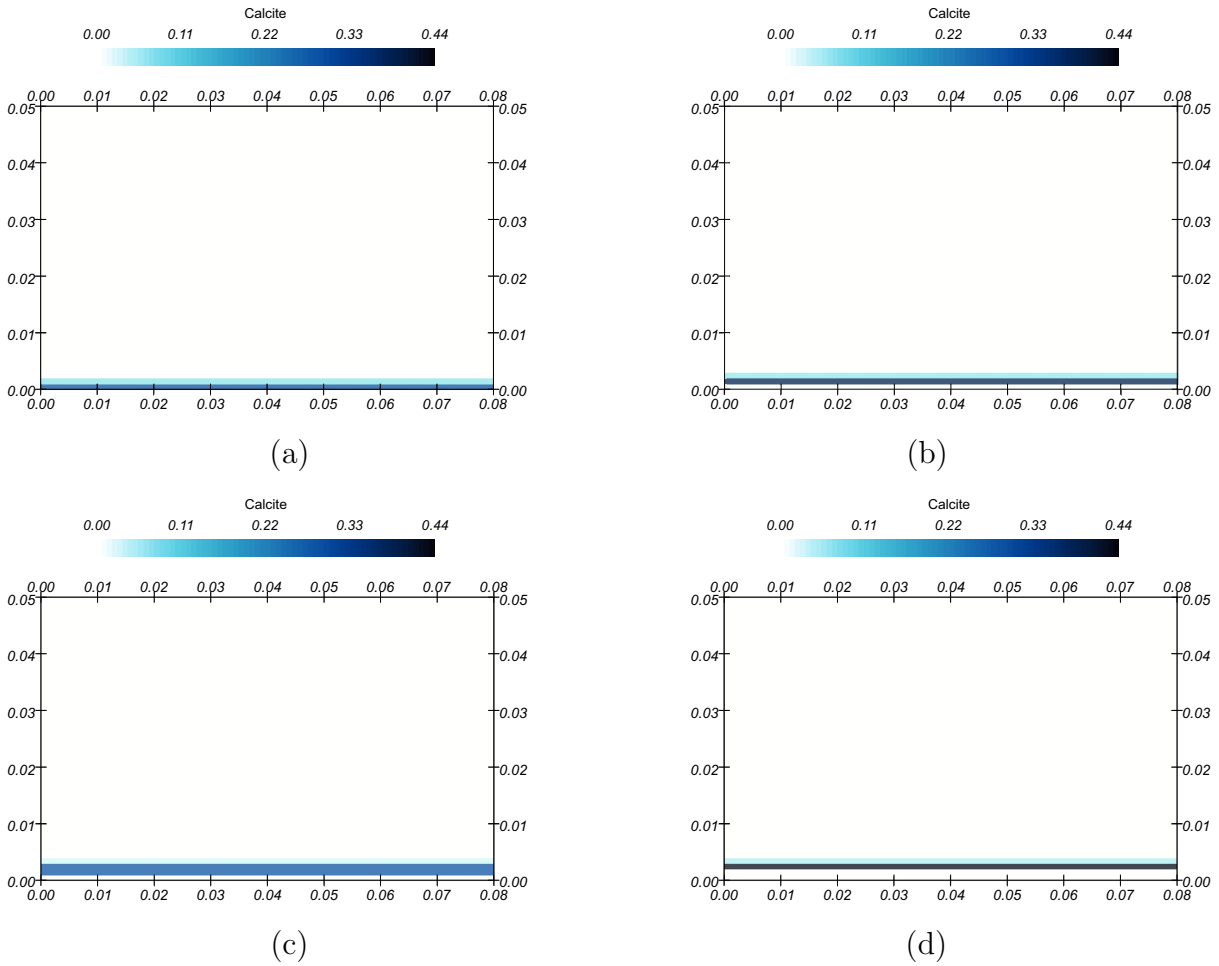

Figure 4.9: Profiles of calcite volume fractions in the cement paste beam exposed to carbonated brine (pH=3.7 and 30 mM dissolved CO_2) for (a) 150 days, (b) 500 days, (c) 900 days and (d) 1400 days.

4.4.2 The residual elasticity of cement-based material exposed to carbonated brine

The formation of a calcite layer occurs in the context of a series of chemical reactions between the cement matrix and pore solution. The dissolution of portlandite and decalcification of C-S-H are the primary mechanisms for the elasticity reduction due to cement degradation [33], which is measured that the Young's modulus of cement paste reduces from 21.65 GPa to 3.15 GPa in the experiment [57]. The reduction of elasticity is supposed to be accommodated with the strengthening effect of calcite precipitation to evaluate the overall mechanical properties for materials exposed to carbonated brine.

The Young's modulus E_{hom} and Poisson's ratio ν_{hom} of the cement paste are evaluated by the Mori-Tanaka scheme [48] in equation (4.11) by homogenizing the multi phases of cement material as the matrix medium and inclusions. For cement-based materials, C-S-H is considered as the matrix medium accommodating the inclusions as the macroscopic cement material. In context of calcite precipitated in the material, calcite replaces C-S-H as the matrix medium if the volume of calcite exceeds that of C-S-H in the representative elementary volume (REV).

$$E_{hom} = \frac{9\psi_{hom}\mu_{hom}}{3\psi_{hom} + \mu_{hom}}; \nu_{hom} = \frac{3\psi_{hom} - 2\mu_{hom}}{6\psi_{hom} + 2\mu_{hom}} \tag{4.11}$$

The bulk modulus ψ_{hom} and shear modulus μ_{hom} in Mori-Tanaka scheme are described in equation (4.12) and (4.13).

$$\psi_{hom} = \sum f_i\psi_i\Big(1 + A^m\Big(\frac{\psi_i}{\psi_m} - 1\Big)\Big)^{-1} \times \Big[\sum f_i\Big(1 + A^m\Big(\frac{\psi_i}{\psi_m} - 1\Big)\Big)^{-1}\Big]^{-1} \tag{4.12}$$

$$\mu_{hom} = \sum f_i\mu_i\Big(1 + B^m\Big(\frac{\mu_i}{\mu_m} - 1\Big)\Big)^{-1} \times \Big[\sum f_i\Big(1 + B^m\Big(\frac{\mu_i}{\mu_m} - 1\Big)\Big)^{-1}\Big]^{-1} \tag{4.13}$$

$$A^m = \frac{3\psi_m}{3\psi_m + 4\mu_m}; B^m = \frac{6(\psi_m + 2\mu_m)}{5(3\psi_m + 4\mu_m)} \tag{4.14}$$

where the bulk/shear moduli of the matrix medium and inclusions are ψ_m/μ_m and ψ_i/μ_i respectively, while f_i is the volume fraction of the i-th inclusion.

Table 4.5: Intrinsic elastic moduli of minerals in cement paste.

Mineral	Bulk modulus (GPa)	Shear modulus (GPa)	Reference
Calcite	69.8	30.4	[58]
Portlandite	40.0	16.0	[59]
C-S-H (Intact)	15.3	9.6	[33]
C-S-H (Leached)	2.8	1.7	[33]
Ettringite	14.9	9.0	[60]
Monosulphate	40.0	16.0	[60]
Unhydrated clinker	105.4	44.7	[61]

The simulated outcomes of the cement paste beam subject to leaching for 150 days are demonstrated in figure 4.10. The outermost element layer has undergone the complete delcalcificaiton of C-S-H as shown in figure 4.10a and 4.10b, and presents the depletion of portlandite in figure 4.10c. Nevertheless, the Young's modulus remains approximately the initial value (20.9 GPa) demonstrated in figure 4.10d, which is attributed to the precipitation of calcite in this area (figure 4.9a) by contrast to the experimental results [57]. In the depth between 1 mm and 2 mm, the Young's modulus is slightly larger than the initial value due to the moderate decalcification of C-S-H and formation of calcite. The evaluated values of Young's modulus in the present work generally accord with the conclusion of the experiment [36].

Portlandite and C-S-H are thoroughly degraded up to the depth of 2 mm by 500 days, which is demonstrated in figure 4.11a-c. As discussed in figure 4.9b, the calcite layer moves to the depth of 1 - 2 mm rendering the absence of CCP strengthening effect in the outermost element layer, which is reflected in the Young's modulus significantly reducing to approximate 2 GPa in figure 4.11d. By contrast, calcite counteracts the majority of stiffness loss in the depth of 1 - 2 mm.

As the dissolution and re-precipitation of calcite towards the interior developing an uniform calcite layer by 900 days in figure 4.9c, Young's modulus decreases progressively with calcite dissolution in the depth of 1 - 2 mm, and increases remarkably to approximate 47 GPa (figure 4.12d) in the depth of 2 - 3 mm as a result of the calcite precipitation and the moderate degradation of C-S-H and portlandite shown in figure 4.12a-c.

The high stiffness zone in figure 4.12d continuously undergoes the degradation process on C-S-H and portlandite, while the precipitated calcite occupies the enlarged

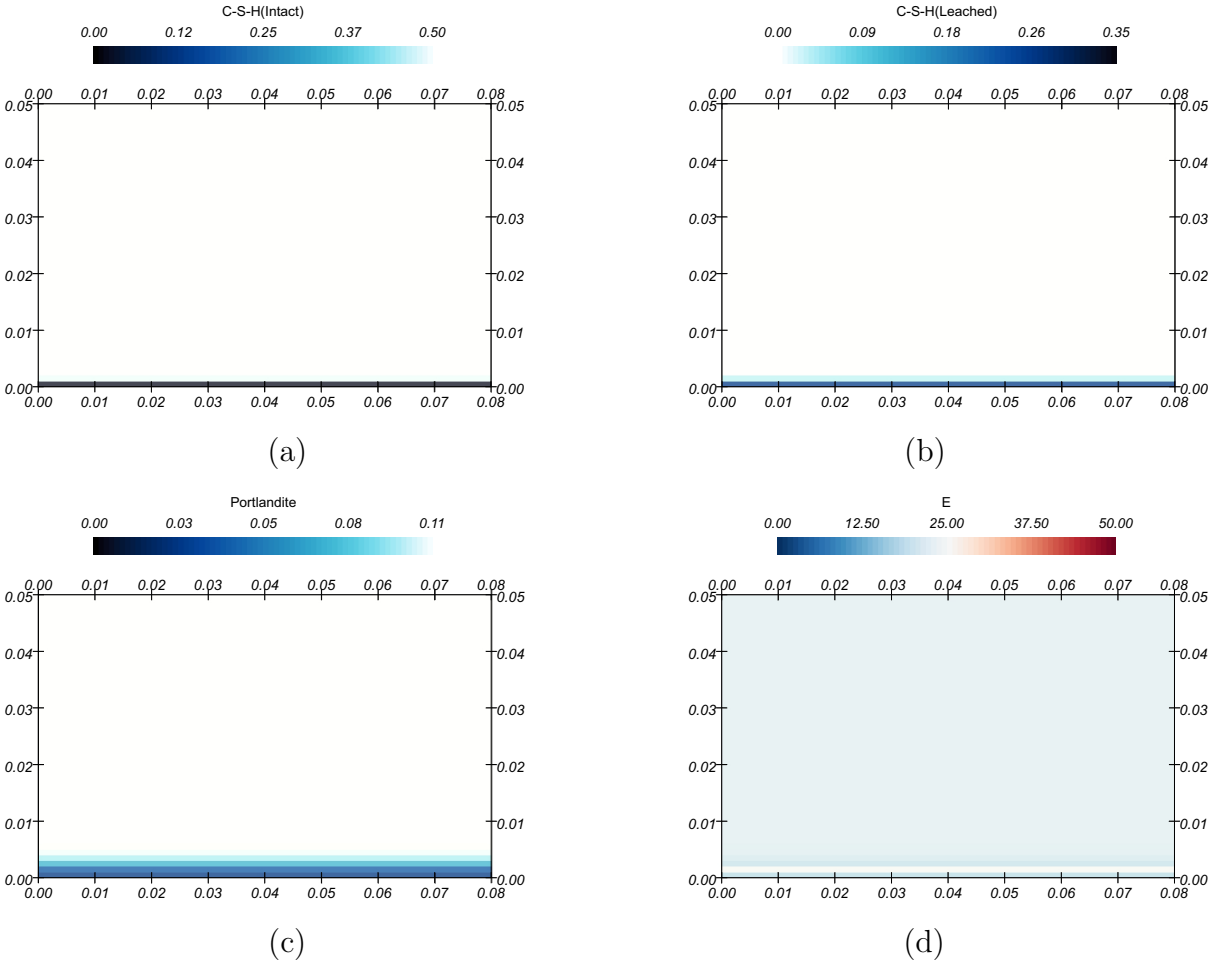

Figure 4.10: The volume fractions of (a) C-S-H(Intact), (b) C-S-H(Leached), (c) portlandite and (d) Young's modulus (GPa) of the cement paste beam exposed to carbonated brine (pH=3.7 and 30 mM dissolved CO_2) for 150 days.

pore space and subsequently becomes the matrix medium, which is depicted in figure 4.13a-c and 4.9d by 1400 days. Therefore, the Young's modulus is approximately reduced to the initial value in figure 4.13d. In the deeper zone adjacent to the calcite layer, the Young's modulus is slightly lower than the initial value throughout the process of chemical degradation as shown in figure 4.10d - 4.13d, which is determined by the moderate dissolution of portlandite.

The enhancement of calcite precipitation on the elasticity of cement paste subject to chemical degradation is qualitatively evaluated by Mori-Tanaka scheme in the present section. In the thoroughly leached zone, C-S-H and portlandite are completely degraded, however the formation of calcite can compensate the elasticity reduction and maintain the Young's modulus approximately at the initial value, which shows agreement with the experimental outcomes [36]. During the process of chemical reac-

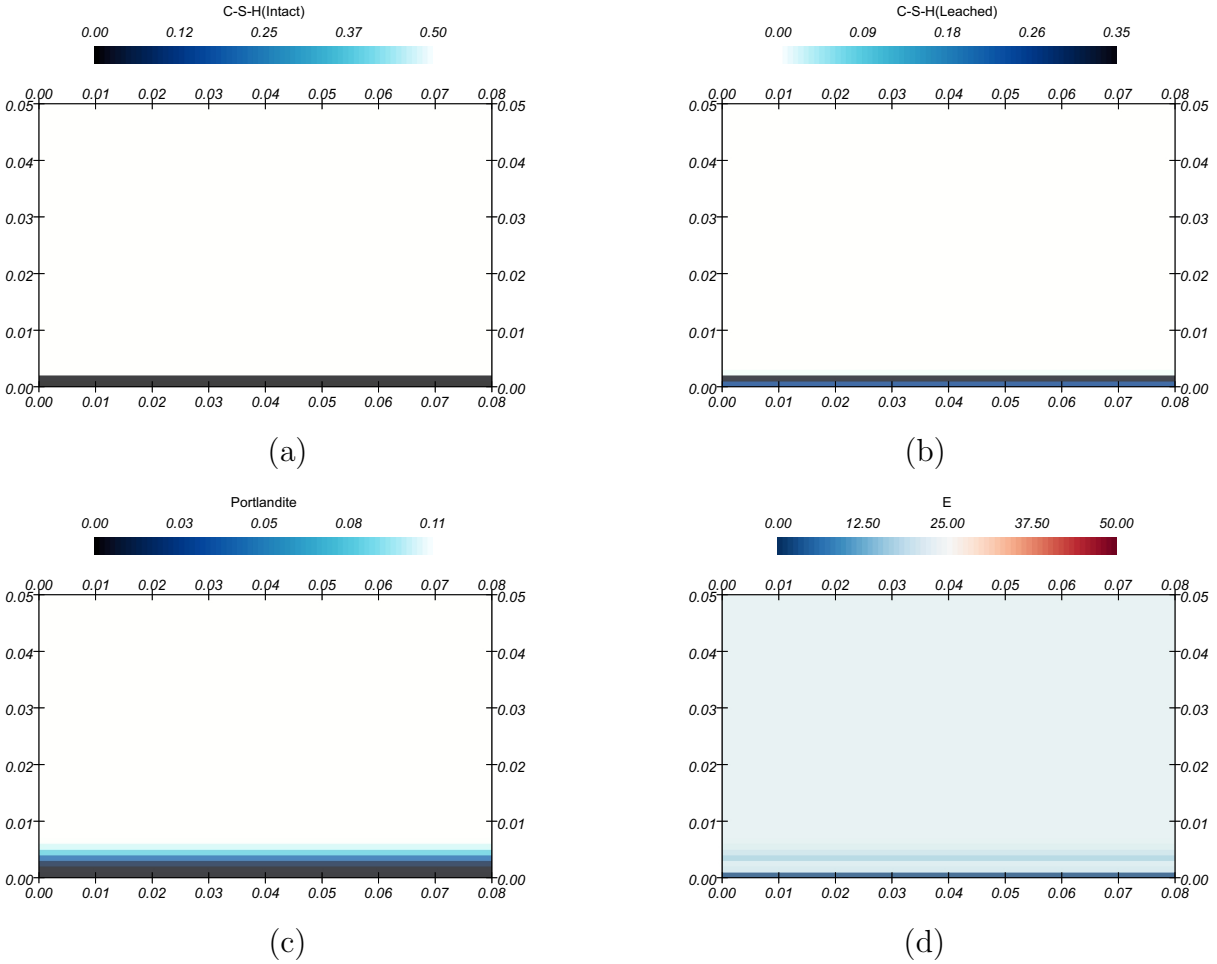

Figure 4.11: The volume fractions of (a) C-S-H(Intact), (b) C-S-H(Leached), (c) portlandite and (d) Young's modulus (GPa) of the cement paste beam exposed to carbonated brine (pH=3.7 and 30 mM dissolved CO_2) for 500 days.

tions, the calcite layer moves to the intermediately degraded zone, and significantly enhances the Young's modulus twice as much as the initial value. The transformation of constituents in cement paste is converted into the variation of elastic properties, which is adopted to investigate the overall mechanical behaviour in the following section.

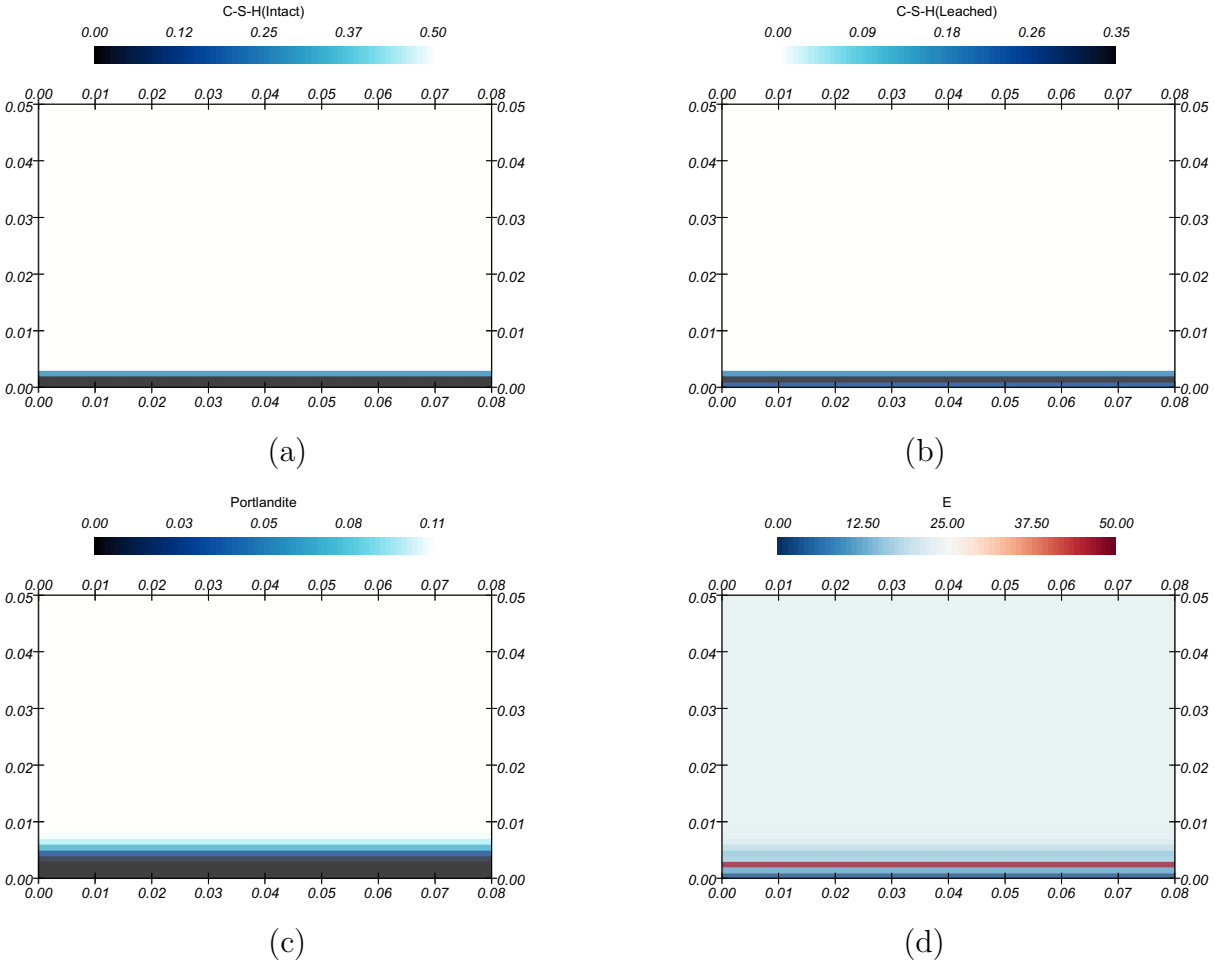

Figure 4.12: The volume fractions of (a) C-S-H(Intact), (b) C-S-H(Leached), (c) portlandite and (d) Young's modulus (GPa) of the cement paste beam exposed to carbonated brine (pH=3.7 and 30 mM dissolved CO_2) for 900 days.

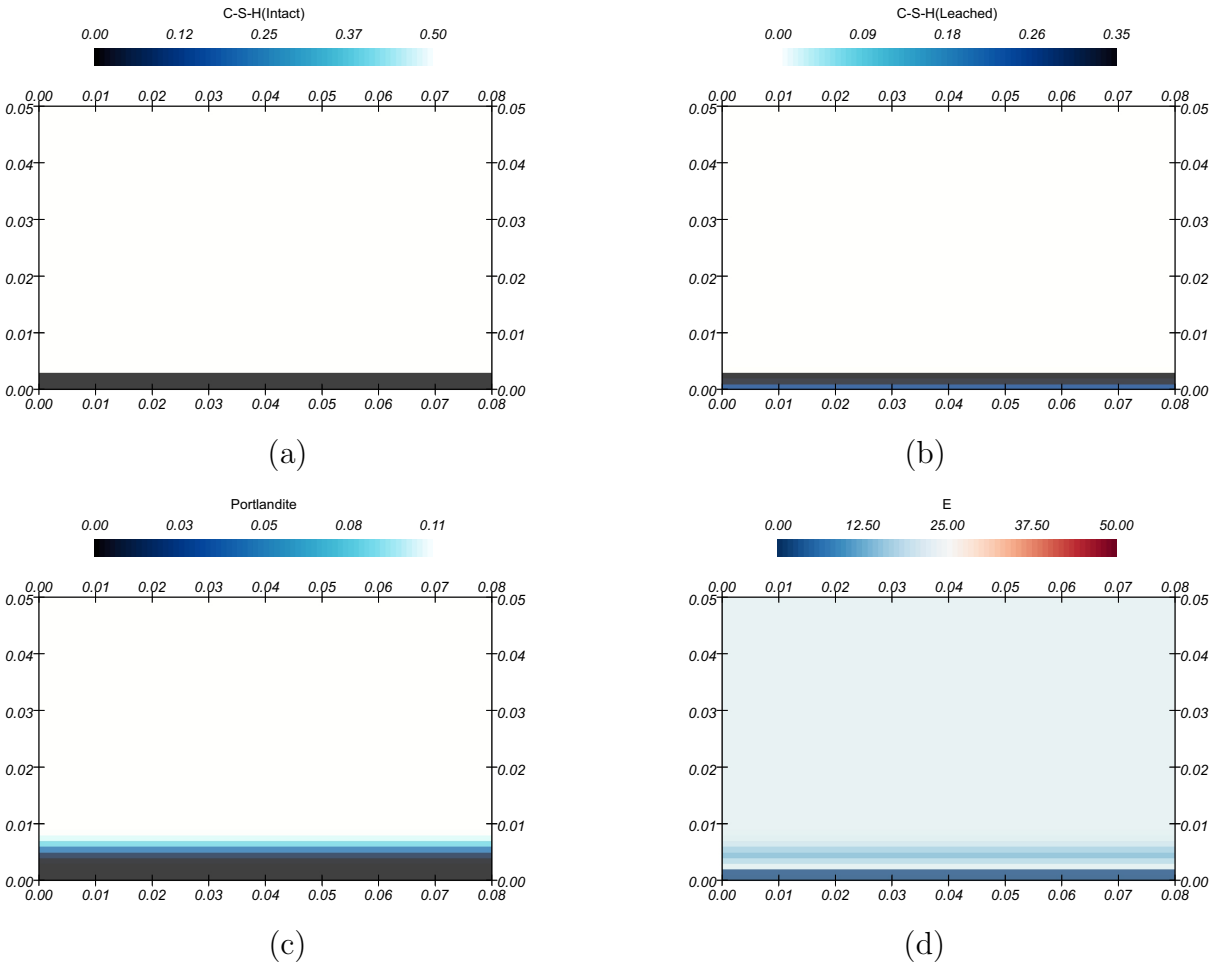

Figure 4.13: The volume fractions of (a) C-S-H(Intact), (b) C-S-H(Leached), (c) portlandite and (d) Young's modulus (GPa) of the cement paste beam exposed to carbonated brine (pH=3.7 and 30 mM dissolved CO_2) for 1400 days.

4.4.3 The mechanical behaviour of cement-based material exposed to carbonated brine

The mechanical behaviour of the degraded cement paste beam is evaluated with the four-point bending test. The displacement loading is imposed 0.03 m away from the centre on both sides on the top surface of the beam, and the simulation setup is depicted in figure 4.14.

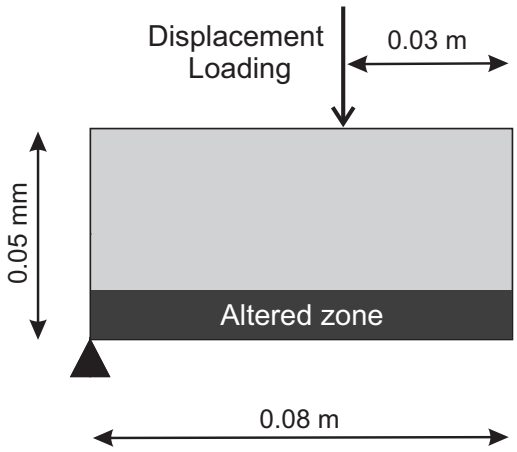

Figure 4.14: Schematic diagram of the four-point bending test for cement paste beam leached by carbonated brine (pH=3.7 and 30 mM dissolved CO_2).

The Young's modulus E_{hom} and Poisson's ratio ν_{hom} of the cement paste are evaluated by Mori-Tanaka scheme in section 4.4.2 after a prescribed duration of chemical degradation, and subsequently employed to update the initial stiffness tensor $\boldsymbol{C}_0$ defining the strain-stress relation in equation (4.15).

$$\boldsymbol{\sigma} = \boldsymbol{C_0} : \boldsymbol{\varepsilon} \tag{4.15}$$

where $\boldsymbol{\sigma}$ and $\boldsymbol{\varepsilon}$ are the stress and strain tensors respectively.

The cement paste is subject to flexure in the four-point bending test, and the isotropic damage model is adopted to evaluate the material non-linearity. A scalar damage variable d is defined in equation (4.16), and represents the reduced proportion of Young's modulus, assuming the Poisson's ratio is unaffected during the process of damage evolution [62].

$$d = 1 - \frac{\kappa^0}{\kappa}\left[1 - \alpha + \alpha \exp\left[\beta[\kappa^0 - \kappa]\right]\right] \tag{4.16}$$

where κ^0 and κ are the initial threshold and current damage threshold individually, while α and β are material parameters.

The damaged stiffness tensor $\boldsymbol{C}$ is subsequently described as

$$\boldsymbol{C} = (1 - d)\boldsymbol{C_0} \tag{4.17}$$

To avoid the convergence difficulty and capture the post-peak behaviour, the displacement based non-local damage model is incorporated in the present work, and the detailed numerical implementation is presented in the literature [63–65]. The initial strain threshold is 0.86 $\times 10^{-4}$ [32], while the model parameters α and β are set to 0.9 and 2000 respectively.

The simulation of the four-point bending test is to qualitatively assess the overall behaviour of the degraded beam, which requires to make assumptions due to the complex constituents change in chemical reactions. For the REV undergoing stiffness reduction in chemical degradation, the evolution of strain threshold is considered as the same as that of mechanical damage in equation (4.16). In terms of the REV where Young's modulus is larger than that of the intact cement paste due to calcite precipitation, the strain threshold is set to the initial threshold of intact cement paste for simplification.

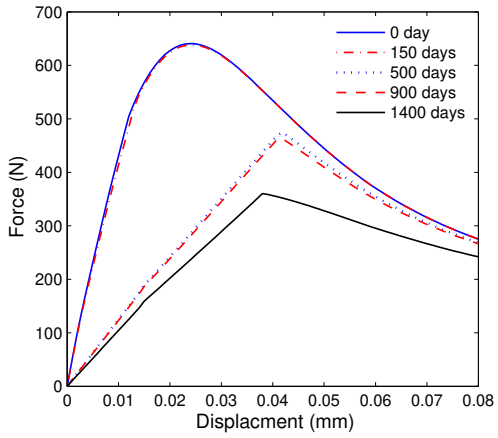

Figure 4.15: Curves of force versus displacement in the four-point bending test for cement paste beam subject to carbonated brine (pH=3.7 and 30 mM dissolved CO_2) after different time durations.

The force-displacement relation in four-point bending simulation is demonstrated in figure 4.15 after the cement paste beam submitted to carbonated brine for various durations. The curve of the intact beam (0 day) is approximately the same as that of

beam subject to carbonated brine for 150 days. According to figure 4.9a and 4.10, the outermost layer of the beam undergoes complete degradation on portlandite and C-S-H, meanwhile the precipitation of calcite counteracts the weakening effect in stiffness, which maintains the overall stiffness of the beam generally unchanged comparing with the intact beam.

The curves of 500 and 900 days exhibit a high similarity in figure 4.15, and remarkably differ from the curve of intact beam. In the two cases as shown in figure 4.11 and 4.12, the stiffness in outermost layer reduces significantly, due to the completely degraded portlandite and C-S-H as well as the absence of calcite, which can account for the weakening of the overall mechanical behaviour. From 500 days to 900 days, the calcite layer is shifting towards the interior between 1 mm and 3 mm demonstrated in figure 4.9b and c, the difference of stiffness distribution (figure 4.11d and 4.12d) is unable to influence the overall flexural behaviour of the beam. By 1400 days, the calcite layer moves to the depth of 2 mm in figure 4.11d, and subsequently the stiffness reduced zone is further developed in figure 4.13d, which contributes to the reduction of maximum load and post-peak behaviour in figure 4.15.

4.5 Conclusions

The crystallization pathway and polymorph type of CCP highly depends on the reactive environment, which can result in the different chemical and mechanical effect in cement-based materials.

It has been studied in extensive experimental works that magnesium ions can stabilize ACC due to the higher dehydration energy, and the formation of ACMC by incorporating Mg into ACC is investigated on the basis of the Mg/Ca ratio. The experiments of Schwotzer et al. [46] and Matteo et al. [3] provide an advantageous support that the formation of ACMC layer occurs on the water/cement interface with the presence of Mg, Ca and HCO_3^- in the leaching solution, while calcite layer forms in the interior of cement material in the absence of Mg. The ACMC layer on the interface demonstrates a feature of preventing the cement paste from chemical degradation, which is numerically reproduced with the solubility product of ACMC measured in the latest experiment [25].

The calcite layer occurs in the conditions of moderate and high concentration of dissolved CO_2, while the typical diffusion-controlled leaching process is observed with low CO_2 concentration. The pore-clogging effect is realized due to calcite precipitation

in the case of moderate concentration, and ceases the further chemical degradation in cement paste. The high concentration of dissolved CO_2 is the most aggressive case in terms of the degradation rate. The interplay between pH and CO_2 concentration can negate the pore-clogging effect by the dissolution and re-precipitation of calcite, presenting the shifting calcite layer within cement matrix.

The transformation of cement constituents is incorporated with micromechanical model to evaluate the variation of elastic moduli. The calcite layer can counteract the stiffness loss of completely decalcified cement paste, and approximately maintain the Young's modulus at the initial value. In the moderately decalcified zone, the Young's modulus can increase to twice as the initial value. However, the overall performance of the beam in the four-point bending test is determined by the depth of the completely decalcified zone, which is located between the water/cement interface and shifting calcite layer.

The formation and sealing effect of ACMC are potentially conducive to the CCP related application in industry and investigation of biomineralization. The stability and crystallization of ACMC require experimental studies to further reveal the relevant mechanisms. The enhancement of CCP on the degraded cement-based materials is qualitatively demonstrated in the present work, and the constitutive behaviour of decalcified-strengthened cement-based materials none the less requires to be thoroughly studied in theory and experiment.

References

[1] H. F. W. Taylor. *Cement chemistry*. Thomas Telford, London, second edition, 1997.

[2] Ribooga Chang, Semin Kim, Seungin Lee, Soyoung Choi, Minhee Kim, and Youngjune Park. Calcium carbonate precipitation for CO_2 storage and utilization: A review of the carbonate crystallization and polymorphism. *Frontiers in Energy Research*, 5:17, 2017.

[3] Edward N. Matteo, Bruno Huet, Carlos F. Jové-Colón, and George W. Scherer. Experimental and modeling study of calcium carbonate precipitation and its effects on the degradation of oil well cement during carbonated brine exposure. *Cement and Concrete Research*, 113:1 – 12, 2018.

[4] Rita G.W. Vasconcelos, Nicolas Beaudoin, Andrea Hamilton, Neil C. Hyatt, John L. Provis, and Claire L. Corkhill. Characterisation of a high pH cement backfill for the geological disposal of nuclear waste: The nirex reference vault backfill. *Applied Geochemistry*, 89:180 – 189, 2018.

[5] J. Cowie and F. P. Glasser. The reaction between cement and natural waters containing dissolved carbon dioxide. *Advances in Cement Research*, 4(15):119–134, 1992.

[6] C. Edvardsen. Water permeability and autogenous healing of cracks in concrete. *ACI Materials Journal*, 96:448–454, 1999.

[7] A. Neville. Autogenous healing - A concrete miracle? *Concrete International*, 24:76–82, 2002.

[8] Eva Loste, Rory M. Wilson, Ram Seshadri, and Fiona C. Meldrum. The role of magnesium in stabilising amorphous calcium carbonate and controlling calcite morphologies. *Journal of Crystal Growth*, 254(1):206 – 218, 2003.

[9] Brian Jones and Xiaotong Peng. Amorphous calcium carbonate associated with biofilms in hot spring deposits. *Sedimentary Geology*, 269-270:58 – 68, 2012.

[10] Attila Demény, Péter Németh, György Czuppon, Szabolcs Leél-Őssy, Máté Szabó, Katalin Judik, Tibor Németh, and József Stieber. Formation of amorphous calcium carbonate in caves and its implications for speleothem research. *Scientific Reports*, 6:155–164, 2016.

[11] G. Cobourne, G. Mountjoy, J.D. Rodriguez-Blanco, L.G. Benning, A.C. Hannon, and J.R. Plaisier. Neutron and X-ray diffraction and empirical potential structure refinement modelling of magnesium stabilised amorphous calcium carbonate. *Journal of Non-Crystalline Solids*, 401:154 – 158, 2014.

[12] C.R. Blue and P.M. Dove. Chemical controls on the magnesium content of amorphous calcium carbonate. *Geochimica et Cosmochimica Acta*, 148:23 – 33, 2015.

[13] J.D. Rodriguez-Blanco, S. Shaw, P. Bots, T. Roncal-Herrero, and L.G. Benning. The role of pH and Mg on the stability and crystallization of amorphous calcium carbonate. *Journal of Alloys and Compounds*, 536:S477 – S479, 2012.

[14] J.D. Rodriguez-Blanco, S. Shaw, and L.G. Benning. The kinetics and mechanisms of amorphous calcium carbonate (ACC) crystallization to calcite, via vaterite. *Nanoscale*, 3(1):265–271, 2011.

[15] Bettina Purgstaller, Vasileios Mavromatis, Adrian Immenhauser, and Martin Dietzel. Transformation of Mg-bearing amorphous calcium carbonate to Mg-calcite - In situ monitoring. *Geochimica et Cosmochimica Acta*, 174:180 – 195, 2016.

[16] Yael Politi, David R. Batchelor, Paul Zaslansky, Bradley F. Chmelka, James C. Weaver, Irit Sagi, Steve Weiner, and Lia Addadi. Role of magnesium ion in the stabilization of biogenic amorphous calcium carbonate: A structure-function investigation. *Chemistry of Materials*, 22(1):161–166, 2010.

[17] P. Bots, L.G. Benning, R.E.M. Rickaby, and S. Shaw. The role of SO_4 in the switch from calcite to aragonite seas. *Geology*, 39(4):331–334, 04 2011.

[18] Xia Long, Yurong Ma, and Limin Qi. In vitro synthesis of high Mg calcite under ambient conditions and its implication for biomineralization process. *Crystal Growth & Design*, 11(7):2866–2873, 2011.

[19] D. Wang, L. M. Hamm, A. J. Giuffre, T. Echigo, J. Donald Rimstidt, J. J. De Yoreo, J. Grotzinger, and P. M. Dove. Revisiting geochemical controls on patterns of carbonate deposition through the lens of multiple pathways to mineralization. *Faraday Discuss.*, 159:371–386, 2012.

[20] Nan Xu, Yanan Li, Lei Zheng, Yuxi Gao, Hongwei Yin, Jiating Zhao, Zhigang Chen, Jianping Chen, and Ming Chen. Synthesis and application of magnesium amorphous calcium carbonate for removal of high concentration of phosphate. *Chemical Engineering Journal*, 251:102 – 110, 2014.

[21] S. Raz, S. Weiner, and L. Addadi. Formation of high-magnesian calcites via an amorphous precursor phase: Possible biological implications. *Advanced Materials*, 12(1):38–42, 2000.

[22] Pao-Tao Yu, Chieh Tsao, Chun-Chieh Wang, Chun-Yu Chang, Chia-Hsin Wang, and Jerry Chun Chung Chan. High-magnesium calcite mesocrystals: Formation in aqueous solution under ambient conditions. *Angewandte Chemie International Edition*, 56(51):16202–16206, 2017.

[23] M.M. Reddy and G.H. Nancollas. The crystallization of calcium carbonate: IV. The effect of magnesium, strontium and sulfate ions. *Journal of Crystal Growth*, 35(1):33 – 38, 1976.

[24] Cang-Jie Lin, Sheng-Yu Yang, Shing-Jong Huang, and Jerry C. C. Chan. Structural characterization of Mg-stabilized amorphous calcium carbonate by Mg-25 solid-state NMR spectroscopy. *The Journal of Physical Chemistry C*, 119(13):7225–7233, 2015.

[25] Bettina Purgstaller, Katja E. Goetschl, Vasileios Mavromatis, and Martin Dietzel. Solubility investigations in the amorphous calcium magnesium carbonate system. *CrystEngComm*, 21:155–164, 2019.

[26] I.G Richardson. The nature of C-S-H in hardened cements. *Cement and Concrete Research*, 29(8):1131 – 1147, 1999.

[27] A.W Harris, M.C Manning, W.M Tearle, and C.J Tweed. Testing of models of the dissolution of cements-leaching of synthetic CSH gels. *Cement and Concrete Research*, 32(5):731 – 746, 2002.

[28] U.R. Berner. Modelling the incongruent dissolution of hydrated cement minerals. *Radiochimica Acta*, 44(45):387 – 393, 1988.

[29] Kazuko Haga, Masahito Shibata, Michihiko Hironaga, Satoru Tanaka, and Shinya Nagasaki. Change in pore structure and composition of hardened cement paste during the process of dissolution. *Cement and Concrete Research*, 35(5):943 – 950, 2005.

[30] C. Perlot, J. Verdier, and M. Carcassès. Influence of cement type on transport properties and chemical degradation: Application to nuclear waste storage. *Materials and Structures*, 39(5):511 – 523, Jun 2006.

[31] Christophe Carde, Raoul François, and Jean-Michel Torrenti. Leaching of both calcium hydroxide and C-S-H from cement paste: Modeling the mechanical behavior. *Cement and Concrete Research*, 26(8):1257 – 1268, 1996.

[32] F. H. Heukamp, F.-J. Ulm, and J. T. Germaine. Does calcium leaching increase ductility of cementitious materials? Evidence from direct tensile tests. *Journal of Materials in Civil Engineering*, 17(3):307–312, 2005.

[33] Georgios Constantinides and Franz-Josef Ulm. The effect of two types of C-S-H on the elasticity of cement-based materials: Results from nanoindentation and micromechanical modeling. *Cement and Concrete Research*, 34(1):67 – 80, 2004.

[34] James Vanzo. *A nanochemomechanical investigation of carbonated cement*. M.Sc, Massachusetts Institute of Technology, 2009.

[35] Veronique Barlet-Gouédard, Gaëtan Rimmelé, Bruno Goffé, and Olivier Porcherie. Well technologies for CO_2 geological storage: CO_2-Resistant cement. *Oil & Gas Science and Technology*, 62(12):325 – 334, 2007.

[36] A. Fabbri, J. Corvisier, A. Schubnel, F. Brunet, B. Goffé, G. Rimmelé, and V. Barlet-Gouédard. Effect of carbonation on the hydro-mechanical properties of portland cements. *Cement and Concrete Research*, 39(12):1156 – 1163, 2009.

[37] Ján Jerga. Physico-mechanical properties of carbonated concrete. *Construction and Building Materials*, 18(9):645 – 652, 2004.

[38] Björn Johannesson and Peter Utgenannt. Microstructural changes caused by carbonation of cement mortar. *Cement and Concrete Research*, 31(6):925 – 931, 2001.

[39] Juan Manuel Galíndez and Jorge Molinero. Assessment of the long-term stability of cementitious barriers of radioactive waste repositories by using digital-image-based microstructure generation and reactive transport modelling. *Cement and Concrete Research*, 40(8):1278 – 1289, 2010.

[40] Zhongcun Zuo and Terry Bennett. Simulation of the degradation of oilwell cement for the prediction of long-term performance. *Construction and Building Materials*, 202:669 – 680, 2019.

[41] Gaëtan Rimmelé, Véronique Barlet-Gouédard, Olivier Porcherie, Bruno Goffé, and Fabrice Brunet. Heterogeneous porosity distribution in Portland cement exposed to CO_2-rich fluids. *Cement and Concrete Research*, 38(8):1038 – 1048, 2008.

[42] Andrew Duguid and George W. Scherer. Degradation of oilwell cement due to exposure to carbonated brine. *International Journal of Greenhouse Gas Control*, 4(3):546 – 560, 2010.

[43] Barbara G. Kutchko, Brian R. Strazisar, David A. Dzombak, Gregory V. Lowry, and Niels Thaulow. Degradation of well cement by CO_2 under geologic sequestration conditions. *Environmental Science & Technology*, 41(13):4787–4792, 2007.

[44] Marcus Wigand, John P. Kaszuba, J. William Carey, and W. Kirk Hollis. Geochemical effects of CO_2 sequestration on fractured wellbore cement at the cement/caprock interface. *Chemical Geology*, 265(1):122 – 133, 2009.

[45] C Dow and F.P Glasser. Calcium carbonate efflorescence on portland cement and building materials. *Cement and Concrete Research*, 33(1):147 – 154, 2003.

[46] M. Schwotzer, T. Scherer, and A. Gerdes. Protective or damage promoting effect of calcium carbonate layers on the surface of cement based materials in aqueous environments. *Cement and Concrete Research*, 40(9):1410 – 1418, 2010.

[47] Tianfu Xu, Eric Sonnenthal, Nicolas Spycher, and Karsten Pruess. *TOUGHREACT: A new code of the TOUGH family of nonisothermal multiphase reactive geochemical transport in variably saturated geologic media.* Lawrence Berkeley National Laboratory, Berkeley, California, 2003.

[48] T Mori and K Tanaka. Average stress in matrix and average elastic energy of materials with misfitting inclusions. *Acta Metallurgica*, 21(5):571 – 574, 1973.

[49] E. Stora, Q.-C. He, and B. Bary. Influence of inclusion shapes on the effective linear elastic properties of hardened cement pastes. *Cement and Concrete Research*, 36(7):1330 – 1344, 2006.

[50] Jun Jiang, Min-Rui Gao, Yun-Hao Qiu, and Shu-Hong Yu. Gram-scale, low-cost, rapid synthesis of highly stable Mg-ACC nanoparticles and their long-term preservation. *Nanoscale*, 2:2358–2361, 2010.

[51] Thomas J. Wolery. EQ3/6, A software package for geochemical modeling of aqueous systems: package overview and installation guide. *Lawrence Livermoer Laboratory, Berkeley, California*, 1992.

[52] Hao Wang, Viveka Alfredsson, Juergen Tropsch, Roland Ettl, and Tommy Nylander. Formation of $CaCO_3$ deposits on hard surfaces - Effect of bulk solution conditions and surface properties. *ACS Applied Materials & Interfaces*, 5(10):4035–4045, 2013.

[53] Fredrik P. Glasser, Jacques Marchand, and Eric Samson. Durability of concrete - Degradation phenomena involving detrimental chemical reactions. *Cement and Concrete Research*, 38(2):226 – 246, 2008.

[54] D. Jacques, L. Wang, E. Martens, and D. Mallants. Modelling chemical degradation of concrete during leaching with rain and soil water types. *Cement and Concrete Research*, 40(8):1306 – 1313, 2010.

[55] Edward N. Matteo and George W. Scherer. Experimental study of the diffusion-controlled acid degradation of Class H Portland cement. *International Journal of Greenhouse Gas Control*, 7:181 – 191, 2012.

[56] Fabien Georget, Jean H. Prévost, and Bruno Huet. Reactive transport modelling of cement paste leaching in brines. *Cement and Concrete Research*, 111:183 – 196, 2018.

[57] Georgios Constantinides. *The elastic properties of calcium leached cement pastes and mortars: A multi-scale investigation.* MSc Thesis, MIT, 2002.

[58] C.-J. Haecker, E.J. Garboczi, J.W. Bullard, R.B. Bohn, Z. Sun, S.P. Shah, and T. Voigt. Modeling the linear elastic properties of portland cement paste. *Cement and Concrete Research*, 35(10):1948 – 1960, 2005.

[59] Paulo J.M. Monteiro and C.T. Chang. The elastic moduli of calcium hydroxide. *Cement and Concrete Research*, 25(8):1605 – 1609, 1995.

[60] E. Stora, B. Bary, Q.-C. He, E. Deville, and P. Montarnal. Modelling and simulations of the chemo–mechanical behaviour of leached cement-based materials: Leaching process and induced loss of stiffness. *Cement and Concrete Research*, 39(9):763 – 772, 2009.

[61] A. Boumiz, D. Sorrentino, C. Vernet, and F. Cohen Tenoudji. *Modelling the development of the elastic moduli as a function of the degree of hydration of cement pastes and mortars.* In: A. Nonat (Ed.), Proceedings 13 of The 2nd RILEM Workshop on Hydration and Setting, Dijon, France, 1997.

[62] René de Borst, Mike A. Crisfield, Joris J. C. Remmers, and Clemens V. Verhoosel. *Non-Linear Finite Element Analysis of Solids and Structures.* John Wiley & Sons, Ltd, 2012.

[63] Antonio Rodríguez-Ferran, Irene Morata, and Antonio Huerta. A new damage model based on non-local displacements. *International Journal for Numerical and Analytical Methods in Geomechanics*, 29(5):473–493, 2005.

[64] M. Jirásek and S. Marfia. Non-local damage model based on displacement averaging. *International Journal for Numerical Methods in Engineering*, 63(1):77–102, 2005.

[65] Terry Bennett and Sivakumar Kulasegaram. On the use of a damage model based on non-local displacements in the Element-Free Galerkin method. In C. A. Motasoares, J. A. C. Martins, H. C. Rodrigues, Jorge A. C. Ambrósio, C. A. B. Pina, C. M. Motasoares, E. B. R. Pereira, and J. Folgado, editors, *III European Conference on Computational Mechanics*, page 362. Springer Netherlands, 2006.

Chapter 5

Conclusions and recommendations

5.1 Conclusions

The modelling methodology of fully coupled chemo-mechanical degradation is developed in the present thesis, which consists of reactive transport, non-local damage and micromechanical model. The proposed coupled damage model is able to predict the long-term performance of cement-based materials in various real service conditions based on chemical degradation, and subsequently evaluate the residual mechanical properties/behaviour in the instantaneous interaction with the progress of chemical reactions. In the perspective of engineering practice, the presented model can assess the serviceability of cement-based materials in contact with aggressive aqueous solutions, and contribute to the decision-making of remediation and replacement. In the perspective of theoretical study, the present model successfully accommodates interdisciplinary methodologies to integrate the modelling of coupled chemo-mechanical degradation, and is able to demonstrate the physical and chemical variation of cement-based materials from the constituents on microscale to structural behaviour on macroscale.

According to the objectives in section 1.2, the major research outcomes of the present thesis are summarised as following innovations:

Objective 1 :

- According to service conditions of oilwell cement, the long-term chemical degradation up to 1000 years is investigated with reactive transport model for the integrity of cement sheath subject to groundwater, and the model parameters are calibrated by existing experiments, which overcomes the difficulties of extrapolating experimental results. The interaction between cement constituents

and pH of pore solution reveals the process of chemical degradation on microscale. The corrosion depth of cement annulus is predicted versus the square root of time, which is practical for the assessment and forecast in industrial projects.

- The difference of corrosion rate for cement sheath subject to groundwater is demonstrated with dissolution/precipitation of cement minerals, which provides a deep insight of long degradation in real service conditions. The precipitation of calcite has an important impact on corrosion rate by reducing/clogging the pore space within material matrix, which accord with experimental outcomes. In addition, the precipitation of ettringite with the dependence of pH is captured, which is essential for studying the expansive effect of ettringite and the subsequent mechanical damage on cement-based materials.

Objective 2 :

- Based on existing studies on coupled chemo-mechanical degradation, the non-local damage model is coupled with reactive transport model to overcome the existing difficulty of capturing the post-peak behaviour of the material. With the integration of aquatic chemistry and proper development of microcracks in the proposed model, the simulated flexural performance of three-point bending test show good agreement with experimental outcomes, which verifies the significance of non-local damage model in coupled degradation modelling.
- The fully coupled chemo-mechanical degradation demonstrates remarkable difference with the non-coupled case, which results in different residual properties and subsequent mechanical behaviour. The propagation of microcraks is influenced by the degraded area, of which the elastic moduli are evaluated by Mori-Tanaka scheme and the evolution of elastic threshold is qualitatively determined on the basis of experimental outcomes.

Objective 3 :

- The detailed review of magnesium ions incorporated into amorphous calcium carbonate is performed to reveal the influence of Mg/Ca ratio on amorphous calcium magnesium carbonate (ACMC) formation, which can explain the conflicting experimental outcomes in literature. The sealing layer of ACMC on the surface of cement-based materials is demonstrated by existing experimental outcomes, which is simulated with the latest data of solubility product.

- The chemo-mechanical behaviour of calcium carbonate precipitation is evaluated with the proposed model on the basis of the dependence to reactive environments. The enhancement of calcium carbonate precipitation on cement elastic moduli is accommodated by Mori-Takana scheme, which generally accords with experimental results. The interaction of pH and CO_2 concentration is successfully simulated to demonstrate the pore-clogging effect and dissolution/re-precipitation of calcium carbonate layer.

5.2 Recommendations

The present research project is an interdisciplinary science, covering geochemistry, continuum damage and micromechanics, and inevitably involves assumptions and limitations. In this context, the study of coupled chemo-mechanical degradation can potentially be further consummated as following recommendations.

- Mass transport is defined by Fick's law in reactive transport model, and negate the electrical potential caused by the motion of charged particles. The Poisson–Nernst–Planck equations can describe the electro-diffusion to account for electroneutrality. The diffusivity and tortuosity are primary aspects determining movement of ion species, and approximatively evaluated by saturation and porosity based on homogenization, which is to be further studied heterogeneously.

- Corrosion depth of cement-based materials subject to aggressive aqueous solutions is an essential indicator for degradation assessment, and the available measuring methods suffer limitations. It is suggested to apply advanced testing technology to develop an universal measuring method, especially non-destructive inspection, which can provide solid validations for the outcomes of numerical simulations.

- The present study is focusing on the coupling effect of chemical and mechanical degradation, and has not involved other issues like temperature effect on chemical reactions, material plasticity and creep. The proposed methodology could incorporate above mentioned issues and fulfil future studies.

- In order to be consistent with the adopted reactive transport model, the mechanical damage is converted to an equivalent porosity change to evaluate the diffusivity and tortuosity, which is a phenomenological assumption to realize the

complicated interdisciplinary project. However, the influence of microcracks on transport properties of materials has yet to be comprehensively studied, which can further be extended to the impact of fractures on the process of reactive transport.

- The presence of magnesium in carbonated brine has been widely recognized and studied in chemical engineering, however has not yet been highlighted in carbonation studies on cement-based materials. The formation and subsequent sealing effect of ACMC is discussed in the thesis, which has real potential in $CaCO_3$ related research and application.

- The enhancement of calcium carbonate precipitation on elastic moduli is qualitatively evaluated with Mori-Tanaka scheme in the thesis. The constitutive behaviour of calcium carbonate strengthened cement involves both theoretical and experimental studies to quantitatively evaluate the current mechanical properties. The measurement of elastic threshold and Young's modulus evolution can vastly promote theoretical study and numerical simulation, however is challenging due to difficulties of accurately realizing and testing the mixture of totally/intermediately leached cement matrix and calcium carbonate.

- The premise of the chemo-mechanical degradation in the present study is saturated condition, which means that diffusion is the predominant mechanism initiating the degradation process. However, advection is a crucial scenario for the application of chemo-mechanical process, which can be further investigated on the basis of the present study.